STUDIES RELATING TO CYCLOTRON EMISSION FROM SEMICONDUCTORS

David A. Cowan

A Thesis Submitted for the Degree of PhD
at the
University of St Andrews

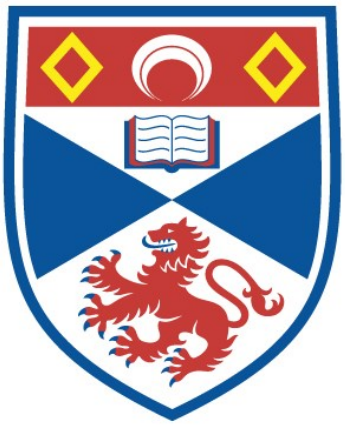

1985

Full metadata for this item is available in
St Andrews Research Repository
at:
http://research-repository.st-andrews.ac.uk/

Please use this identifier to cite or link to this item:
http://hdl.handle.net/10023/14664

This item is protected by original copyright

STUDIES RELATING TO CYCLOTRON EMISSION

FROM SEMICONDUCTORS

A thesis presented by David Cowan to the University of St. Andrews in application for the Degree of Doctor of Philosophy

ProQuest Number: 10167168

All rights reserved

INFORMATION TO ALL USERS
The quality of this reproduction is dependent upon the quality of the copy submitted.

In the unlikely event that the author did not send a complete manuscript
and there are missing pages, these will be noted. Also, if material had to be removed,
a note will indicate the deletion.

ProQuest 10167168

Published by ProQuest LLC (2017). Copyright of the Dissertation is held by the Author.

All rights reserved.
This work is protected against unauthorized copying under Title 17, United States Code
Microform Edition © ProQuest LLC.

ProQuest LLC.
789 East Eisenhower Parkway
P.O. Box 1346
Ann Arbor, MI 48106 – 1346

Th A279

Declaration

I hereby certify that this thesis has been composed by me, is a record of work done by me and has not previously been presented for a Higher Degree. The research was carried out in the physical sciences laboratory of St. Salvador's College, in the University of St. Andrews under the supervision of Professor R.A. Stradling.

David Cowan

Certificate

I certify that David Cowan has spent nine terms of work in the laboratories of the School of Physical Science, University of St. Andrews, under my direction, that he has fulfilled the conditions of the Resolution of the University Court, 1967, no.1, and that he is qualified to submit the accompanying thesis in application for the Degree of Doctor of Philosophy.

Research Supervisor

Career

In october 1981, following the award of an S.E.R.C. studentship I enrolled as a research student under Resolution of the University Court, 1967, No.1, as a Candidate for the Degree of Doctor of Philosophy.

Acknowledgements

The author wishes to express his thanks to:

His parents.

His supervisor, Prof. R.A. Stradling for his help and advice.

His colleagues: Chris Armistead, Dave Marks, Steve Najda, Clivia Sotomayor-Torres, Tony Thorley, Carol Trager and Zbyczek Wasilewski for much appreciated help and companionship.

Phil Gribbon for many good days in the hills.

The technical and cryogenic staff in the physics department, in particular:
Bob Mitchell for valuable help on a variety of technical problems;
Doug Irons for invaluable assistance in sample preparation and related feats of coordination.

Dr P. Knowles for the gift of samples.

The S.E.R.C. for providing a C.A.S.E. studentship with R.S.R.E Malvern and Dr N. Apsley for his supervision at Malvern.

Finally my fellow research students for helping me to drink many pints of Guinness and the Guinness Brewing Company for supplying it.

Abstract

In this thesis studies relating to cyclotron emission in GaAs, InSb, InP and $Cd_xHg_{1-x}Te$ (C.M.T.) are described.

The effect of the electric field bias on the emission intensity and linewidth in GaAs and InP is studied and a theoretical model is proposed. The study indicates the importance of nonparabolicity and polar mode scattering in determining the intensity and linewidth in these materials. Inter-excited state transitions are observed for the first time in emission. Nonparabolicity splitting is observed in InP and that in GaAs, originally observed in by Gornik (1983),is confirmed.

The application of hydrostatic pressure to InSb is observed to narrow the emission line by a factor of three.

In experiments on the magnetoimpurity effect in GaAs transitions between the 1S and $2P_-$, $2P_o$, $3D_{-2}$ and $3D_{-1}$ impurity states are observed and central cell structure is observed for the first time .

In bulk C.M.T. cyclotron resonance is studied as a function of hydrostatic pressure and reasonable agreement is achieved with accepted values for the variation of band gap with pressure. In the surface layer cyclotron resonance is observed as are Shubnikov de Haas oscillations and electric subband energies are calculated for each of these experiments.

Finally the use of cyclotron emission as a spectroscopic source is demonstrated and future developments discussed.

Table of Contents

	page
1. Introduction	1
2. Theory	8
2.1 Introduction	9
2.2 Band Structure	9
2.2.1 Effective Mass	11
2.2.2 Nonparabolicity	12
2.3 Effect of a Magnetic Field	14
2.4 Cyclotron Resonance	15
2.4.1 Classical Theory	15
2.4.2 Quantum Theory	16
2.4.3 Cyclotron Resonance Linewidths	16
2.5 Hot Electron Theory	21
2.6 Impurity Levels	24
2.6.1 Central Cell Structure	25
2.6.2 Compensation	26
2.6.3 Effect of a Magnetic Field	27
2.7 Cyclotron Emission	28
2.7.1 Nonparabolicity Broadening	30
2.7.2 Linewidths due to the Broadening of the Landau Levels	31

Page

3. Experimental Method 32

3.1 Double Magnet System 33

3.2 Emission Experiment 35

3.2.1 Analysis of Emission Spectra 38

3.3 Sample Preparation 39

3.3.1 GaAs and InP 39

3.3.2 InSb 40

3.4 Pressure bomb 40

3.5 Far-infra-red Laser System 42

4. Cyclotron Emission from GaAs and InP 44

4.1 Introduction 45

4.2 Cyclotron Emission 47

4.3 Samples 49

4.4 Linewidth-Sample Dependence 50

4.5 Electric Field Dependence on Linewidth 53

4.5.1 Lineshape Model 55

4.5.2 Comparison of Experimental and Theoretical Results 57

4.6 Other Transitions

4.6.1 Splittings of the Cyclotron Lines Resulting from Nonparabolicity of the Conduction Band 61

4.6.2 Impurity Transitions 63

4.7 Conclusions 65

Page

5. Cyclotron Emission in InSb under Pressure 66

5.1 Characteristics of InSb and Review of Previous Work 67

5.2 Effect of Hydrostatic Pressure 70

5.3 Experimental 74

5.3.1 Cyclotron Resonance 75

5.3.2 Cyclotron Emission 76

5.4 Discussion of Narrowing Mechanisms 78

5.5 Future Work 81

6. Magnetoimpurity Effect in GaAs 82

6.1 Introduction 83

6.2 Experimental 85

6.2.1 Sample characteristics 87

6.3 Results 88

6.3.1 'Heating' or 'Cooling 89

6.3.2 Effect of Electric Field 91

6.3.3 Central Cell Structure 92

6.4 Relevance of the Magnetoimpurity Effect to Cyclotron Emission 95

6.5 Conclusion 96

Page

7. Cyclotron Resonance in C.M.T. 98

7.1 Introduction 99

7.2 Cyclotron Resonance and the Effect of a Magnetic Field 99

7.3 Surface Electronic States 101

7.4 Experimental 102

7.5 Results and Analysis 103

7.5.1 Cyclotron Resonance Data 103

7.5.2 Accumulation Layer Data 104

7.6 Conclusion 106

8. Cyclotron Emission as a Spectroscopic Source 107

8.1 Description of Source 108

8.2 Detectors 109

8.3 Spectrometer 110

8.4 Spectrometer modes 101

8.4.1 Fixed Wavelength Mode 110

8.4.2 Swept frequency Mode 112

8.5 Other Examples of Spectrometer Application 114

8.5.1 Ion Implanted Silicon 114

8.5.2 Central Cell Structure 115

8.5.3 Phonon Spectra 116

8.6 Conclusions 116

References 117

List of Diagrams

2.1 Typical band structure for materials of interest

2.2 Effect of magnetic field on band structure

2.3 Electron energy distribution (Gornik(1980))

2.4 Impurity state binding energies

3.1 Schematic diagram of the double magnet system

3.2 Schematic diagram showing the emission experiment

3.3 Detector Response

3.4 Energies of detector lines

3.5 Pressure Bomb

3.6 Schematic diagram of the F.I.R. laser system

4.1 Schematic diagram showing cyclotron emission in and InP

4.2 Graph of linewidth vs. total impurity concentration

4.3 Linewidth vs electric field - GaAs

4.4 Intensity vs electric field - GaAs

4.5 Linewidth and intensity vs electric field -InP

4.6 Examples of calculated lineshapes

4.7 Nonparabolicity splitting in GaAs

4.8 Nonparabolicity splitting in InP

4.9 'A' lines in GaAs and InP

4.10 'A' lines and cyclotron resonance energies

5.1 Central cell structure of donors in InSb

5.2 Band structure in InSb

5.3 Effect of pressure on the conduction band and ground impurity states in InSb

5.4 Schematic diagram of the conduction band and impurity in InSb

5.5 Configuration coordinate diagram showing lattice relaxation after electron transfer

5.6 Cyclotron resonance in InSb under pressure

5.7 Cyclotron resonance in InSb under pressure

5.8 Cyclotron emission in InSb under pressure

5.9 Graph of linewidth vs pressure

5.10 I-V characteristic in InSb

6.1 Differentiation circuits

6.2 Magnetoimpurity effect results

6.3 Transition energies for the magnetoimpurity effect

6.4 Effect of electric field

6.5 Central cell structure-m.i.r.

6.6 Central cell structure-photoconductivity

7.1 Band structure showing C.M.T. alloys

7.2 Schematic diagram of accumulation layer

7.3 Diagram showing transmission set up on pressure bomb

7.5 Graph of pressure vs. effective mass

7.6 Shubnikov de Haas oscillations in C.M.T. under pressure

7.7 Surface subband cyclotron resonance

8.1 Broadband detector response

8.2 Schematic diagram of spectrometer

8.3 Cyclotron resonance absorption in InSb

8.4 Impurity and phonon spectra in CdTe

8.5 Interference fringes on ion implanted silicon

8.6 Central cell structure

8.7 Phonon spectra

List of Tables

2.1 Table showing band structure parameters

2.2 Table showing shallow impurity parameters

4.1 Sample characteristics

4.2 Linewidths-experimental

4.3 Linewidths-theoretical

6.1 Summary of results from magnetoimpurity effect

7.1 Results on the accumulation layer on C.M.T.

Note on the use of symbols

The meanings of symbols are mostly explained in the text, however, the letter E is used both for energy and electric field. Where conflicts arise the letter W is used for energy.

CHAPTER 1

INTRODUCTION

Introduction

Spectroscopy in the region of the spectrum between microwave and infrared wavelengths has never been easy and this is largely as a result of the lack of a high power tunable source.

At the low frequency end of the spectrum conventional radio transmitters give way to valve oscillators as the frequency is increased and at higher frequencies semiconductor oscillators based on negative differential resistance characteristics are used. These devices stop working, however, at frequencies much above 100GHz.

In applications not requiring coherent sources a variety of spectrometers are available. In the infra-red grating spectrometers using Nernst sources are used but they become very difficult below about 30000GHz($1000cm^{-1}$). Fourier transform spectrometers work reasonably well as low as 300GHz($10cm^{-1}$) but in the far infrared we are working in the tail of the black body emission spectrum and only very low powers are available.

The advent of optically pumped molecular gas lasers provided a boost to spectroscopy in the far-infra-red in the late 1960's but, although they can produce very high power outputs, they work at fixed frequency and spectra must be obtained by scanning some other variable.

In the 1970's the search for a tunable source in the far infrared increased and it was mostly centred on emission from semiconductors at low temperatures. One of the most promising of these is cyclotron emission. The object of the research described in the thesis was the study of cyclotron emission and its development into a tunable source in the far-infra-red.

Cyclotron emission is the reverse process to cyclotron resonance- photons are emitted from a hot electron gas at the cyclotron frequency

$$w_c = eB/m^*$$

as the electrons decay from one Landau level to the next. The potential applications for a tunable incoherent source are discussed at length in Chapter 8 on the use of cyclotron emission as a spectroscopic source and the potential is considerable.

Aside from cyclotron emission other possibilities have been considered and for completeness these are briefly described below.

1. Two dimensional subband emission - In this case the electrons are confined to move in an inversion, accumulation layer or quantum well. As a consequence the energy levels are quantised in the direction perpendicular to the the surface. The electrons are only free to move along the surface and so they form what are known as two dimensional

subbands. Emission is observed once the carriers are heated out of equilibrium by an electric field into higher subbands and radiatively decay from one subband to the next. This emission would be tunable by applying a gate voltage in an metal-insulator-semiconductor(m.i.s.) device but the power levels are very small and it must be doubted whether this can be considered to be a viable source. The possibility of using a multiple quantum well and increasing the power many times over has to be considered. At present it is possible to grow structures with as many as 500 layers of 100Å thickness.

2. Minigap Emission- This is a variant on subband emission which produces much higher power levels. The silicon is cut at an angle a few degrees from the (1,0,0) plane and the electrons in the surface layer of the m.i.s device experience an additional periodicity when the (1,0,0) planes emerge at the surface. This periodicity and the effect of valley orbit splitting conspire to form additional bandgaps in the surface subbands. Gate voltage tunable emission is obtained from recombination across the minigaps.

3. 2D-Plasmon emission- Plasma oscillations are excited with d.c.. electric field bias applied to the surface layer. A grating on the surface couples the nonradiative plasma oscillation to the electromagnetic field. The periodicity of the grating defines, according to the plasmon dispersion relation ($w_p^2 \propto k$), the emitted frequency. This again will be tunable with gate voltage bias or magnetic fields.

4. Emission from streaming carriers- For sufficiently pure

semiconductors electrons can be accelerated by an electric field to the optical phonon energy without scattering. They are then scattered back to zero energy by the emission of optical phonons. With appropriate electric and magnetic fields there is a region in k-space where electrons are in closed orbits which do not cross the optical phonon energy. Carriers will gradually accumulate in this region through weak scattering processes and a population inversion may even occur. Emission can occur between Landau levels or, in the case of the valence band, from radiative transitions between the light and heavy hole bands. Since the strongest nonradiative relaxation mechanism has been eliminated (i.e. that of scattering by L.O. phonons) this must be a candidate for stimulated emission. A great deal of work on GaAs is described in this thesis which raises the interesting question of whether streaming is occurring in this material. For GaAs the time for an electron to accelerate to the L.O.phonon energy in a field of 100V/cm is 10^{-11}s. The scattering time measured from the narrowest emission linewidths is of the order $5x10^{-12}$s and so the electron would probably be scattered before it reached the L.O. phonon energy.

For a review of (1) and (2) see (Gornik et al (1980)) and (Gornik(1982) for (3) and (4).

Although all of these have considerable potential, cyclotron emission has been developed to the greatest extent and has most to offer in terms of linewidth and tunability. In this thesis work on GaAs and InP(Chapter 4) and InSb(Chapter 5) is described. In the case of GaAs and InP the importance of nonparabolicity and polar mode scattering in determining the linewidth and the emission intensity is demonstrated. The effect of hydrostatic pressure in InSb was studied because of the remarkable line narrowing which occurs.

The final aim of the development of cyclotron emission as a radiation source must be the creation of a laser device. However a number of problems have still to be overcome. Firstly, the probability of stimulated emission P_e is always less than that of a further cyclotron absorption transition P_a. For an equally spaced series of Landau levels:

$$P_a/P_e = (n+1)/n$$

where n is the Landau index.

The problem is easily overcome by choosing a material which has unequally spaced Landau levels because of nonparabolicity. In this respect even GaAs is significantly nonparabolic. Secondly energy relaxation times tend to increase towards the band edge making it difficult to achieve a steady state population inversion. This is why the magnetoimpurity effect was studied as it

provides a mechanism for emptying a particular Landau level(Chapter 6). In this effect the conduction band electrons are heated or cooled at the expense of electrons in shallow impurity states as the spacing between two Landau levels corresponds to the spacing between two impurity levels. In these experiments the effect is observed through a change in the resistance of the sample as the magnetic field is swept.

At this start of the research project one of the aims was to study cyclotron emission from $Cd_xHg_{1-x}Te$ (c.m.t.) and in particular from the inversion/accumulation layer on the surface of that material. Although cyclotron emission was not in fact studied related measurements were made. Shubnikov de Haas oscillations and cyclotron resonance were studied as a function of pressure (Chapter 7). The periodicity of the Shubnikov de Haas oscillations gave the energy and population of the subbands in the surface accumulation layer and the cyclotron resonance gave the pressure dependence of the effective mass and bandgap.

Theoretical aspects and previous work are reviewed in Chapter 2, a description of the experimental method follows in Chapter 3. Finally an evaluation of cyclotron emission as a spectroscopic source is presented in Chapter 8.

CHAPTER 2

THEORY AND REVIEW OF PREVIOUS RESULTS

2.1 Introduction

In this chapter a background review of the theory and some previous experimental results will be given. Where necessary more detailed theoretical ideas will be explained in the individual chapters. The chapter starts by introducing band structure and the effect of magnetic fields and goes on to discuss cyclotron resonance, cyclotron resonance linewidths, impurity states, hot electron transport and finally cyclotron emission.

2.2 Band Structure

A schematic diagram of the band structure, typical of the materials used, is shown in fig 2.1. The lowest conduction band minimum lies at the gamma point of the Brillouin zone with higher lying minima at the 'L' and 'X' points. The Bloch functions associated with electrons at the conduction band minimum originate from 'S' like atomic orbitals and, neglecting spin, the band is singly degenerate. Normally the 'L' and 'X' minima in the Brillouin zone are of sufficiently high energy that they do not contribute to conduction even under the hot electron conditions used in many of the experiments.

Typical Band Structure for Materials of Interest

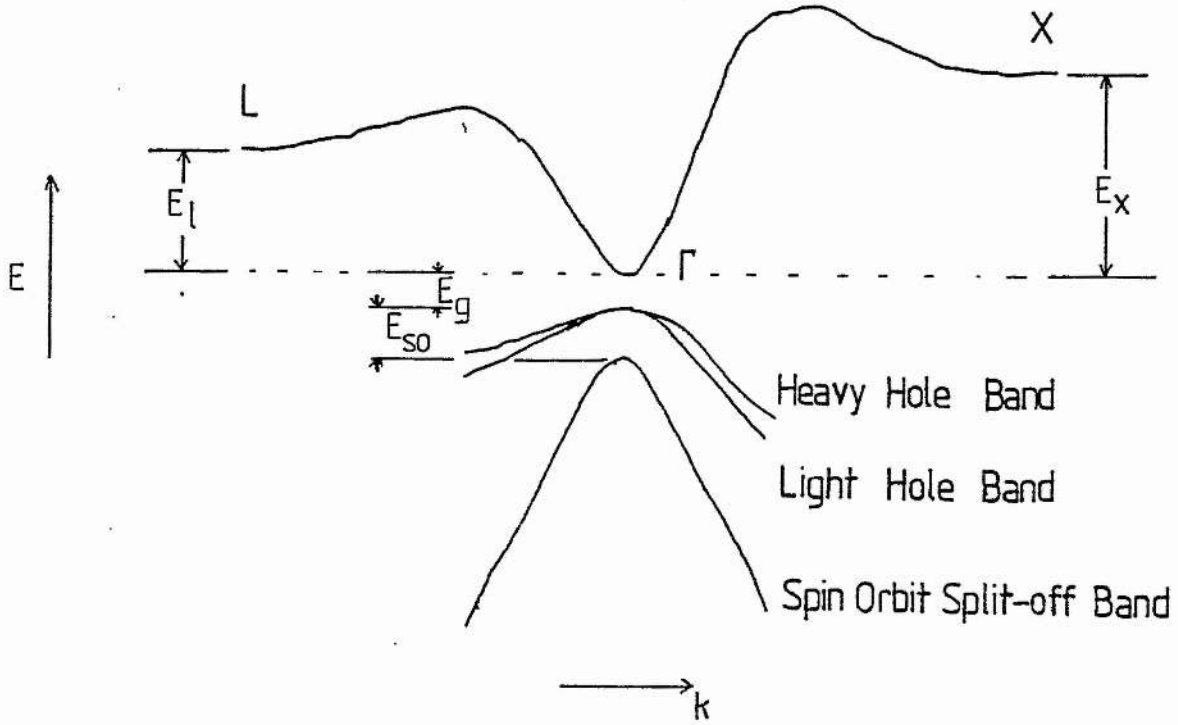

The valence band maxima all lie at the gamma point. The three bands originate from 'P' like atomic orbitals. Two bands are degenerate at the gamma point with different effective masses and a lower lying band separated by spin-orbit splitting also exists. In all the experiments n-type material was used and the primary interest was in electron states close to the conduction band edge. The other conduction band minima were of interest only in respect of the pressure work on InSb where impurity states associated with these minima can be introduced into the band gap. The valence bands were only of concern for calculating second order effects in the conduction band.

Neglecting the effects of spin, phonon coupling and wavefunction admixture from other bands the energy of electrons in the gamma conduction band can be described by the relation

$$E = \frac{\hbar^2 k^2}{2m^*} \qquad -(1)$$

where m^* is the mass of the electron modified by its interaction with the rigid lattice and other electrons.

2.2.1 Effective Mass

The effective mass can be defined in a number of ways:

1) By assuming equation (1) which relates E and k;

2) The conductivity effective mass is given by:

$$m^* = \hbar^2/(d^2E/dk^2) \qquad -(2)$$

where the acceleration produced by an electric field is related to the magnitude of that field;

3) The cyclotron mass is defined by the relation:

$$\hbar w_c = eB/m^* \qquad -(3)$$

Where w_c is the cyclotron frequency of the charge carrier in a magnetic field, B;

4) Another definition is the density of states effective mass which is defined by the equation:

$$D(E) = (2E^{1/2})(m^*)^{3/2}/(\pi^2\hbar^3) \qquad -(4)$$

This gives an average effective mass for non-isotropic and nonparabolic bands whereas 1, 2 and 3 are in general tensors.

When the bands are nonparabolic each of these definitions will produce a different value and possibly even a different sign of effective mass. When the band is parabolic all definitions yield the same value. However,

with the exception of c.m.t. the bands are reasonably parabolic for the materials and energies of interest in this thesis. The 4.2K band-gaps, band edge effective masses and band structure parameters are shown in table 2.1 along with some phonon frequencies and phonon coupling constants.

Table 2.1.

	GaAs	InP	InSb	C.M.T.(x=0.2)
m^*/m(Gamma)	0.0665	0.0803	0.0139	0.0008
E_g/eV	1.52	1.42	0.235	0.10
m^*_{hh}	0.50	0.56	0.40	
m^*_{lh}	0.08	0.12	0.016	
m^*_{so}	0.15	0.12	0.43	
E_X/eV	0.52	0.94	1.60	
E_L/eV	0.31	0.69	0.80	
E_{so}/eV	0.35	0.21	0.82	
Froelich const.	0.068	0.113	0.022	
$\hbar\omega_{lo}$/cm^{-1}	296	350	196	143

2.2.2 Non-Parabolicity

It was mentioned in the previous paragraph that the energy of the electrons may not be given by the energy wave-vector relation

$$E=\hbar^2k^2/2m^* \qquad -(1)$$

with constant m^*.

A deviation from a parabolic relationship can be caused by interactions with LO phonons and always arises in any

explicit form of band theory.

The latter can be seen by using $\underline{k}.\underline{p}$ theory (Kane (1957)). Using a two band model, valid only when $E<<E_g+2E_{so}/3$, it is possible to derive the relation

$$E = E_g/2 + ((E_g/2)^2 + E_g(\hbar^2k^2/2m^*))^{1/2} \quad -(5)$$

Which, when expanded, gives a parabolic relation close to the band edge with higher order terms for higher values of k.

The other important deviation from a parabolic band is due to the interaction with longitudinal optical phonons. In this case the electron becomes a polaron, which is a quasi-particle comprising an electron surrounded by a polarisation in the lattice or, equivalently by a cloud of L.O. phonons. Apart from a uniform shift in band energies and a small increase from the unperturbed effective mass in the weakly polar materials which we use, the polaron dispersion relation is very similar to that of the electron near to the band edge. Close to the optical phonon energy, however, the interaction becomes resonant and the polaron dispersion relation deviates strongly from that of the electron (see Gornik et al (1983)).

2.3 Effect of a Magnetic Field

In a magnetic field the band structure in a solid is modified. The Shroedinger equation for the conduction band of a solid can be written as

$$(1/2m^*)p^2u_k=E_ku_k \qquad -(6)$$

where u_k is an envelope function. When a field is applied one has to add an extra term to the momentum operator, $\underline{P}=\underline{p}+e\underline{A}$ where $\underline{A}$ is the magnetic vector potential. If the field is in the z direction $\underline{A}$ can be written

$$\underline{A}=(0,Bx,0) \qquad -(7)$$

After some algebra we get

$$H = (p_x^2 - (m^*)^2w_c^2q^2)/(2m^*) + \hbar^2k_z^2/(2m^*) \qquad -(8)$$

where

$$q = X + \hbar k_y/m^*w_c$$

The first term is in the form of the Hamiltonian for a simple harmonic oscillator of frequency w_c, resulting from motion in the plane perpendicular to the magnetic field, while the second term represents the energy of a free electron moving in a direction parallel to the magnetic field. The energy of the system is thus given by

$$E = (n+1/2)\hbar w_c + \hbar^2k_z^2/(2m^*) \qquad -(9)$$

If spin is included an extra term $+/- 1/2g^*\mu_bB$ must be added(g^* is the effective g-factor and μ_b the Bohr magneton). The conduction band of a semiconductor in a magnetic field is shown in figure 2.2. The impurity states shown are discussed in section 2.6.

Band Structure in a Magnetic Field

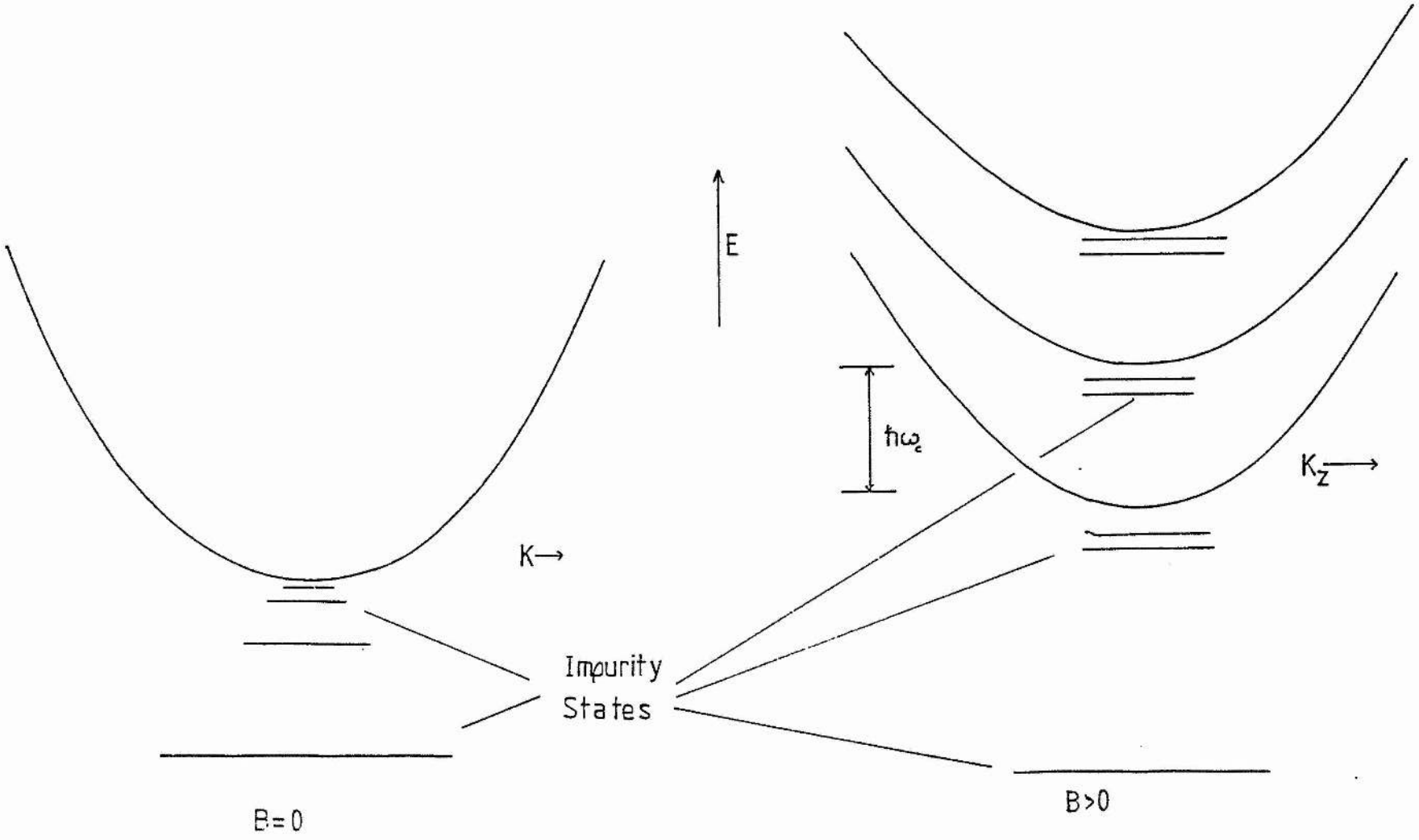

2.4 Cyclotron resonance

2.4.1 Classical Theory

The force on an electron in the presence of an electric and magnetic field can be written as

$$\underline{F} = -e(\underline{v} \times \underline{B}) - \underline{E}e \qquad -(10)$$

where $\underline{F} = m^* d\underline{v}/dt$

and

$$d\underline{v}/dt = -\underline{w}_c \times \underline{v} - e\underline{E}/m^* \qquad -(11)$$

where $\underline{w}_c = q\underline{B}/m^*$

Now we know that the velocity decays after an electron has been accelerated in a time T_{dc} and we can obtain an average velocity

$$\langle \underline{v} \rangle = \int_o^\infty \underline{v} \exp(-t/T_{dc})\, dt \,/ \int_o^\infty \exp(t/T_{dc})\, dt \qquad (12)$$

where T_{dc} is the momentum relaxation time.

Suppose we are applying a circularly polarised electric field

$$\underline{E} = \underline{E}_o \exp(+/- iwt) \qquad (13)$$

then the first order solution for the drift velocity is

$$\underline{v} = \underline{v}_o \exp(+/- iwt) \qquad (14)$$

in the steady state.

Substituting into equation (11) and averaging each term as in equation (12) we obtain

$$\sigma = \langle v \rangle ne/\langle E \rangle = (ne^2/m^*)T/(1 + i(w +/- w_c)T) \qquad -(13)$$

The power absorbed is given by

$$P = Re(\sigma E^2) = P_o/(1 + (w +/- w_c)^2 T^2)$$

where $P_o = Ne^2T/m^*$.

The expression with $w-w_c$ clearly gives resonance when $w=w_c$ also. At half peak height

$$(w - w_c)^2T^2 = 1$$

Thus $$w - w_c = 1/T$$

and $$w_c/\Delta w_{1/2} = wT.$$

or $$B/\Delta B_{1/2} = wT$$

where $\Delta w_{1/2}$ and $\Delta B_{1/2}$ are the half half widths depending on whether the experiment is performed at constant frequency or constant field.

2.4.2 Quantum Theory

Quantum mechanically the cyclotron resonance is an electric dipole transition corresponding to a change

$$\Delta n = +1$$

in the Landau level index.

The probability P_n of transition between the n and n+1 levels is proportional to

$$(n+1)/m^*$$

where I is the power of the incident radiation.

2.4.3 Cyclotron Resonance Linewidths

The cyclotron resonance lineshape has been extensively studied under a large variety of conditions. The final shape is given by the combination of a number of effects. Line broadening mechanisms can be divided into two categories - homogeneous and inhomogeneous broadening (broadening on both and one side of the resonance line respectively

Homogeneous broadening is made up of two components:

1. The natural linewidth, which is the length of time it takes for an electron to radiatively decay from an excited Landau state.
2. The collision linewidth, which is related to the transport properties in the semiconductor.

In all practical situations the natural linewidth is small compared with the collision linewidth. The characteristic lifetime can be defined as the high frequency magneto-current decay time (Kawabata(1967)) in the classical model (see previous section) or by the length of time an electron stays in any particular conduction band state in a quantum model.

For an energy independent scattering time this will yield a Lorentzian lineshape . If the scattering time is energy dependent then one must take the average over the electron energy distribution. The effect is to enhance the peak and to broaden the wings but the broadening will

continue to be homogeneous.

Inhomogeneous broadening may come partly from Stark effects i.e. from changes in the energies of the conduction band electrons as they pass through the stray electric fields of the ionised impurities. Nonparabolicity also has an effect even at low temperatures; lines can be shifted and broadened on the high field or low energy side. Landau transitions have lower energies as one goes away from the conduction band edge because the effective mass of the electrons increases. At weak electric fields and low temperatures the nonparabolicity contributes less than 10% to the linewidth of the cyclotron resonance in the materials and energies of interest in this thesis (see Simmonds(1973) and Kaplan et al(1973).

Scattering Mechanisms which Contribute to the Linewidth

When studying the collision cyclotron resonance linewidth two parameters are of some importance -

1. l/a, where l is the cyclotron radius and a is the characteristic range of the scatterer.
2. $\hbar\omega_c/kT$ which determines whether the cyclotron resonance is occurring in the classical limit with many subbands participating ($\hbar\omega_c/kT<<1$) or in the quantum limit with just two levels participating ($\hbar\omega_c/kT>>1$).

It is also important to understand the meaning of the various relaxation times. $T_{dc}=T_p$ is the momentum relaxation time and is a measure of the length of time that an electron distribution takes to be randomised after it has been accelerated by a pulsed electric field. In a steady state T_p controls the resistivity of the sample.

The energy relaxation time T_w is the average length of time a carrier takes to return to thermal equilibrium after it has been excited out of equilibrium impulsively either electrically or optically.

The cyclotron resonance time T_{cr} is defined by the relation

$$B/\Delta B = w/\Delta w = wT_{cr}$$

In the classical derivation, above, this will equal T_{dc} if an energy independent scattering time is assumed. In other situations T_{cr} can differ markedly from T_{dc} in a way which is determined by the exact form of the scattering potential.

In the classical limit when $1/a>>1$ it is reasonable to assume that the momentum scattering time T_{dc} follows closely the cyclotron resonance time T_{cr}. This is the case for acoustic phonon scattering when $1/a>>1$ (a is the wavelength of the acoustic phonon in this case) at temperatures greater than 20 or 30K. In many semiconductors acoustic phonons

limit both the mobility and the cyclotron resonance linewidth in this range and generally good agreement is found between T_{cr} and T_{dc}. Under quantum limit conditions, i.e. at low temperatures in the far-infra-red (Meyer et al (1962)), considerable deviations are observed.

For ionised impurity scattering considerable deviations are also observed. Two forms of scattering are important- intra Landau level scattering (adiabatic scattering) and elastic scattering between two Landau levels (nonadiabatic scattering). The two lifetimes are normally calculated independently but this is not always valid. Shin(1973) calculated T_{cr} for adiabatic scattering and found

$$T_{cr} \propto n_i^{-1/2} T^o \cdot (1-(c/B^{1/2}))$$

Kawamura et al (1964), using a different impurity potential, found that

$$T_{cr} \propto n_i^{-1/2} B^{1/4} T^o$$

which agreed well with his experimental results on germanium. For nonadiabatic scattering Kawabata(1967) found

$$T_{cr} \propto BT^{1/2}/n_i$$

The expressions for adiabatic scattering were based on a long range couloumb potential scatterer ($1/a<1$) and those for the nonadiabatic scattering on a short range point defect scatterer ($1/a>1$).

More recently Lodder and Fujita (1976) have performed a more rigorous calculation from a statistical mechanical point of view. Their results are in agreement with Kawabata for very low carrier concentrations but then follow the semiclassical theory of Kawamura et al (to within a proportionality constant).

Experimentally, a minimum is observed in the linewidth of the cyclotron resonance in InSb as w_c is increased (Kaplan et al(1973)). This was explained qualitatively by saying that adiabatic scattering (Shin(1973)) is taking over from Kawabata's expression at the minimum. In GaAs and InP the cyclotron resonance linewidth decreases monotonically with field in agreement with Lodder and Kawamura and it is possible that the minimum in InSb is due to a combination of nonparabolicity and an energy dependent scattering time. Another explanation of the minimum is given by Prasad et al (1980). It is claimed that the minimum is due to a combination of acoustic phonon scattering and ionised impurity scattering.

It is quite clear that in the case of ionised impurity scattering not only is T_{dc} much smaller than T_{cr} but also it has a quite different temperature dependence $T^{3/2}$ as compared with T^{o} for the formula derived by Lodder and Fujita . However the dependence on the impurity concentration is the same $\sim n_i^{-1/2}$. It is not clear how T_{dc}

should be changed to account for the effect of the magnetic field. Roth et al (1965) and Kubo et al((1965) found that at low fields (1/a>1) $T_{dc} \sim B$ and that at high fields (1/a<1) $T_{dc} \sim B^{o}$.

2.5 Hot Electron Theory

When a sufficiently large electric field is applied to a semiconductor the electrons are heated out of equilibrium with the lattice and they are then said to have a 'hot' or 'warm' electron energy distribution. If there are sufficient electrons for electron- electron scattering to be strong then a Maxwellian distribution will result(Yamada and Kurasawa (1973)). This distribution can then be characterised by an electron temperature T_e defined such that $3/2k_bT_e$ is the average energy of the electrons:

$$f(W) = \exp(-W/kT_e) \qquad -(14)$$

In dynamic equilibrium the rate of energy gain is equal to the rate of energy loss through phonon emission

$$e\mu E^2 = -\langle dW/dt \rangle = \langle W \rangle - \langle W_o \rangle / T_W \qquad -(15)$$

If the mobility and energy relaxation rates are independent of the electron distribution then we can say that the change in the total energy of the electron system is

$$\langle W \rangle - \langle W_o \rangle = eEv_dT_W$$

and $$v_d = \mu E$$

Then $$(\langle W \rangle - \langle W_o \rangle)/k = T_e - T_o = e\mu T_W E^2/k = aE^2 \qquad -(17)$$

$\langle W \rangle$ is the mean energy of the electron gas

$\langle W_o \rangle$ is the mean energy of the gas in equilibrium

T is the energy relaxation time

v_d is the drift velocity and μ the mobility

In fact if the electron distribution is said to be warm the mobility is dependant on the electron distribution and it can be approximated by

$$\mu = \mu_{E=0}(1 + bE^2)$$

where b is the warm electron coefficient, therefore

$$T_e - T_o = a(1 + bE^2)E^2$$

For bigger fields this approximation no longer holds and the distribution is said to be hot. It is generally assumed that optical phonon scattering dominates the energy relaxation process under warm electron conditions.

All this depends on there being sufficient electrons in the conduction band for interelectronic collisions to result in a Maxwellian energy distribution. If there are insufficient electrons there is a tendency for many of them to be accelerated to the optical phonon energy and then be scattered to the bottom of the conduction band. This leaves effectively two distributions, one associated with high energy electrons with a sharp cut off at the optical phonon energy and another associated with the thermal electrons with a peak around the band edge. Stratton (1958) calculated the carrier concentration necessary for interelectronic collisions to be effective in this way. Even if sufficient interelectronic collisions occur then the distribution will still not be Maxwellian. A strong cut off will occur as a result of energy relaxation by optical phonons and this will be particularly apparent at electron temperatures above about 100K because large numbers of electrons will then be around the optical phonon energy. Electron energy distributions are plotted in figure 2.3 for

Electron Energy Distribution for InSb (After Gornik 1978)

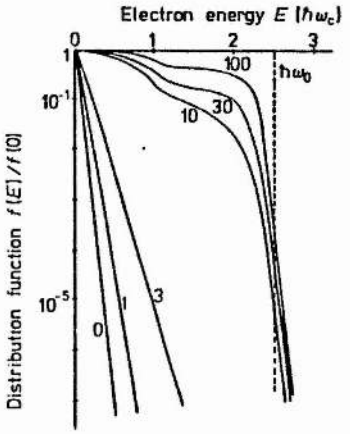

Without el-el Scattering

Distribution function $f(E)$ for different F_{tot} (in V/cm^{-1}) $H = 12$ kG, $n_{imp} = 7 \times 10^{14}$ cm^{-3}, $T_0 = 4{\cdot}2$ K, $\Gamma = 10$ K, but for $n_e = 0$.

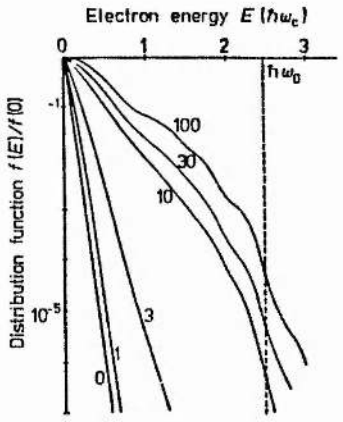

With el-el Scattering

Distribution functions $f(E)$ for different F_{tot} (in V cm^{-1}). $H = 12$ kG, $n_{imp} = 7 \times 10^{14}$ cm^{-3}, $n_e = 1{\cdot}5 \times 10^{14}$ cm^{-3}, $T_0 = 4{\cdot}2$ K, $\Gamma = 10$ K.

calculations which include and neglect electron-electron scattering. It can be seen that electron-electron scattering smooths out the cut-off to some extent.

2.6 Impurity Levels

When an impurity is substituted into the crystal it often has a different valence and consequently a different number of electrons available for bonding than have atoms in the host crystal. When the impurity has fewer electrons it accepts an electron from the crystal to complete the bonding and it is called an acceptor atom. When an atom has a higher valence than the host lattice it gives an electron to the crystal and it is called a donor atom. Interstitials, vacancies and defect complexes can also act as donors or acceptors.

A donor atom, having 'given' its extra electron to the crystal has a net positive charge and similarly the acceptor has a net negative charge and they provide a potential well for electrons and holes respectively. This potential well can be approximated by

$$V(r) = e^2/4\pi\varepsilon_0\varepsilon_r r \qquad -(18)$$

away from the impurity atom.

At low temperatures some electrons bind to the potential and the energy levels of these electrons are those of electrons in the hydrogen atom

i.e. $$E_n = -R_h.(m^*/m)/\ \varepsilon_r^2 n^2 \qquad -(19)$$

$$n = 1,2,3.....$$

measured below the bottom of the conduction band or above the bottom of the valence band. The energy levels are modified by the effective mass ratio and the dielectric constant ε_r which takes into account the polarisation of the lattice. The impurity binding energies, Bohr radii and dielectric constants are given for different materials in table 2.2.

Table 2.2.

	GaAs	InP	InSb
R^*/cm^{-1}	46.1	59.5	4.0
a^*/nm	9.5	8.0	50
ε_r	12.6	12	16.8

The effective mass theory is only valid when $a^* >> a_o$, i.e. it does not include the local potential close to the impurity. (a_o is the lattice spacing)

2.6.1 Central Cell Structure

The ground state of the hydrogenic impurity is the 1S state. The s states are the only ones with a probability density at the impurity atom itself and therefore these are the only states which are strongly sensitive to the chemical nature of the impurity. Transitions from the ground state are split into different components corresponding to each chemical species present. The chemical shifts associated with the nS impurity states (n>1) are much smaller than those associated with the 1S state because the wave function amplitudes of these states are much smaller in the central

cell. In GaAs, InP and InSb these central cell shifts are of the order of $1 cm^{-1}$. If the chemical shift is greater than the effective mass Rydberg then the states can no longer be said to be shallow and the effective mass theory no longer holds.

2.6.2 Compensation

If we have equal numbers of acceptors and donors (N_A and N_D) in the crystal then the extra electron from each donor will complete the binding for each acceptor and we will be left with no net extrinsic carrier concentration and a number $2N_a$ ($=2N_d$) of ionised impurities. For every extra donor or acceptor atom an extra electron or hole respectively will either be bound to an impurity or free to move in the crystal and a carrier concentration of $N_d - N_a$ electrons or $N_a - N_d$ holes will occur if no charge carriers are frozen onto impurities. If $N_d \sim N_a$ then the material is said to be compensated. In these experiments the GaAs samples from the Wright Patterson Air Force Base tended to be very uncompensated (sometimes the compensation ratio could be as low as 5%, see Colter et al (1983)); other samples were somewhat more compensated but the compensation was never great. The InP samples showed a bigger range in compensation and were in general less pure. The InSb samples were fairly highly compensated, but were in general quite pure e.g. $N_d - N_a = 5 \times 10^{13} cm^{-3}$ and $N_d + N_a = 2 \times 10^{14} cm^{-3}$.

2.6.3 Effect of a Magnetic Field

The effect of a magnetic field is to cause Zeeman splitting of the impurity states and to compress the wavefunctions around the impurity atoms in directions perpendicular to the magnetic field. The effect of the magnetic field on a hydrogenic impurity is much stronger than in a real hydrogen atom because the magnetic energy is increased by $1/(m^*/m)$ and the binding energy is reduced by $m^*/m/\ \varepsilon_r^2$. In contrast to cyclotron resonance, where the linewidth is limited by the scattering time, the impurity states are broadened because stray fields from ionised impurities cause shifts in the energies of shallow impurity transitions. These shifts occur at random and the spatial distribution of electric fields causes an inhomogeneous broadening of the line. The compression of the wavefunctions in a magnetic field leads to a narrowing of the impurity transitions when only electric dipole perturbations are considered since the interactions with the stray fields from ionised impurities are decreased. Broadening due to perturbations from quadrupolar interactions associated with electric field gradients reduces initially as the field is applied and then increases to become dominant at high fields. The binding energy of various impurity states is plotted against magnetic field in fig 2.4.

Impurity State Binding Energies

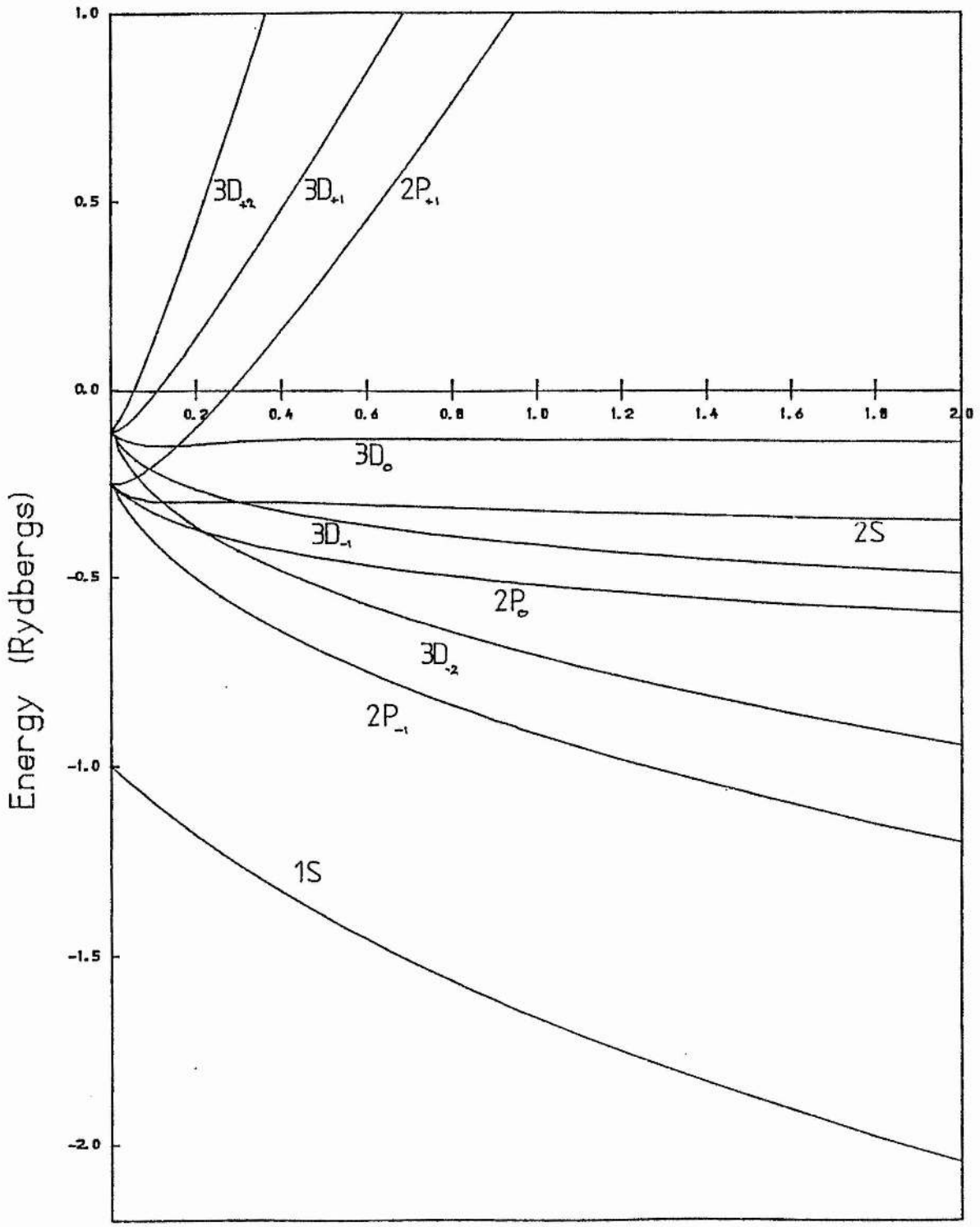

2.7 Cyclotron Emission

A hot electron distribution is a system in dynamic equilibrium at times >> T_w after an electric field is applied. The energy gained by the electron system through an accelerating field is exactly balanced by the energy relaxation of carriers as they try to attain thermal equilibrium with the lattice. Most of the energy is dissipated by phonon emission but small amounts of energy are released in the form of photons (~0.01%).

If a magnetic field is applied to the sample most of these photons result from vertical transitions between Landau levels (at the cyclotron frequency). Cyclotron emission was first observed in InSb by Gornik et al (1972) and has since been observed in GaAs (Waldman et al (1974)), n-Ge (Holtzman (1981)) and p-Ge (Komiyama et al (1982)), InP (Gornik et al (1981)), and c.m.t. (Dornhaus et al (1974)). It has also been observed in Si inversion layers (Gornik et al(1978)). Both electrical and photo (Gornik et al(1976)) excitation have been used to produce a hot electron distribution.

Owing to possible tunable source applications there has been interest in linewidth and emitted power. These are investigated in detail in this thesis and the potential of cyclotron emission as a spectroscopic source is

demonstrated. Gornik has shown that, at least for non-polar elemental semiconductors and weakly polar III-V semiconductors, that the power output is almost independent of the material used. Assuming the radiation is emitted from the semiconductor to a vacuum he has shown that the power output is given as follows:

$$P = KAT_e w_c^2 (1 - (n-1)^2/(n+1)^2)$$

where A is the area and K a constant and n is the refractive index, i.e., the power emitted will be the same for semiconductors with the same refractive index, electron temperature, cyclotron frequency and area. For more strongly polar materials like c.m.t. the optical phonon relaxation is stronger and the power output has been observed to have been a factor of 100 lower.

The linewidth is more problematical. Two components contribute to the linewidth - nonparabolicity of the conduction band and broadening of the landau levels due to electron scattering.

Gornik et al have claimed that in InSb (McCombe et al (1976)), GaAs (Gornik et al (1980)) and InP (Gornik et al (1980)) the emission linewidth is dominated by ionised impurity scattering and that it is proportional to the square root of the total impurity concentration. This would be the same as cold electron cyclotron resonance. Indeed, it is claimed that the emission linewidth is a more reliable way of estimating the total impurity concentration than are

conventional electrical methods. In germanium (Holtzman(1981)) band nonparabolicity is said to be the dominant broadening mechanism at sub-mm wavelengths. At electron temperatures greater than 100K optical phonon emission should also contribute directly to the emission linewidth but its effect will be limited because there is a strong cut-off in the electron energy distribution above this energy.

2.7.1 Nonparabolicity Broadening

The introduction of a magnetic field changes the conduction band energies of a semiconductor which are written as

$$E = E_g/2 - E_g/2(1 + (2/E_g)((\hbar^2 k_z^2/2m^*) + (n + 1/2)\hbar w_c))^{1/2} \quad -(20)$$

(neglecting spin) when a two band model can be applied.
It can be seen that a higher effective mass and a smaller spacing between Landau levels results on going away from the band edge. Emission will occur from different Landau levels and over a range of k_z values. This will result in a broadening on the high field, low frequency side of the emission line. Polaron nonparabolicity also has a similar effect. It is even possible to resolve different Landau level transitions in the highest purity InP and GaAs (Gornik(1983)) and also in InSb where the Landau transitions associated with spin-up and spin-down states are resolved because of the higher effective g-value.

2.7.2 Linewidths due to the Broadening of the Landau levels

It was explained in the section on cyclotron resonance that the width of the Landau levels is often related to the length of time an electron stays in a particular state. This depends on the individual scattering mechanism and it is extremely difficult to derive a satisfactory analytical expression for the linewidth.

The problem with cyclotron emission and hot electron cyclotron resonance is that we are dealing with a much broader range of energy and wavevector than we are with cold electron cyclotron resonance, at least when performed at low temperatures. We must therefore take into account the electron distribution which may not be Maxwellian when calculating the lineshape which is then unlikely to be Lorentzian.

For these reasons, and the fact that emission linewidths can be much bigger than the low temperature resonance linewidths it is reasonable to be suspicious of the claim that the same scattering mechanisms are responsible for the lifetimes of the state in both cases.

CHAPTER 3

EXPERIMENTAL METHOD

Experimental Method

In this chapter the equipment and method used in the experiments are described as is the interpretation of results.

3.1 Double Magnet System

In 1983 a double superconducting magnet system was commissioned at St. Andrews. The system, made by Thor Cryogenics, consisted of two magnets wound on the same former each with a bore of 4cm; one magnet had a maximum field of 8 Tesla and the other 4 Tesla. The field centres were 20cm apart and the coils were each 10cm long. The reason for having a double magnet system is that in the cyclotron emission experiment the ability to tune the emitter in one magnet was required as was the ability to change the photoconductive response of the detector by changing the field in the other magnet so that we could observe emission at different energies.

A schematic diagram of the circuit used with the magnet system is shown in figure 3.1. Superconducting switches enable the operation of both magnets with one power supply. The switches consist of a piece of superconducting wire in parallel with the magnet. In its superconducting state the switch shorts out the high inductance magnet so that the

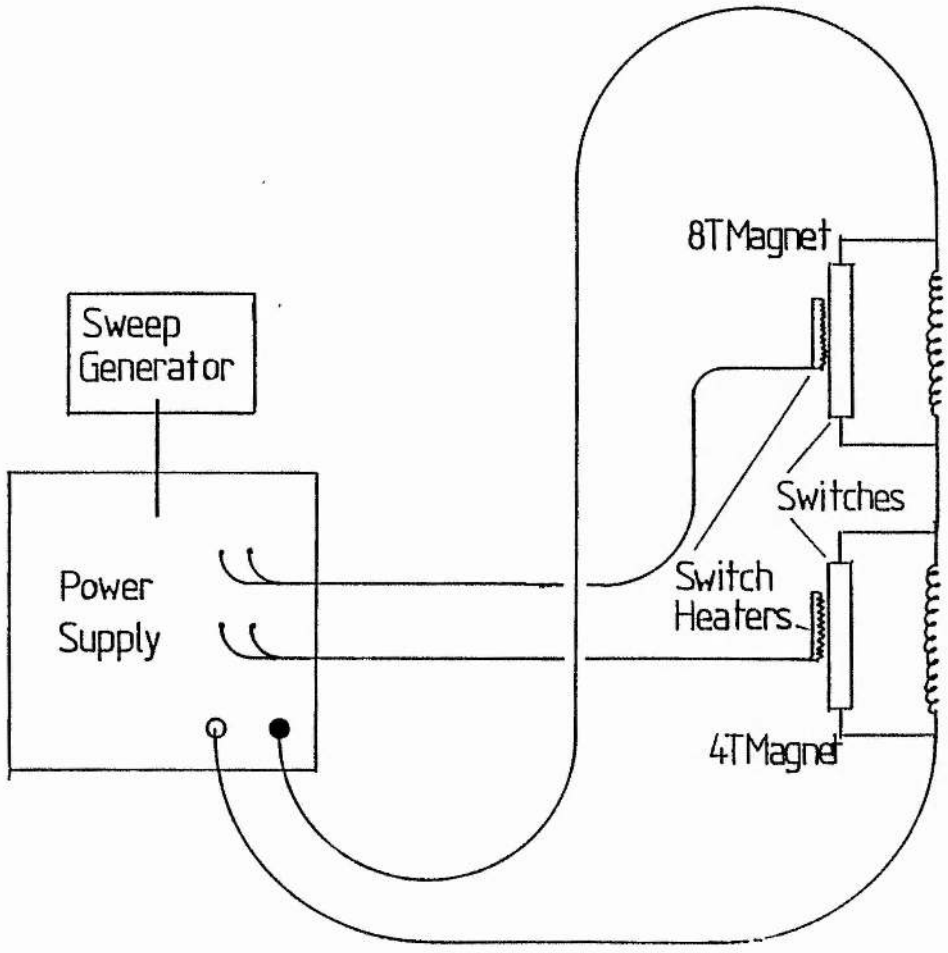

Schematic of the Double Magnet System

field is not changed by a change in the current from the supply. A heater coil is wound round the superconducting link which can heat the wire beyond the critical temperature for superconductivity. Then the lowest impedance path is through the superconducting magnet, thus if the current is increased the field will increase. In this way the magnet can be effectively connected or disconnected to the power supply.

For example if one wanted to set a particular field on the detector and then study the effect of changing the field on the emitter the procedure might be as follows:

1. Put on the superconducting switch heater in the detector magnet; wait 30s.
2. Increase the current from the power supply to the required value, say 30A.
3. Turn off superconducting switch; wait 30s; note the value of the current.
4. Decrease the current from the supply to zero.

The detector magnet is now in persistent mode and the emitter magnet could be swept at will once the switch heater has been on for 30s. To deenergise the magnet the procedure would be as follows:

1. Sweep the emitter magnet to zero.
2. Switch off the switch heater in the emitter magnet; wait 30s.
3. Sweep power supply to 30A exactly.
4. Switch on the switch heater in the detector magnet;

wait 30s.

5. Decrease current to zero, switch off heater and power supply.

Care must be taken to ensure that the power supply is delivering the same current as is flowing in the magnet when the switch heater is turned on.

The power supply is controlled by a linear sweep generator making it possible to sweep the magnet at a constant rate. The finite resistance of the switches and the quench protection resistors means that the increase in current carried in the magnet lags behind the change in the current from the supply. This is taken into account by averaging the positions of features on the up and down sweeps. It is possible to sweep the 8 Tesla magnet to full field in ten minutes and the 4 Tesla magnet in five minutes. The current (and field) were measured with a 50m resistor in series with the power supply.

3.2 Emission Experiment

The set-up for the emission experiment is shown schematically in figure 3.2. The emitter is placed in one magnet and the detector in the other. A light pipe of 12.5mm diameter joins the emitter and detector with a condensing cone at the detector end to focus the light on to the detector as shown.

Schematic of the Cyclotron Emission Experiment 32

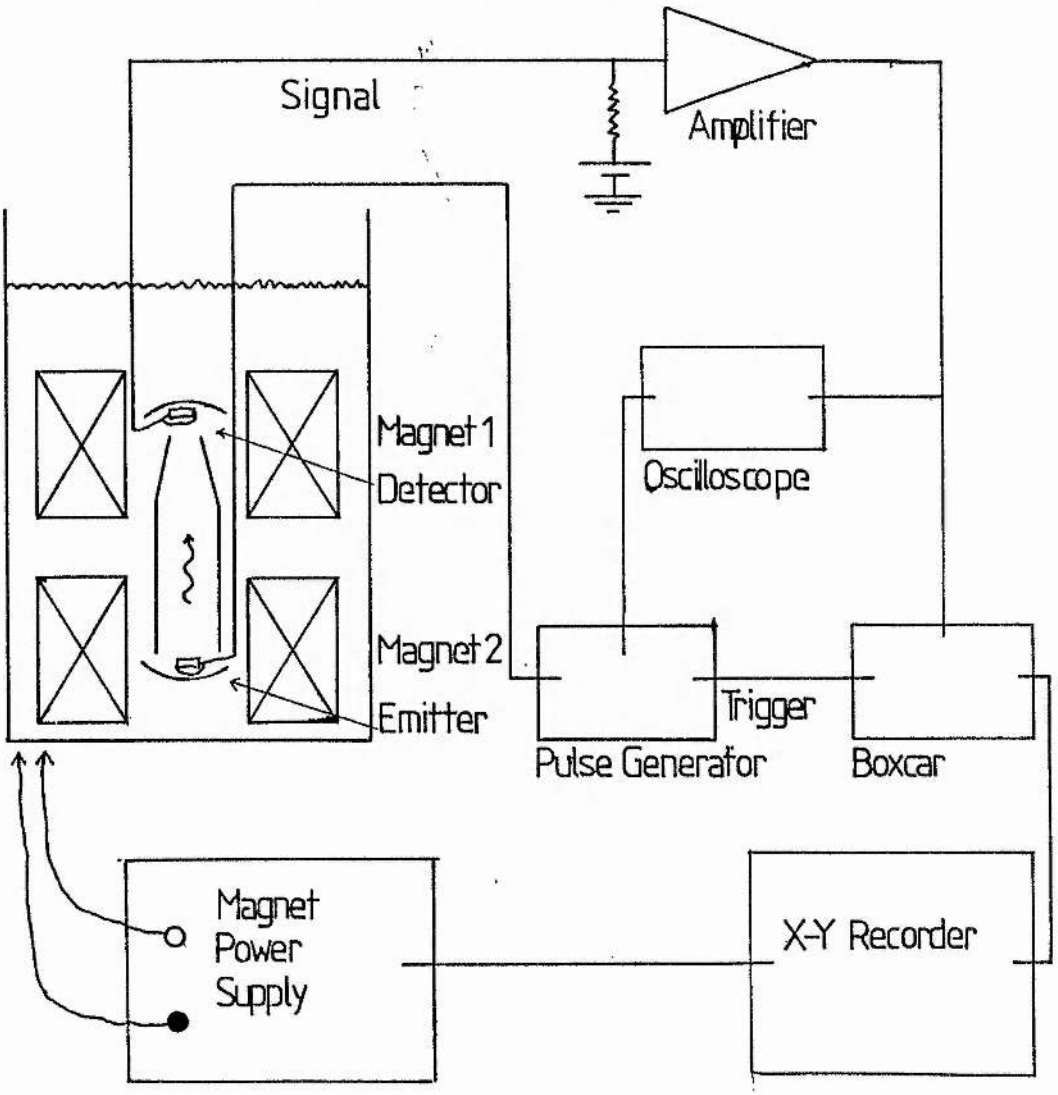

The emitter and detector samples are contacted and mounted in P.T.F.E. rings. Miniture coaxial cable connects the samples in the rings to the top of the cryostat. The whole assembly is put in a sleeve and purged before cooling with helium gas to avoid any unwanted water vapour absorptions. In the cyclotron emission experiment the emitter is subjected to voltage pulses in order to heat the carriers out of equilibrium with the lattice and the detector picks up the resulting radiation. Initially there was a problem with the rather high impedance of the pulse generator ($4k\Omega$) making difficult the application of voltages to low impedance samples. It also meant that often the amplitude of the voltage pulses changed due to the magnetoresistance of the sample as the magnetic field was swept. This is overcome by using a trigger box made here and a low impedance D.C. supply. The box allows the D.C. voltage from the supply to be applied to the sample when the pulse generator is on. Typically pulses of 1ms and duty cycles of 10 are used although shorter duty cycles are used when large voltage pulses are applied to the sample to avoid sample heating.

The detector consisted of n-GaAs sample (RR125, $\mu=156000 cm^2/vs$ and $n_d-n_a=3.5x10^{14} cm^{-3}$ measured at 77K). Low resolution Fourier transform photoconductivity spectra for this sample are shown in figure 3.3 at zero Tesla and 3 Tesla. In figure 3.4 the energies of the principle peaks

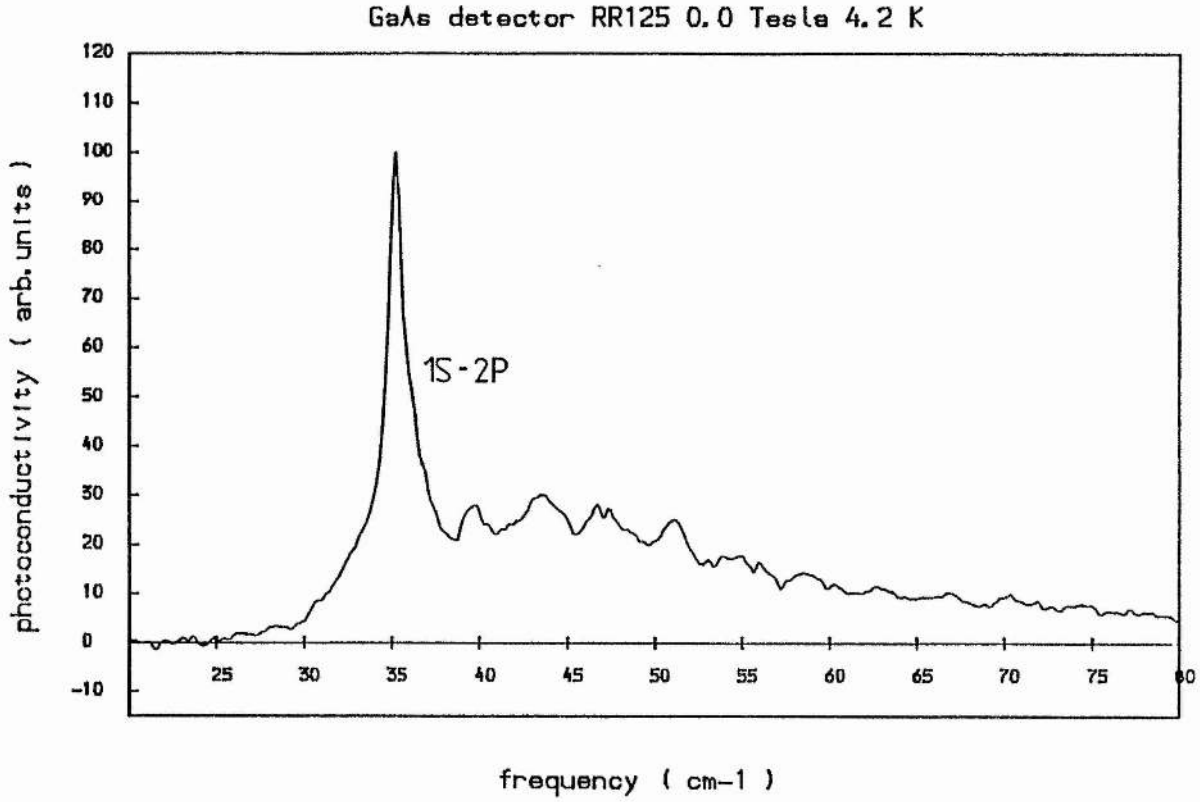
GaAs detector RR125 0.0 Tesla 4.2 K
photoconductivity (arb. units)
frequency (cm-1)
1S-2P
120
110
100
90
80
70
60
50
40
30
20
10
0
-10
25
30
35
40
45
50
55
60
65
70
75
80

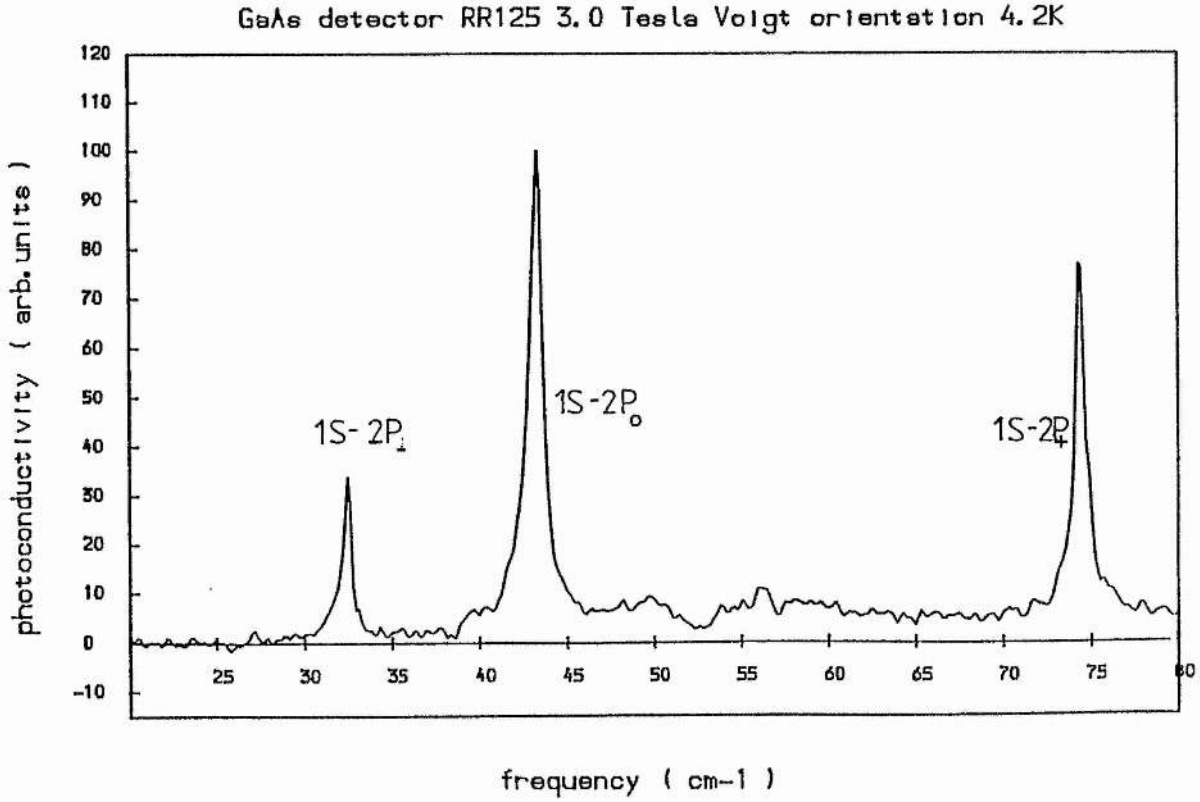
GaAs detector RR125 3.0 Tesla Voigt orientation 4.2K
photoconductivity (arb. units)
frequency (cm-1)
1S-2P-
1S-2P0
1S-2P+
120
110
100
90
80
70
60
50
40
30
20
10
0
-10
25
30
35
40
45
50
55
60
65
70
75
80

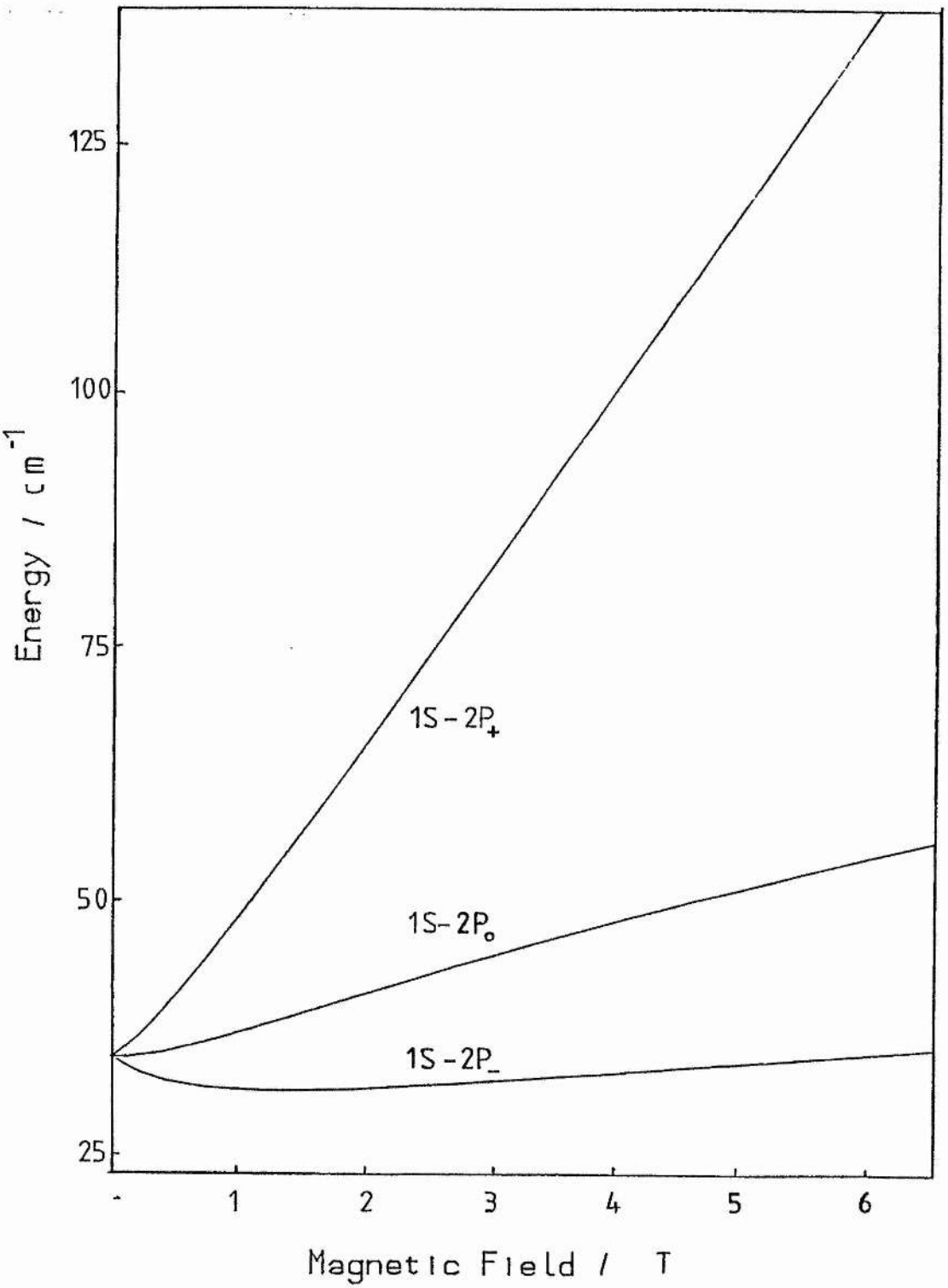
125
100
75
50
25
Energy / cm^{-1}
1S - 2P$_+$
1S - 2P$_o$
1S - 2P$_-$
1
2
3
4
5
6
Magnetic Field / T

are plotted against magnetic field. RR125 is chosen because one peak dominated the central cell structure simplifying the analysis of the emission spectra. When a broadband detector is required at higher energies a Ga doped Germanium detector can also be used. The GaAs detector has a linewidth, defined as the half half width at half height, of $0.8cm^{-1}$ without field and less than $0.4cm^{-1}$ at 3 Tesla. It should be noted that spectra shown in the figure 3.3 were taken in the Voigt orientation whereas in the emission work the Faraday orientation was used; this meant that the $1S->2P_o$ peak was normally weaker than the $1S->2P_{-1}$ and $1S->2P_{+1}$ peaks in the emission work.

When a magnetic field is applied to a GaAs sample being used as a detector a considerable increase in noise is often observed. This is probably due to a combination of the strong magnetoresistance of the material and an increase in contact noise. Because of this emission spectra were normally taken with zero field on the detector to give a spectrum at $35cm^{-1}$ before the field was applied and spectra could be taken, using the $1S->2P_{+1}$ transition at $70cm^{-1}$(~3T).

The detector is operated by applying a constant current to the detector sample and measuring the voltage drop across it. The A.C. component of the detector signal is amplified and a standard boxcar integrator, using the pulse generator as a trigger, is used to improve the signal to noise ratio.

The result is displayed as a function of emitter magnetic field on an X-Y recorder.

3.2.1 Analysis of Emission Spectra

A number of problems arise when attempting to analyse the emission spectra. Often experiments are done as a function of electric field bias and problems are encountered when trying to characterise the electric field properly. This is because the samples are contacted with dots of indium which would tend to concentrate the electric field around the contacts. The fields are calculated on the straight-forward basis of measuring the voltage dropped across the sample and dividing by the distance between the indium dots. The nonuniform field distribution however must be borne in mind when analysing experimental results. In future experiments in the longitudinal orientation it might be better to evaporate a contact over a wider area. However in the transverse orientation problems may be encountered with large circulating currents.

Another problem is that of deconvoluting the cyclotron emission spectrum from that of the detector. In most cases the emission line was broader than the detector line and so true emission spectra were observed as the emitter energy was swept through the detector line. Normally the detector linewidth was simply subtracted from the emitter linewidth. Clearly for emission lines which are narrower than the

detector lines large experimental errors will be incurred in the measurement of the linewidth.

3.3 Sample Preparation (Contacting Proceedure)

3.3.1 GaAs or InP

In order to contact these materials the sample surface is cleaned with toluene, acetone, methanol and distilled water in that order and the sample is placed on a graphite stage in the furnace. Pure indium is cleaned with acetone in an ultrasonic bath and small dots are placed on the sample surface. A quartz cover is then placed over the furnace and a mixture of 90% nitrogen and 10% hydrogen gas was allowed to flow over the sample creating a reducing atmosphere. While the graphite stage is heated with a projector bulb located outside the quartz to a temperature of about 400°C the indium melted. The gas is bubbled through hydrochloric acid for a time to flux the indium contacts and cause them to alloy with the material. Normal gas is again allowed to flow before the furnace is switched off and the sample allowed to cool.

Thin copper wire is tinned with clean indium and is soldered to the dots of indium on the sample by the conduction of heat from the soldering iron down the wire. The samples are then mounted in teflon rings.

3.3.2 InSb

With InSb a similar procedure was followed except that the InSb was normally cut on the wire saw and etched before contacting and kept under methanol until it was put into the furnace to avoid surface oxidation. With this material the alloying temperature is somewhat lower (250^{o}C) and it was not necessary to heat InSb to the same extent.

3.4 Pressure Bomb

In the work on C.M.T. and InSb hydrostatic pressure is used as a parameter in the experiments. The pressure is applied with a pressure cell described by Wasilewski(1984) using a mixture of petrols as a pressure transmitting medium. The cell shown in figure 3.5 consists of a 2% Be-Cu cylindrical case and Be-Cu pistons at either end. The pistons allow optical access via a saphire window at one end and electrical access via a high pressure perofollite feed through at the other. The cell is sealed at either end by deformed brass gaskets.

The pressure is applied on a hardened steel rod pressing on element 9 of figure 5 by a hydraulic press and the Be-Cu nuts are tightened as the pressurisation proceeds so that the pressure is maintained after the cell is removed from the press.

Pressure Bomb

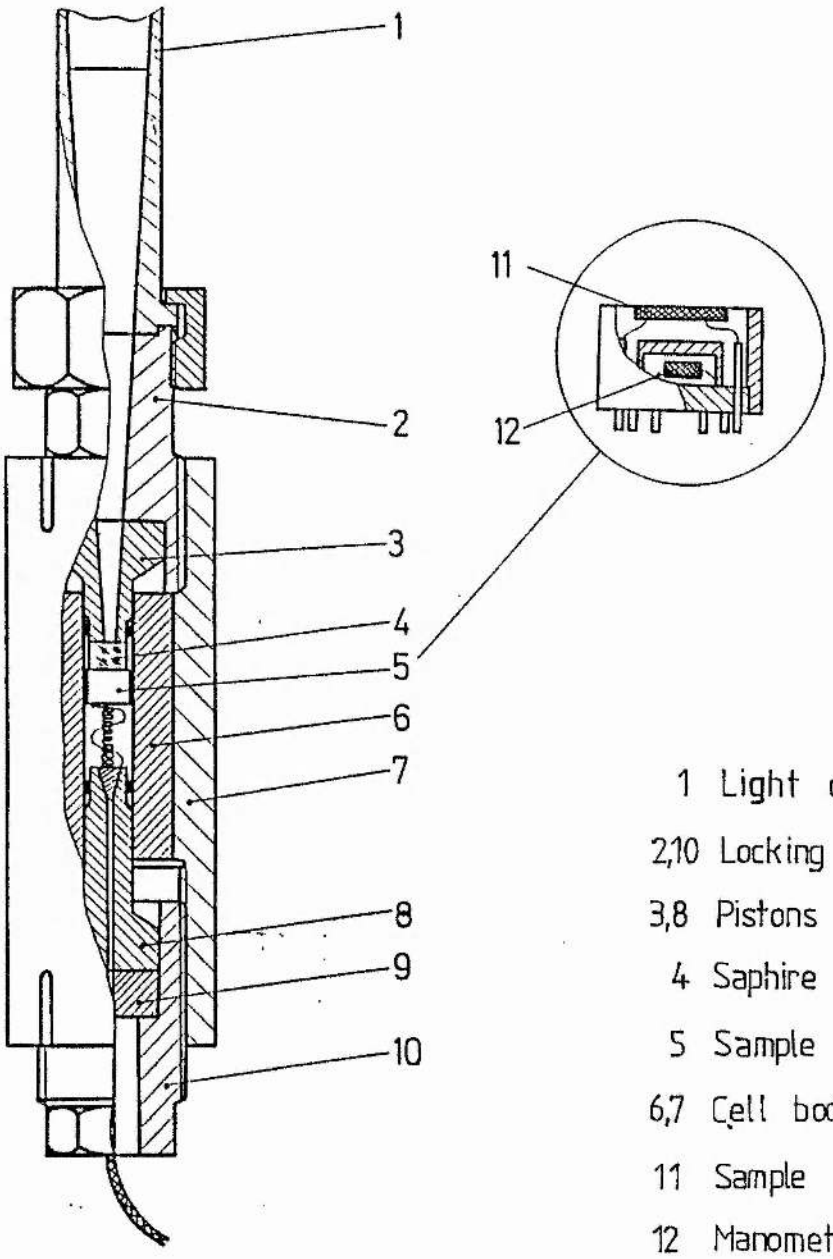

1 Light cone
2,10 Locking Screws
3,8 Pistons
4 Saphire window
5 Sample mount
6,7 Cell body
11 Sample
12 Manometer

The sample is mounted on a stage (element 5 of figure 3.5), enlarged in the inset. It is located in position next to a sapphire window by a spring as shown. It can thus be maintained at field centre regardless of the travel of the piston.

The manometer is also shown in the inset. It consists of a piece of heavily doped InSb. A four terminal resistance measurement can give an value of the pressure at room and helium temperatures to an accuracy of at worst 2%.

The reason for choosing petrol as a pressure transmitting medium is that petrol forms a glass type structure when solid thus preserving hydrostatic pressure as the bomb is cooled. The linewidth of the cyclotron resonance in InSb under pressure indicates that the pressure is uniform to better than 0.1%.

As far as the optics are concerned Wasilewski et al (1984) have shown that the petrol and saphire cause no serious attenuation of radiation up to $400cm^{-1}$.

3.5 Far-Infra-Red Laser System

The far-infra-red laser spectrometer was used to study cyclotron resonance in InSb and C.M.T.. A schematic diagram is shown in figure 3.6. The entire spectrometer consists of a discharge excited CO_2 laser producing 10um radiation which pumped a molecular gas far-infra-red laser. The output of this was used to study the magnetooptical properties of semiconductors at low temperatures.

The CO_2 laser consists of a tube containing 7% CO_2, 18% nitrogen and 75% helium at a pressure of around 20mbar. The laser operates on a continuous flow basis, the gas flow being controlled by a needle valve. A discharge of 20mA to 30mA, 20kV to 40kV pumps the laser. The laser, using vibrational transitions in the CO_2 can produce as much as 50W in the wavelength range between 9um and 11um. A fine screw adjustment at one end controls the length of the cavity allowing a particular transition to be selected and a piezo electric drive allows much finer adjustment of the length to select a cavity mode and maximise power output.

The output of the CO_2 laser is directed down the centre of the far-infra-red laser filled with a molecular gas. Certain vibrational and rotational modes are excited and far-infra-red laser emission takes place. On the strongest lines as much as 100mW can be produced. The modes and

Schematic Diagram of the F.I.R. Laser Spectrometer 3.6

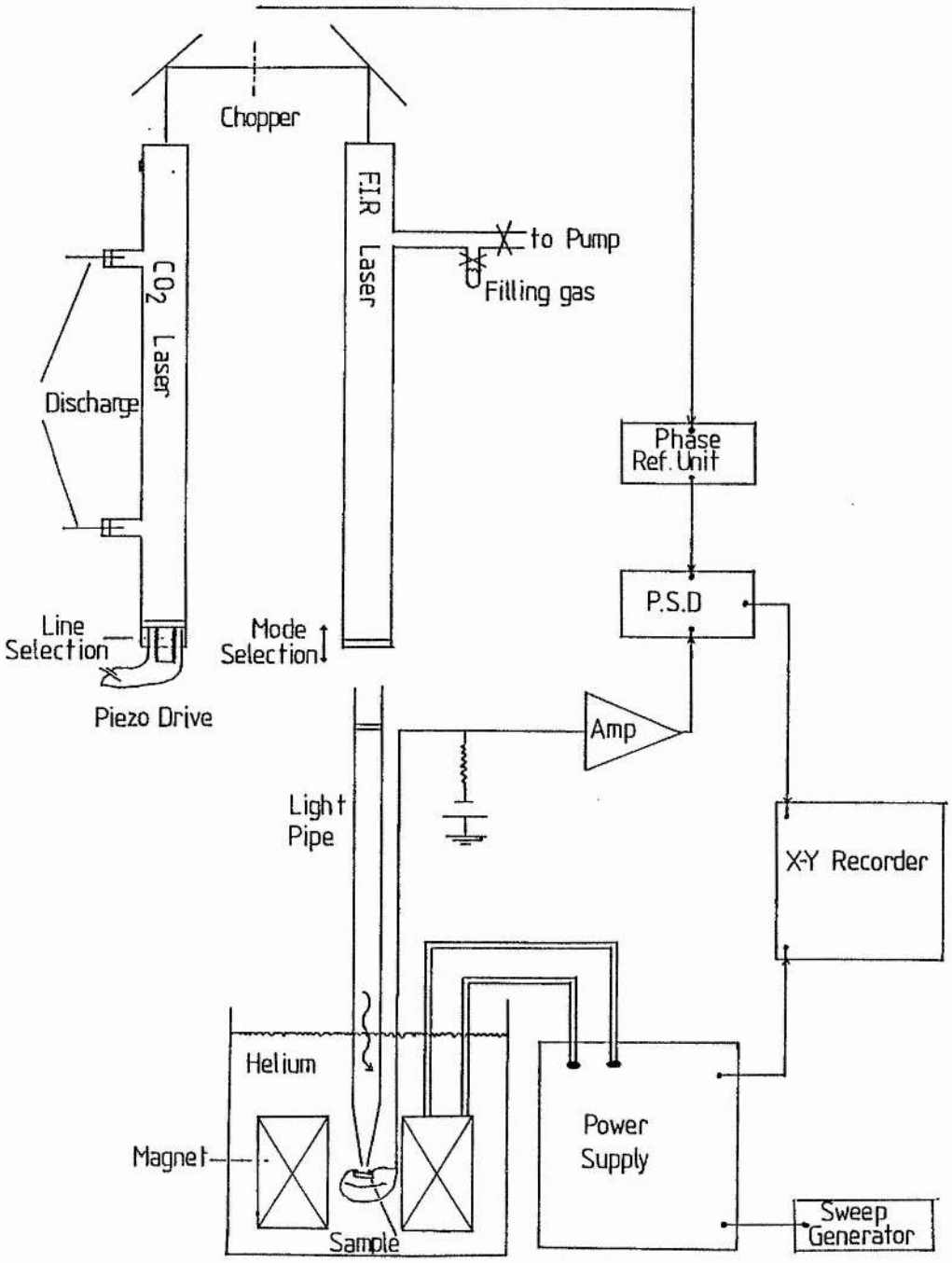

transitions are again selected by adjusting the length of the cavity which in this case consists of a cylindrical metal waveguide. The laser is filled with a gas (e.g. methanol) by pumping it to high vacuum and leaking in the particular gas until the pressure reaches about 0.2mbar. Often at ambient pressure the medium is in the form of a liquid.

The output of the far-infra-red laser was channeled by metal light pipes and allowed to fall on a semiconductor sample in a magnetic field. The magnetooptical properties of the material could then be studied. The laser light was chopped at the output of the CO_2 laser and photoconductivity spectra were obtained by passing a constant current through the sample and amplifying the ac component of the voltage across the sample. Absorption spectra were taken from the response of a carbon bolometer placed behind a baffled sample. Although it works on a different principle the bolometer was biased in the same way as the sample in the photoconductivity measurements. The signal was then passed through a P.S.D. using the chopper as reference to enhance the signal to noise figures.

CHAPTER 4

CYCLOTRON EMISSION IN GaAs AND InP

Cyclotron Emission in GaAs and InP

4.1 Introduction

GaAs and InP are materials of considerable technological importance. Both are used to produce Gunn devices and both are candidates in the development of fast computers. Alloys of these materials are used to produce semiconductor lasers at 'windows' in the transmission of silica optical fibres.

As a result there has been a considerable effort in materials development and samples of high purity have been produced. Since GaAs can be grown at lower temperatures than InP the best samples of GaAs are somewhat purer than the best samples of InP.

Both materials have band structures and shallow impurity states qualitatively similar to those described in Chapter 2. It should be noted, however, that in contrast to InSb, impurity freeze-out does occur in pure samples of both materials at temperatures below about 10K. The detailed characteristics of GaAs and InP are given in tables 2.1 and 2.2 in Chapter 2.

Cyclotron resonance was first observed by Palik et. al. in 1961 in both materials. Exact determinations of the effective mass were obtained by Stillman et al(1969) in GaAs who found that $m^*/m = 0.0665+/-0.0005$ and in InP by Chamberlain(1972) who found that $m^*/m = 0.0810+/-0.0005$.

Less work has been done on cyclotron emission and hot electron effects in quantising magnetic fields at low temperatures though studies have been done in both materials. Hot electron magnetophonon and magnetoimpurity oscillations have been studied in both materials (see Nicholas and Portal(1979) for review). Cyclotron resonance has been studied under electrical and optical (Ohyama et al(1982)) excitation in GaAs. More recently Allan et al(1984) and coworkers have performed saturation cyclotron resonance absorption measurements on electrons in the conduction band and impurity absorption on electrons in impurity states. These workers have concluded that the lifetime of electrons in the Landau levels is considerably longer than in InSb(Gornik et al (1978)). They also concluded that there was a linewidth dependence on the carrier concentration due to electron-electron scattering. Cyclotron emission has been studied in both materials. For example Gornik et al (1980) studied the sample dependence of the emission linewidth concluding that the linewidth was proportional to the square-root of the total impurity concentration. In 1983 Gornik et al reported the

observation of a splitting in the emission lines due to transitions between different pairs of Landau levels.

4.2 Cyclotron Emission

In GaAs and InP the electrons are mostly frozen out onto impurity states at 4.2K (in thermal equilibrium the population of the conduction band is $\sim 10^{-3}$ to 10^{-6} times the number of neutral impurities at zero field). In a magnetic field the shallow impurity ground state deepens and freezeout becomes stronger.

When a D.C. electric pulse greater than a threshold value is applied the donor impurities are impact ionised and the electrons are excited into the conduction band. This occurs at between 2V/cm and 6V/cm in both materials.

In compensated material the electrons emerging from the neutral shallow donors screen the ionised impurities. This results in an increase in the mobility of electrons, a greater mean velocity and more impact ionisation. Often a negative differential resistance is observed as a consequence. In uncompensated material the increase in screening competes with the increase in the total number of ionised impurities and a smoother breakdown characteristic is normally observed.

Once electrons are located in the conduction band they form a nonequilibrium energy distribution characterised by an electron temperature T_e. If there are sufficient interelectronic scattering events and interactions with phonons are ignored then the electron distribution can be approximated by Maxwell Boltzman statistics. For example Stratton(1958) estimated the number of electrons required to thermalise a high energy electron through inter-electronic collisions. For GaAs only $2x10^{11}cm^{-3}$ are required at 4.2K for an electron temperature of 30K whereas $2x10^{15}cm^{-3}$ are needed when the electron temperature reaches 100K. These are probably overestimates because the calculation dealt with a single high energy electron and not with the electron gas as a whole.

Cyclotron emission results from the radiative decay of electrons from one Landau level to the next conserving wavevector. The emitted intensity is proportional to the dynamic equilibrium population of electrons in the upper Landau levels and to the spontaneous emission rate. In the emission experiments on GaAs and InP the samples are in the longitudinal ($J \parallel B$) orientation. The process is shown schematically in figure 4.1.

Schematic Diagram Showing Cyclotron Emission in GaAs and InP

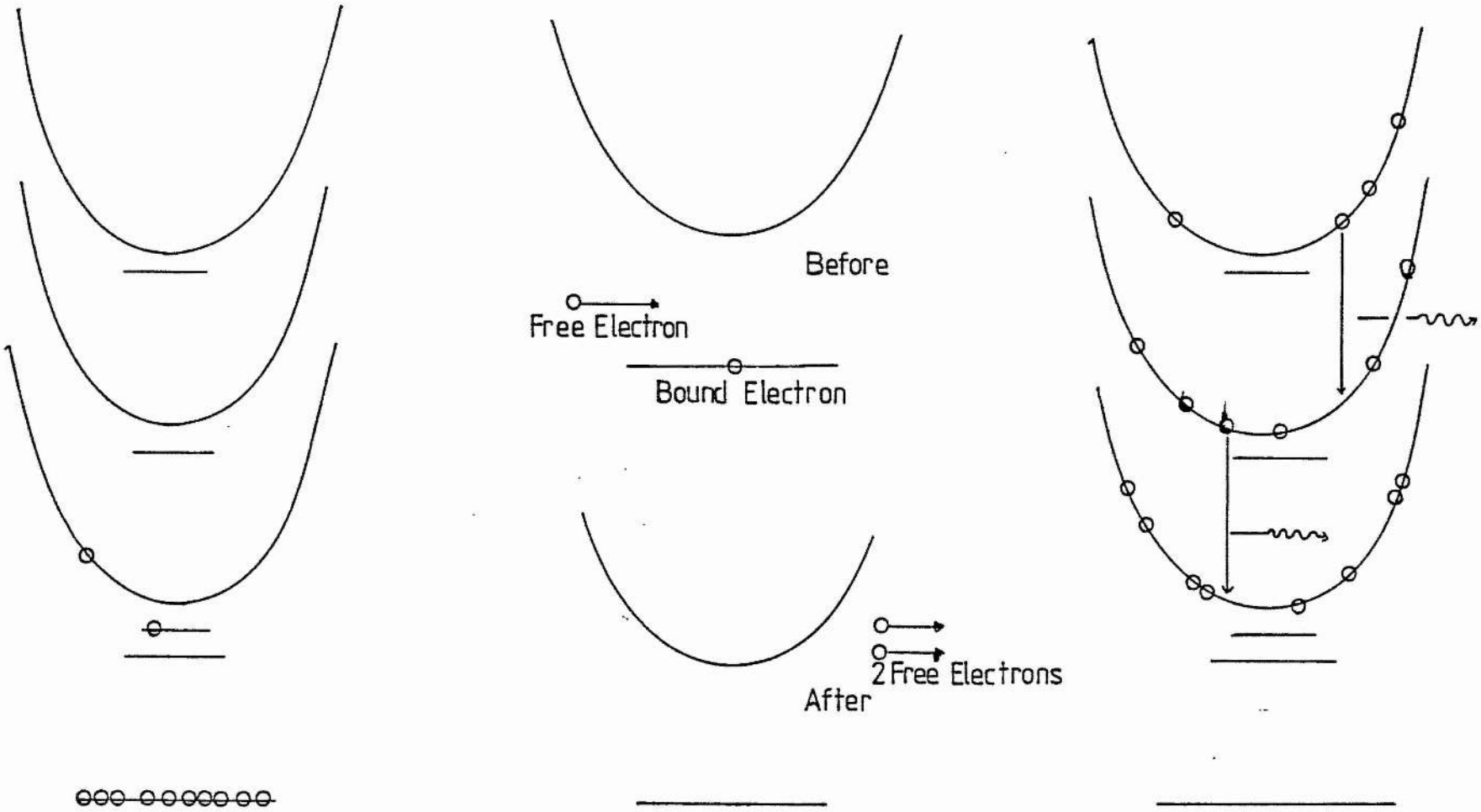

Thermal Equilibrium

$T_e = T_l$, $E = 0$

Impact Ionisation

$E > E_{bd}$

Hot Electron Gas + Cyclotron Emission, $T_e >> T_l$, $E >> E_{bd}$

The sample preparation and experimental method follows that described in the previous chapter.

4.3 Samples

The GaAs samples used were obtained mostly from the Wright- Patterson Air Force Base and the InP samples from R.S.R.E., Malvern. All samples were grown using vapour phase epitaxy (V.P.E.) and their characteristics are shown in table 4.1. On the whole our samples are much less compensated than the GaAs samples used previously (Gornik et al(1980)).

Table 4.1

Characteristics of Samples

Sample	N_d-N_a ($\times 10^{14} cm^{-3}$)	N_d+N_a ($\times 10^{14} cm^{-3}$)	Mobility(77K) (cm^2/vs)
GaAs			
RR98B	2.0	2.1^x	160000
RR17H	6.6	9.2^x	91000
RR17C	2.3	$5,9^x$	105000
RR133	~1.0	-	160000
$S1^+$	~0.5	-	160000
InP			
NAG747	2.0	2.5^o	120000
KV454	1.8	3.3^o	99000
KV584	6.0	20.0^o	38000

+ obtained from Stillman

Graph of Full Linewidth vs. Total Impurity Concentration 4.2

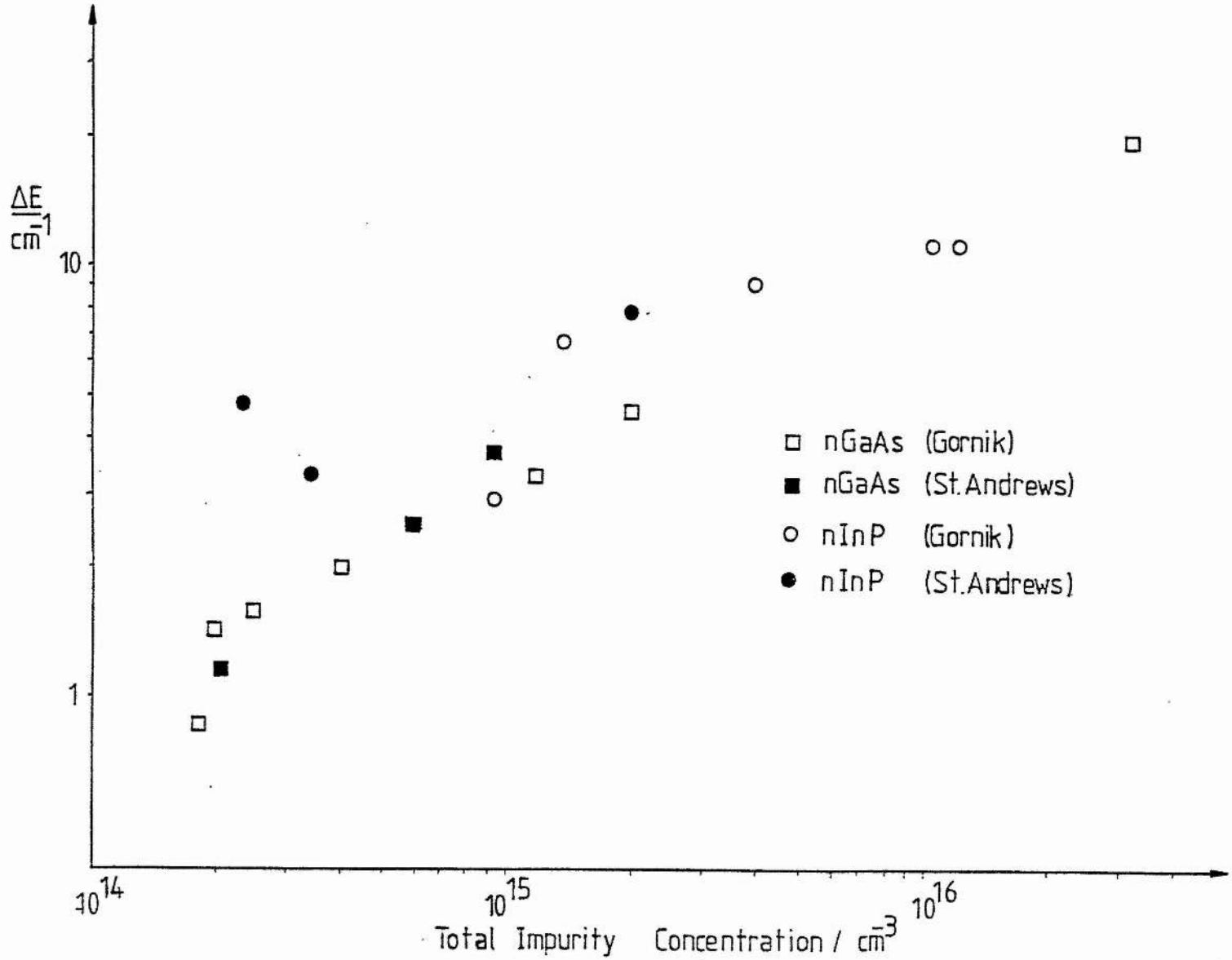

x obtained from a mobility analysis by R.S.R.E, Malvern.

o obtained from tables (Walukiewicz et al (1980))

The samples were characterised by the suppliers.

4.4 Linewidth - Sample Dependence

Previous investigations in GaAs, InP and InSb have assumed that ionised impurity scattering was primarily responsible for the relaxation time limited cyclotron resonance linewidth. Gornik has gone as far as to propose that the emission linewidth is a more reliable guide to the total impurity concentration in GaAs and InP than is a mobility analysis. He has drawn a graph of emission linewidth, defined here as the full width at half height, against total impurity concentration which shows an $N_i^{1/2}$ dependence. Considerable deviations from the stated dependence are accounted for by sample inhomogeneities. Once the data from the samples studied at St. Andrews are added to the graph only a very general trend can be discerned for InP in fig 4.2. The results shown from St Andrews were taken at $35cm^{-1}$ and at a voltage bias where emission was just starting to be observed. The conditions under which Gornik's results were produced are not known. The results for GaAs appear to be consistent.

In a more recent publication (Allan et al(1984)) the conclusion was that a carrier concentration dependence of the cyclotron resonance line-width existed . Presumably a similar mechanism will be present in the emission linewidth.

These authors assumed that the cyclotron relaxation time is controlled by ionised impurity scattering and electron-electron scattering. The scattering times corresponding to these two mechanisms are combined in accordance with Matthiesens rule

$$1/T_{cr} = 1/T_{ii} + 1/T_{ee}$$

where T_{ii} is the component controlled by ionised impurity scattering

and T_{ee} is that controlled by electron electron scattering

Most treatments for T_{ii} conclude that (e.g. Lodder et al(1976))

$$1/T_{ii} \propto N_i^{1/2}$$

Allan et al(1984) plotted the cyclotron resonance scattering time against the carrier density in the conduction band and found a linear relation at high carrier concentrations concluding that

$$1/T_{ee} \propto N_e$$

so that a better relationship for the linewidth might be

$$1/T_{cr} = AN_i^{1/2} + BN_e \qquad (1)$$

Where A and B are constants. On this basis least squares analysis of the data may be attempted but it must be doubted whether good values for A and B could be obtained even with all the present data owing to difficulty in measuring mobilities and carrier concentrations reliably. In any case although the theory explains the increase in linewidth between absorption and emission for uncompensated samples it fails to explain the increase in compensated material.

Using this expression the low temperature cyclotron resonance scattering time under equilibrium conditions is given by

$$1/T_{cr} = A(2N_a)^{1/2} \qquad \text{(ionised impurity)}$$

but under hot electron conditions the impurity states are ionised and the scattering time is given by

$$1/T_{cr} = A(N_d + N_a)^{1/2} + B(N_d - N_a).$$

Clearly for an uncompensated sample where $N_d >> N_a$ a large difference exists between the scattering times in the two cases. This is exemplified by the sample used in the experiment described by Allan et al. Here $N_d = 3x10^{14}$ and $N_a = 0.3x10^{14}$ and a factor of 10 broadening is observed in the cyclotron resonance absorption line as the carrier density is increased from its thermal equilibrium value to $3x10^{14}cm^{-3}$. In compensated samples however $N_d \sim N_a$ and one might expect that the emission and absorption linewidths to be approximately equal. However the smallest emission linewidth observed in GaAs was $0.75cm^{-1}$ reported by Gornik et al(1980) using a highly compensated sample(R137, $N_d - N_a = 10^{13}$) which is almost an order of magnitude broader than the absorption/photoconductivity line in the same sample. Equation 1 therefore breaks down for compensated material and it is concluded that some other factor must also be contributing to the emission linewidth.

Possibly phonon scattering may be contributing in these pure materials and the following section on the electric field dependence on linewidth indicates that nonparabolicity

mass spread may also be important.

4.5 Electric Field Dependence of Linewidth and Intensity

The effect of an electric field is to create a nonequilibrium distribution of electrons. This can influence the linewidth in two ways : firstly, through an energy dependent scattering time $T_{cr}(W)$ and, secondly, because cyclotron transitions from different parts of the band have different energies (nonparabolicity broadening). The former will result in homogeneous broadening and a distortion in the lineshape by enhancing the peak and having greater spread on the wings. The latter will produce broadening on the high field or low energy side of the emission line.

Graphs of experimental linewidth defined as the half half width at half height against electric field bias are shown in figures 4.3 for GaAs and 4.5 for InP and emitted intensity against electric field in figures 4.4 for GaAs and 4.5 for InP. Graphs for typical GaAs(RR133) and InP(KV454) samples are shown and the detector energies were set at $35cm^{-1}$ and $70cm^{-1}$. Qualitatively, the linewidth dependencies on electric field are similar with a steep increase as the electric field bias is increased from breakdown followed by a much more gradual increase at higher fields. The graphs are also qualitatively similar to those drawn (but not shown) for the other GaAs and InP samples

Linewidth vs. Electric Field

GaAs

Theory

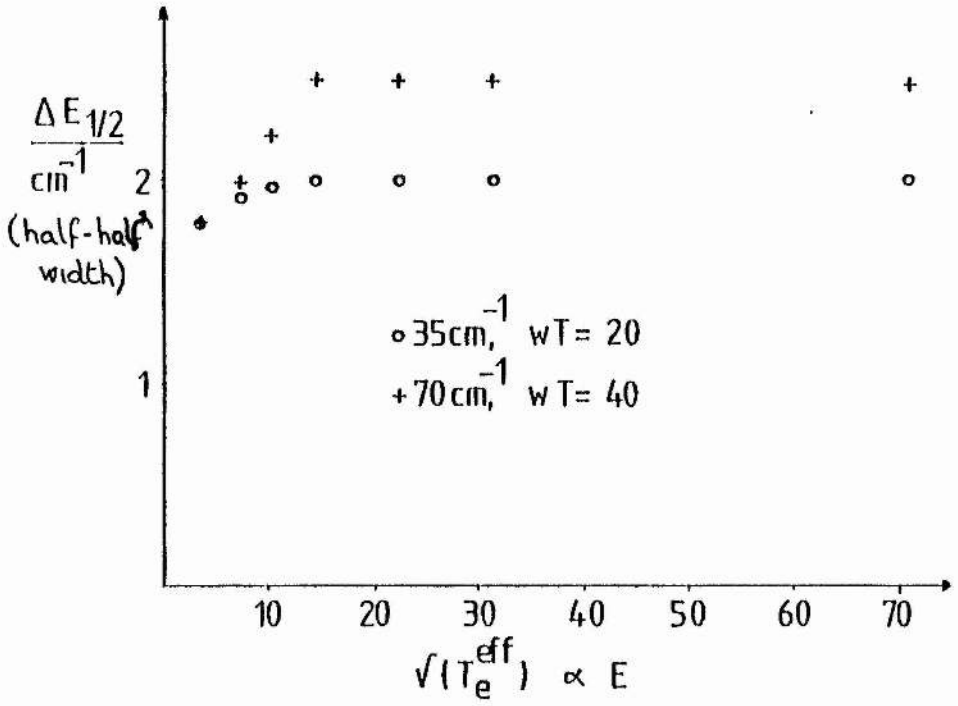

Experiment (RR133)

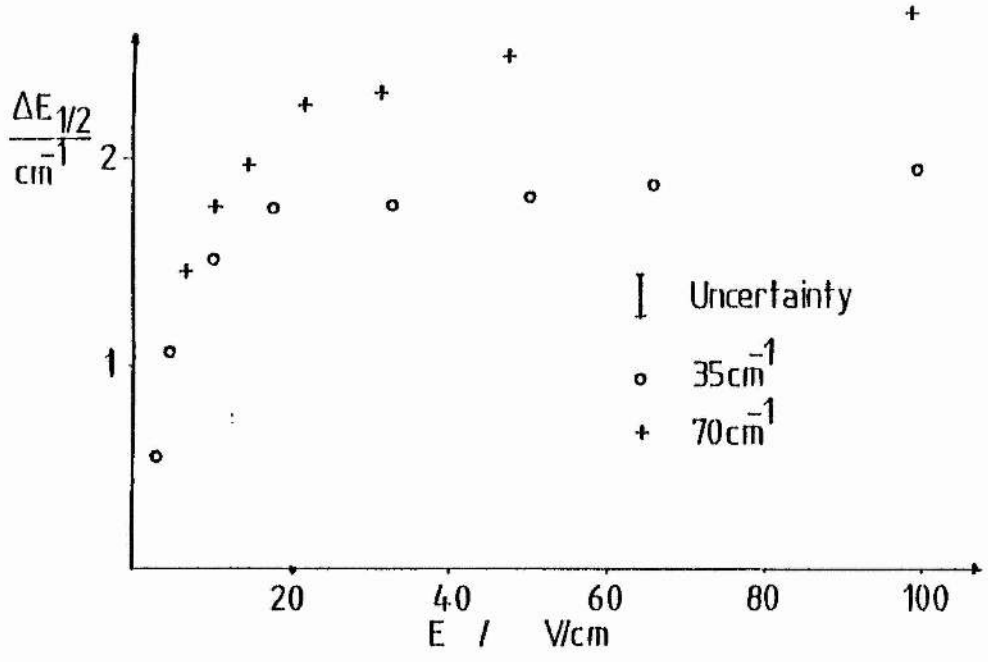

Intensity vs. Bias Field

Theory

GaAs

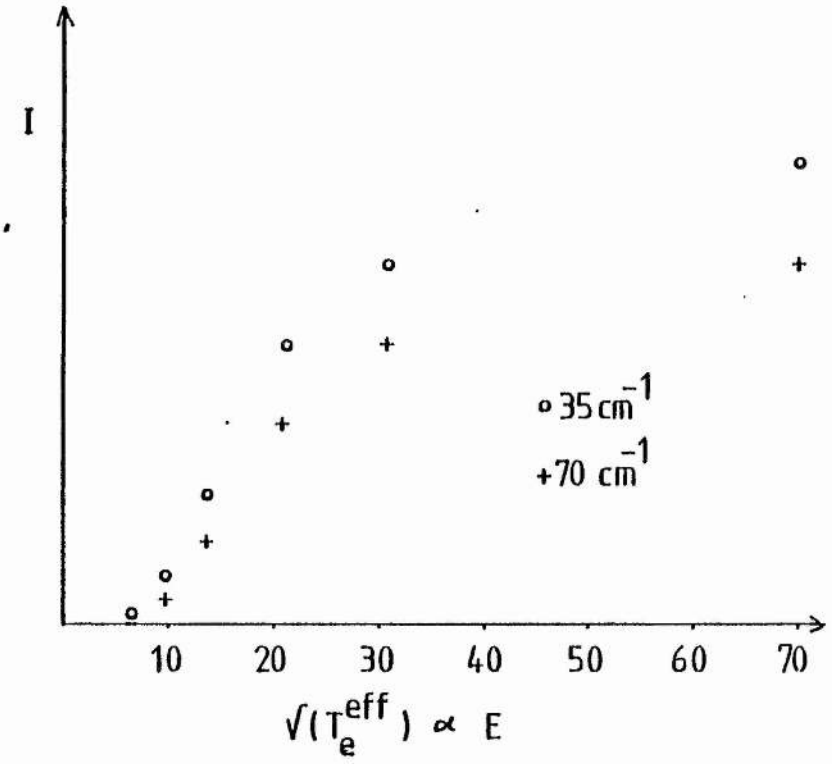

Experimental (RR133)

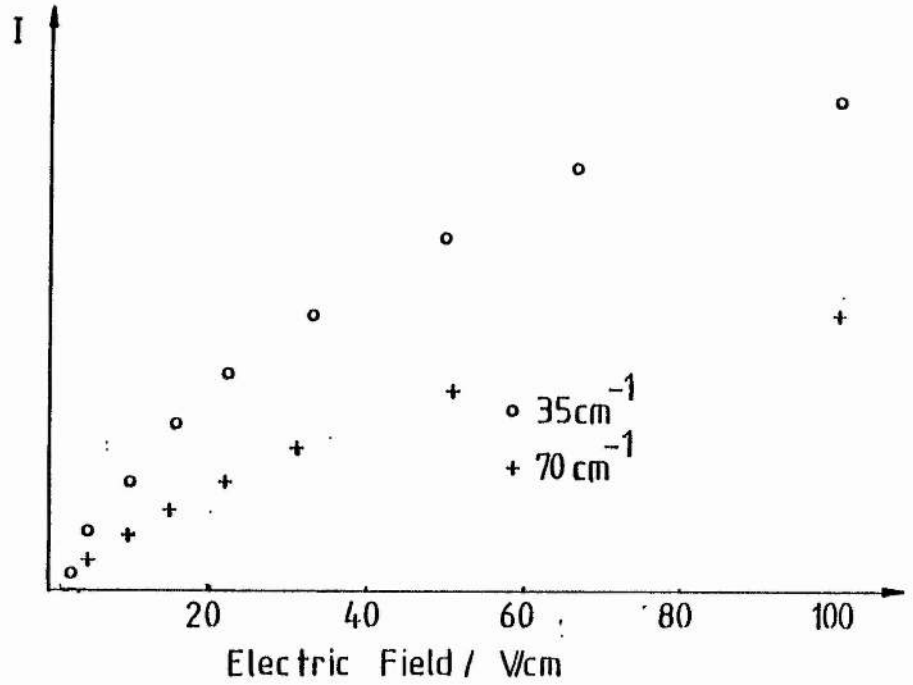

Intensity and Line-width vs. Bias Field

InP (KV454)

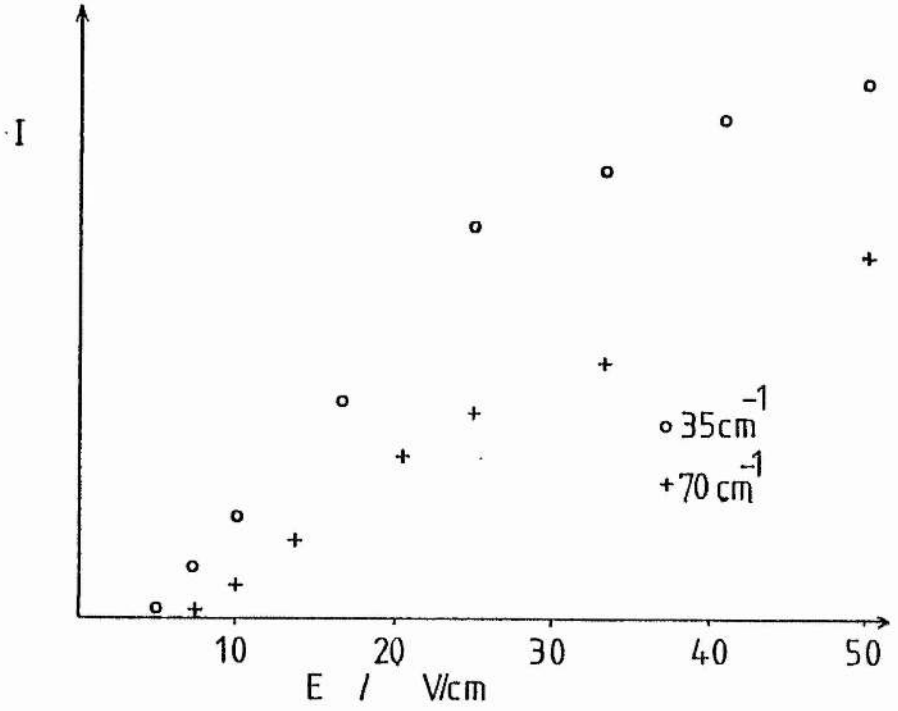

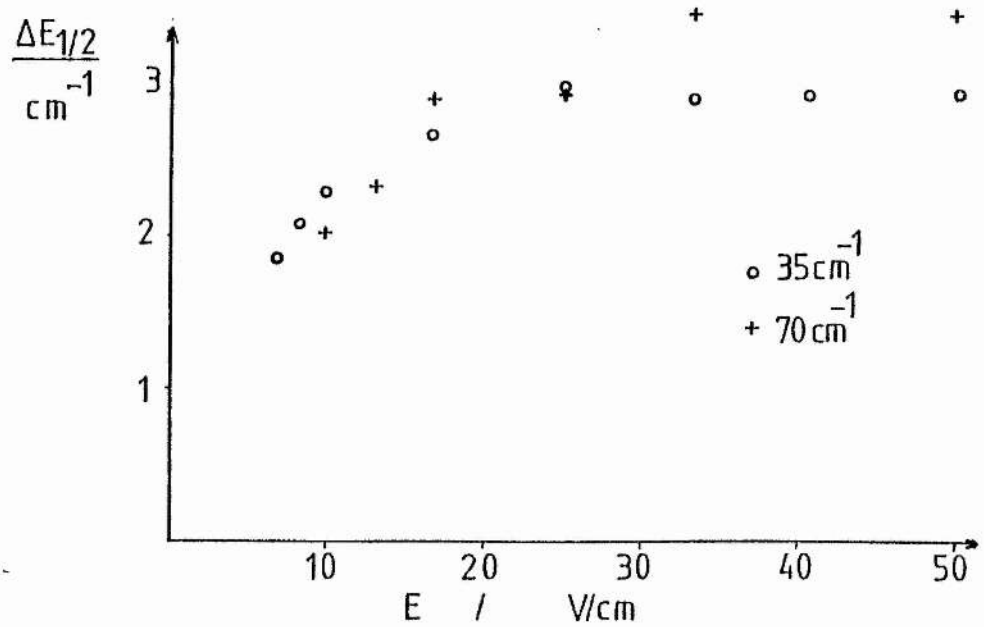

studied. In table 4.2 the linewidths at emission threshold and in the saturation regime and the ratio of saturation linewidth to threshold linewidth at both detector frequencies are given for all the samples.

Table 4.2

Sample	Experimental Linewidths(cm^{-1})					
	$35cm^{-1}$			$70cm^{-1}$		
	Threshold	Saturation	Ratio	Threshold	Saturation	Ratio
nGaAs						
RR133	0.5	1.8	3.6	1.3	2.5	1.9
RR98B	0.65	2.3	3.5	1.0	2.6	2.6
RR17H	1.85	3.25	1.7	2.35	3.45	1.5
RR17C	1.35	2.1	1.6	1.3	2.0	1.5
S1	0.35	0.65	1.9		1.24	
nInP						
KV454	1.6	2.6	1.6	2.0	3.3	1.6
NAG747	2.4	3.4	1.4	1.7	3.2	1.8
KV584	3.8	4.2	1.1	3.2	3.4	1.1

In most cases the emission linewidths was much bigger than the detector linewidth and the detector linewidth was simply subtracted when analysing the spectra. For narrow emission lines however this subtraction leads to large experimental errors especially as the narrowest lines tended to occur at low biases where the signal to noise ratio in the emission spectra was poorest. As the emission linewidth becomes

narrower than the the detector linewidth the amplitude of the peak in the spectra ceased from being a measure of the peak emission intensity to become a measure of the integrated intensity. The intensity shown on the graphs is defined as the maximum signal picked up at the detector. The emission intensity also shows saturation effects as the electric field is increased.

4.5.1 Lineshape Model

In order to model the linewidth and intensity dependence on the electric field bias, lineshapes are calculated assuming an effective electron temperature T_e^{eff} used as an adjustable parameter. T_e^{eff} is defined by assuming that the electron energy distribution function is Maxwellian below the optical phonon energy characterised by T_e^{eff} and zero above the optical phonon energy i.e.

$$f(W) = D(W)\exp(-W/k_B T_e^{eff}), \quad W < \hbar w_{lo},$$

$$f(W) = 0, \quad W > \hbar w_{lo}.$$

The cut-off at the optical phonon energy is introduced to account for the strength of polar mode scattering. For each of the higher subbands the relative electron population is calculated at equal intervals of k_z using the distribution function described above. The energy of the appropriate cyclotron emission transition is also calculated in each case taking into account polaron and nonparabolicity corrections. The nonparabolicity corrections are described in detail in chapter 2, the polaron corrections are taken

from Bajaj (1968) and they were given by

$$E = -3/20\,\alpha^{pol}\hbar w_c 2/w_{lo}(\hbar^2 k_z^2/2m^* w_c + n + 1)$$

which is valid away from the optical phonon energy. Each transition is then assumed to have a Lorentz lineshape characterised by an wT value and the effect of all these transitions is added to produce a final lineshape. Simple energy dependencies for the scattering time, i.e., $T \propto W^p$ with p=0, -1/2 etc could be included in the model.

The model is inadequate in a number of ways:

1. A sharp cut off in the distribution function at the L.O. phonon energy is assumed. This would not be the case because electron electron scattering would smear out the cut off (Gornik et al(1978)).

2. Other relaxation mechanisms could distort the distribution at lower energies e.g. 2T.A. phonon relaxation or L.O. phonon relaxation direct to impurity states. The matrix elements for these processes are small however and the effects should be weak compared with L.O. phonon emission.

3. At high biases the streaming effects discussed by Komiyama et al (1982) can occur (i.e. electrons travel from origin in k space up to a threshold value of k for L.O. emission without being scattered, producing a strong distortion of the distribution function).

4. Several authors e.g. Matsuda et al(1979) have claimed that it is necessary to consider two temperatures T_e^{intra} - the temperature within a Landau level and T_e^{inter} the

temperature given by the relative populations of Landau levels. If this is indeed the case it will result in a different electron energy distribution from the one assumed. The sharp peaks in the density of states function in a magnetic field can cause distortion in the distribution function leading to abrupt changes at each Landau level edge.

5. Absorption and stimulated emission of blackbody radiation are not included in the model.

4.5.2 Comparison of Theoretical and Experimental Results

The linewidths and relative emission intensities resulting from the lineshape calculations are plotted against the square root of the effective electron temperature in figure 4.3 and 4.4. assuming an energy independent T. Some examples of the calculated lineshapes are shown in figure 4.6. The electron temperature which is related to the mean energy can be written (see Chapter 2)

$$T_e = A(1+bE^2)E^2$$

However the higher order term with coefficient b(the warm electron coefficient) usually arises as a result of polar optical scattering. (Strictly speaking the left hand side of the equation for T_e should be the difference between the electron and lattice temperatures. However we are mostly dealing with situations where $T_e >> T_l$ and the equation, as it stands, is a very good approximation.) In our model T_e^{eff} describes the electron distribution up to the L.O. phonon

Examples of Calculated Lineshapes

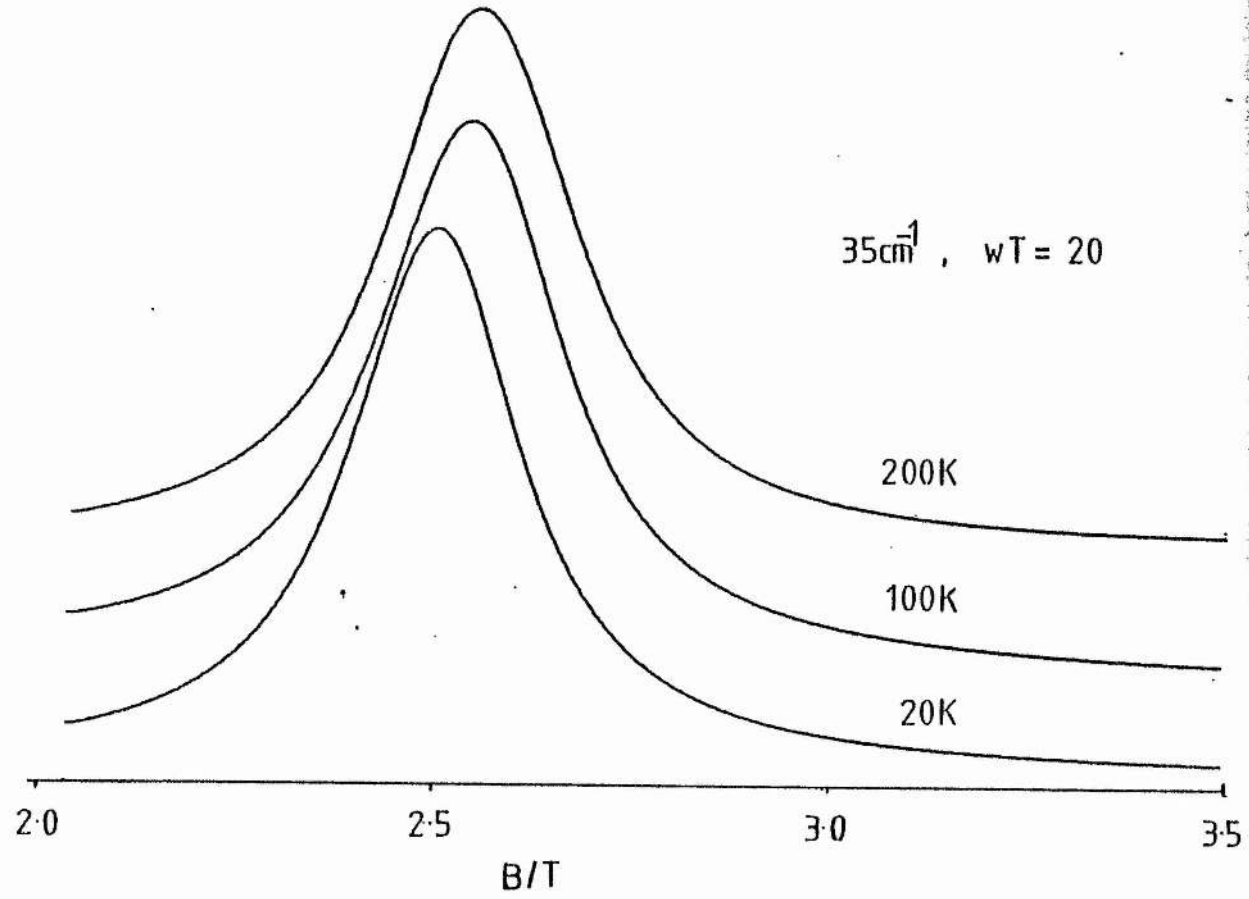

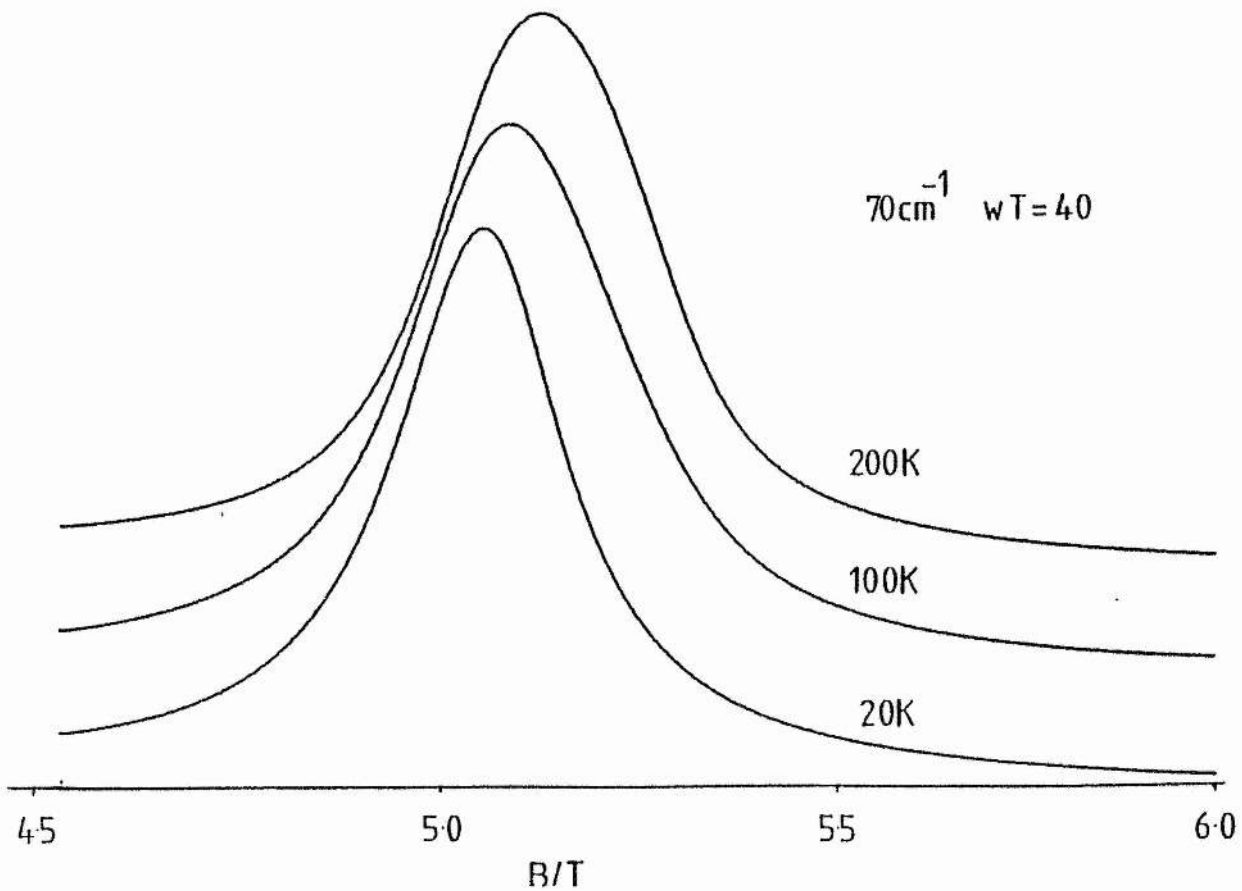

energy and in that sense the effects of L.O. phonon emission are decoupled from T_e^{eff}. It therefore seems reasonable to assume that

$$E = \text{const.}\ (T_e^{eff})^{1/2}$$

(where the constant is adjustable)

to first order and this is why the intensities and linewidths have been plotted against the square root of the effective electron temperature. It is nevertheless difficult to relate E to T_e^{eff} precisely using the lineshape model because the constant cannot be easily determined. Some idea of the electron temperature could however be obtained by comparing theory and experiment at the point at which linewidth saturation occurs. In the experimental case saturation occurs at between 20V/cm and 30V/cm in both materials. In the theoretical case saturation occurs at around 200K and so we can estimate that a bias of the order of 50V/cm will produce a T_e^{eff} of around 1000K. This gives an energy relaxation time of 0.35×10^{-9}s using equation 17 of chapter 2 on the assumption of a mobility of 100000cm^2/Vs. This value certainly yields the right order of magnitude. The effective electron temperatures implied from the graphs of linewidth and intensity against T_e^{eff} appear at first sight to be somewhat high compared to those quoted by other authors (e.g. Gornik et al (1983)) but it must be remembered that the mean electron temperature is given by

$$3/2k_BT_e = \int_0^{\hbar\omega_{LO}} WD(W)\exp(-W/k_BT_e^{eff})dW \Big/ \int_0^{\hbar\omega_{LO}} D(W)\exp(-W/k_BT_e^{eff})dW$$

in the model. T_e will in general be less than T_e^{eff} and at the highest bias fields considered T_e must saturate at

around 200K in GaAs. Comparing the experimental and theoretical graphs for the emission intensity it can be seen that in both graphs the emission intensity increases rapidly at low biases and begins to saturate as the bias, or electron temperature is increased. At low biases the theoretical curve appears to indicate a threshold for emission. In fact under these conditions the calculated emission intensity is very small since it varies as $\exp(\hbar w_c/k_B T_e^{eff})$. There is also a threshold on the experimental curve but this relates to impurity breakdown and there is no account taken of impurity breakdown in our theoretical model. Comparing the linewidth graphs the behaviour of the linewidths is qualitatively similar at both energies; they increase at low bias and saturate as the bias increases. WT values are chosen so that the theoretical linewidths give similar absolute values to those obtained from the experiment in the saturation region. The difference of 30% between the $70cm^{-1}$ saturation value for the linewidth and the $35cm^{-1}$ value is the same in both the experimental and theoretical cases to within experimental error. However the reduction in linewidth at low biases is much greater in the experimental case. In fact using the model it is difficult with an energy independent T to fit the theoretical results to the experimental linewidths in both the low temperature threshold region and the high temperature saturation region. This must be because some of the assumptions on which the model is based are invalid. For example the scattering time is almost certainly

dependent on energy. If an $W^{-1/2}$ dependence is assumed (this would be the dependence for acoustic phonon scattering) and incorporated in the model then a much bigger difference between the theoretical low temperature and high temperature scattering time is found and a better fit to the data can be achieved. The saturation and threshold linewidths are shown in table 4.3 for various wT values for both a $W^{-1/2}$ and a W^{o} dependence of the scattering time. In the energy dependent case the wT value refers to T at the bottom of the first Landau level. The values for RR133 and S1 are shown for comparison.

Table 4.3 Theoretical Values of Linewidth

wT Value	Linewidth(cm^{-1})		wT Value	Linewidth	
	$35cm^{-1}$			$70cm^{-1}$	
	Threshold	Saturation		Threshold	Saturation
W^{o} dependence					
20	1.76	1.98	40	1.76	2.46
40	0.88	1.26	80	0.88	1.82
60	0.62	1.08	120	0.62	1.78
100	0.38	0.98	200	0.40	1.70
$W^{-1/2}$ dependence					
20	1.76	3.20	40	1.76	3.00
40	0.94	1.80	80	0.90	2.18
60	0.64	0.42	120	0.60	1.92
100	0.40	1.14	200	0.36	1.80
S1	0.35	0.65			1.24
RR133	0.5	1.8		1.3	2.5

Possibly some of the substantial decrease in linewidths as

the bias field is reduced towards breakdown in the experimental case is due to the increased probability of impurity capture at low bias fields which would reduce both the number of ionised impurities and free electrons. The results for sample S1 are interesting since they give linewidths in the saturation region which are smaller than the widths which one might expect for nonparabolicity mass spread alone. One explanation of this anomaly could be a distortion of the electron energy distribution. Such a distortion is particularly likely in this sample because of the very low carrier concentration and hence the lack of thermalising interelectronic collisions. The object of attempting to model the cyclotron emission lineshape was to obtain a qualitative understanding of the emission of the mechanisms involved and this has been achieved. The model indicates the importance of polar optical scattering in limiting the intensity and of nonparabolicity in controlling the linewidth.

4.6 Other Transitions

4.6.1 Splittings of the Cyclotron Lines Resulting from the Nonparabolicity of the Conduction Band

In 1983 Gornik et al observed splittings of the cyclotron resonance and emission lines in very pure GaAs under hot electron conditions. These were identified as resulting from transitions from different pairs of Landau levels. It has been mentioned that the conduction band in GaAs is nonparabolic. This means that the transition between the N=2 and N=1 Landau levels is 'turned on' at a slightly higher field than the transition between the N=1 and N=0 Landau levels when working at constant energy In this way structure is resolved on the high field side of the emission line. With our purest sample, 'S1', we also observe nonparabolicity splitting although this is not as well resolved as that seen by Gornik. The samples used by Gornik are mostly more compensated than the samples used at St. Andrews and so the mobility will be higher once the donors are ionised. Gornik used the splitting to estimate the electron temperature, to calculate polaron masses and to verify polaron theories when the energy of the polaron approaches that of the optical phonon. This situation is also modelled quite well by the lineshape calculation described in the previous section assuming an energy independent T. In figure 4.7 typical results due to Gornik,

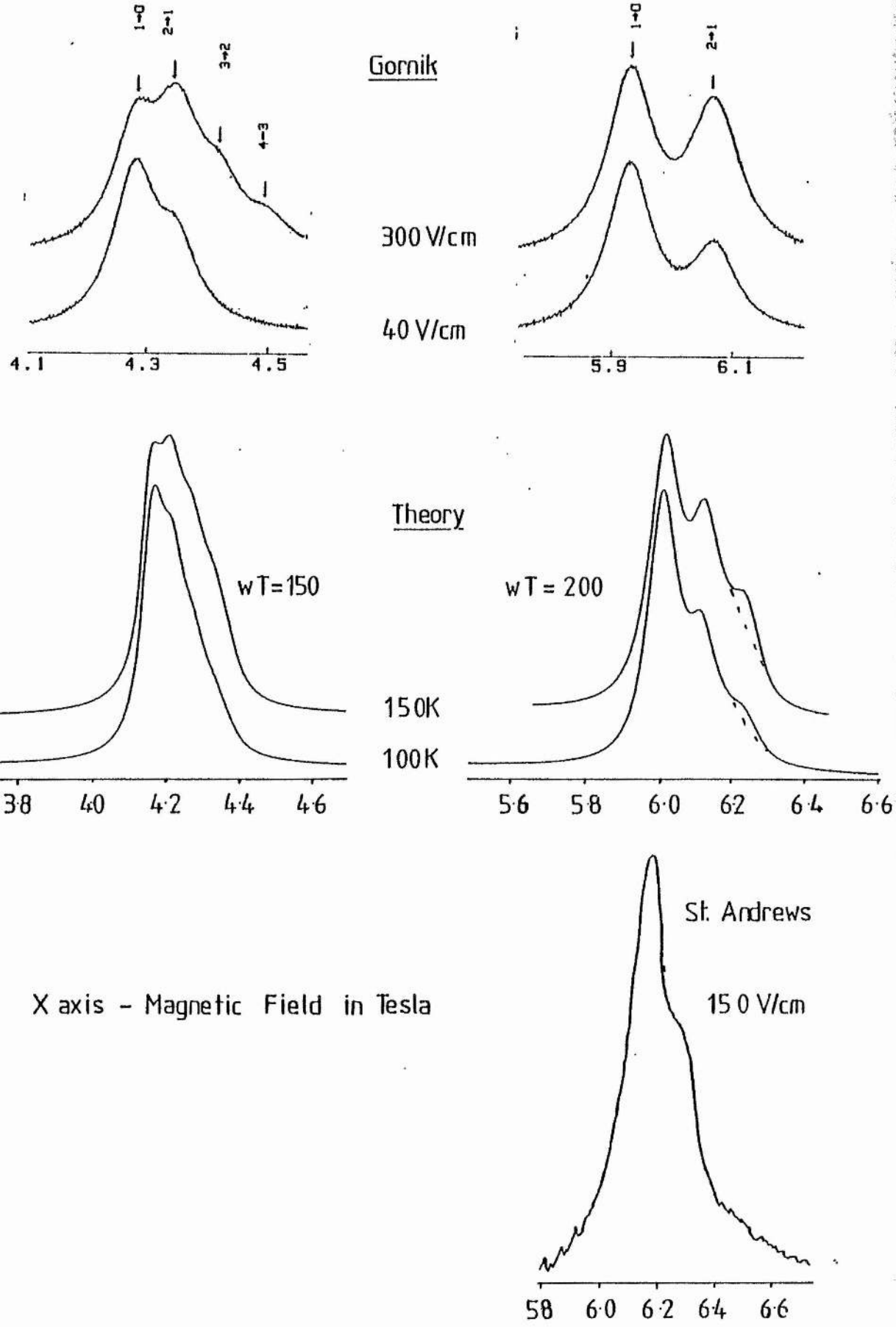

X axis - Magnetic Field in Tesla

from sample 'S1' and from lineshape calculations, carried out as described, are shown. The similarity between the experimental and theoretical curves provides further evidence that the lineshape calculations are valid. (The high field shoulder on the 6 Tesla curve does not appear on the experimental recordings because the n=3 Landau level is becoming close to the polaron level crossing energy.)

In figure 4.8 cyclotron emission spectra in InP are shown. Weak structure is observed on the high field side of the emission line and it is thought likely that this structure is similar in origin to that in GaAs. The structure is hardly observable and the trace was taken at close to the highest field available. Thus, with available magnetic fields, it was not possible to undertake the same analysis as in GaAs.

4.6.2 Impurity Transitions

In 1969 (Mengellis et al(1969)) were the first to observe far-infra-red emission from GaAs. In their case they biased the sample just above breakdown at zero magnetic field and, using a Fourier transform spectrometer and a GaAs detector, they observed emission at $35cm^{-1}$ identified as recombination radiation from the 2p to 1s transition. When a field was applied (Stillman et al(1971)) the line was found to be split into three components, corresponding to recombination via each of the Zeeman split 2p states.

Cyclotron Emission in InP 4.8

Nonparabolicity Splitting

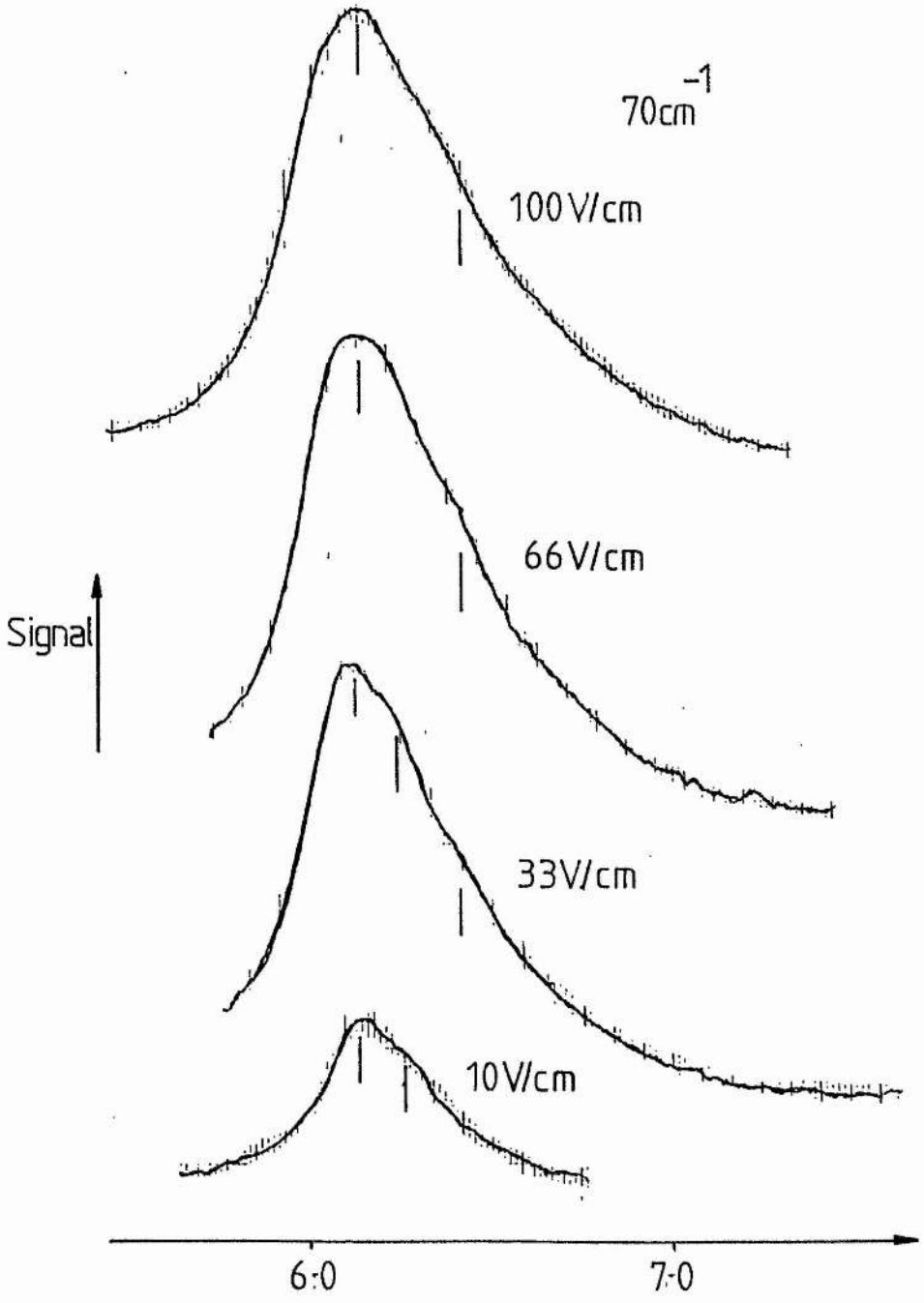

In previous work on InP and GaAs it was thought that some of the emission at zero field was due to emission from electrons in impurity states. However as the magnetic field was applied it was found that cyclotron emission began to dominate (Waldman(1974)).

During experiments on InP (NAG747) when the emission linewidth was being measured with electric fields just above breakdown additional peaks were observed on the low field side of the emission line and they were tentatively identified as the 'A' inter-excited state impurity transitions reported by Chamberlain et.al. in 1972.. These peaks correspond to a group of closely spaced lines corresponding to transitions between impurity states located just below the N=1 Landau level and states below the N=0 Landau level other than the ground state. Similar peaks were observed in GaAs but the signal to noise was much poorer. It appears that in both materials it is preferable to use uncompensated material because the smoother breakdown characteristic allows emission to be observed at lower bias fields. In figure 4.9 emission spectra close to breakdown are shown and in figure 4.10 the energies of the 'A' and cyclotron resonance transitions are shown on a fan chart. It was not possible to observe other impurity transitions such as the 'B' lines because these would occur on the high field side of the detector line and the impurity transitions would be superimposed on the high energy tail of the

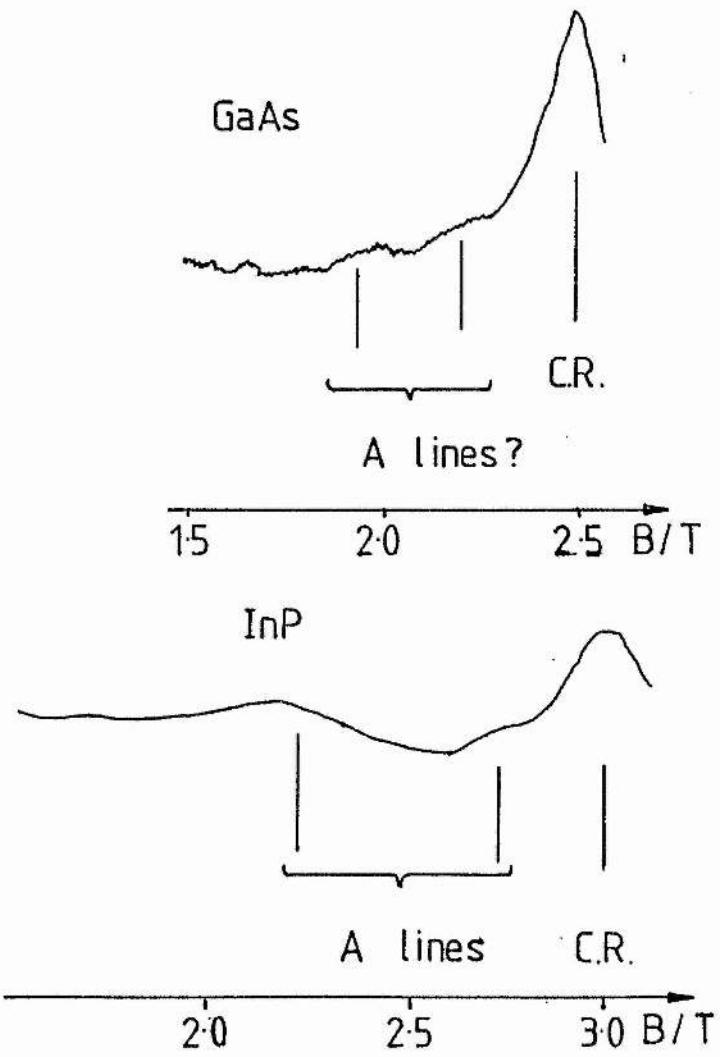
GaAs
C.R.
A lines?
1·5
2·0
2·5 B/T
InP
A lines
C.R.
2·0
2·5
3·0 B/T

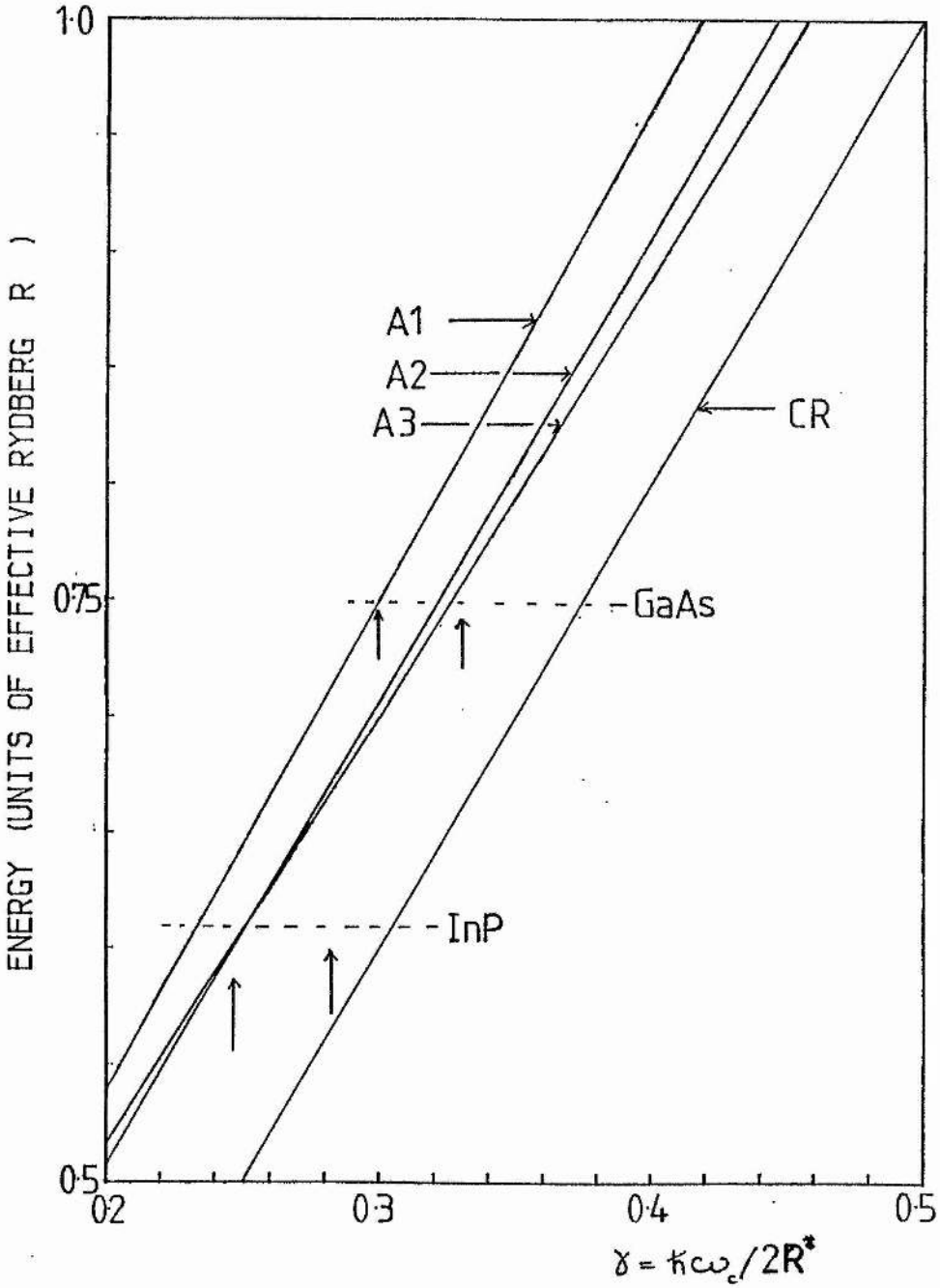
1·0
0·75
0·5
0·2
0·3
0·4
0·5
ENERGY (UNITS OF EFFECTIVE RYDBERG R)
A1
A2
A3
CR
GaAs
InP
γ = ħω_c/2R*

detector line. These results are significant because they show that the probability of electrons being captured by excited states resonant with the conduction band is quite high.

4.7 Conclusions

In this chapter cyclotron emission from InP and GaAs is described. The sample dependence of the emission linewidth is discussed and it is found that electron-electron scattering goes some way to explain the difference in linewidth between the emission and equilibrium cyclotron resonance linewidths at low temperatures for uncompensated samples. However, this cannot explain the difference which remains in pure compensated samples.

An attempt is made to model the way the emission intensity and line-width vary with electric field. The model was based on the following assumptions :

1. A simple energy dependence for the wT value was taken.
2. An electron energy distribution given by T_e^{eff} below the L.O. phonon energy and zero above.
3. $T_e^{eff} \propto E^2$

Lorentzian lineshapes were calculated for each transition taking into account nonparabolicity corrections and all of the lineshapes were summed to produce a final lineshape. Although it was not possible to achieve a quantitative link between theory and experiment good qualitative agreement was

achieved. The model can explain:

1. Saturation of the linewidth as the bias increases.
2. Sublinear variation of I with bias in the same bias range.
3. Increase of linewidth with detector frequency.

In general the model indicated the importance of nonparabolicity and L.O. phonon coupling in determining intensity and linewidth.

Nonparabolicity splitting is observed in InP for the first time and interexcited state transitions are observed in both materials in emission when the samples are biased just above breakdown.

CHAPTER 5

CYCLOTRON EMISSION IN InSb UNDER HYDROSTATIC PRESSURE

Cyclotron Resonance and Emission in InSb under Pressure

5.1 Characteristics of InSb and Review of Previous Work

InSb is a narrow gap semiconductor. It has a band gap of 0.24eV at helium temperatures and an effective mass of $m^*/m = 0.0139$ at the conduction band edge. At these temperatures it has become a model material for the study of magneto-optical and transport properties of narrow gap semiconductors because it can be grown to very high purity with total impurity concentrations as low as $\sim 10^{14} cm^{-3}$. The band is highly nonparabolic and this has a major influence on optical and transport measurements.

The binding energy of an electron in a hydrogenic impurity level is so low ~0.4meV and the Bohr radius so big (e.g. for the 1S state $a^* \sim 50nm$) that, even at 4K, the Fermi level lies in the conduction band. When a magnetic field is applied the impurity binding energies deepen rapidly, the impurity wavefunctions compress about the magnetic field axis ,and to a lesser extent along the field, and magnetic freeze-out occurs. At high field central cell structure is apparent on the 1s state; normally four components are resolved labelled A,B,C and D. The A donor is the deepest and is thought to be oxygen. The central cell structure on 1s to 2p transitions is shown in figure 5.1 (after Wasilewski et al (1982))

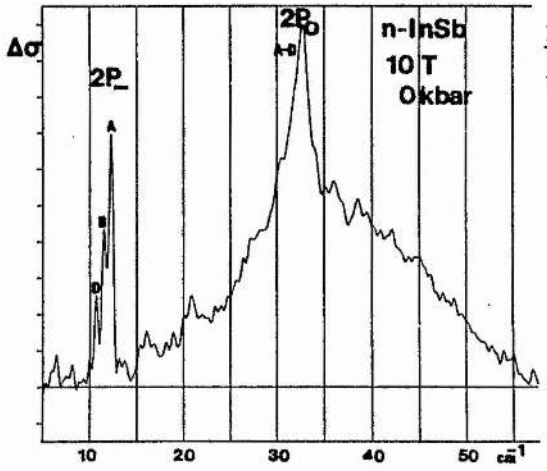

Fig.51 shows the photoconductive spectrum of the donors in InSb in the region of the $1S \rightarrow 2P_-$ and $1S \rightarrow 2P_0$ lines

Cyclotron resonance of the electrons was first observed by Dresselhaus et al (1955) working at 24GHz and at very low temperatures. This was followed quickly by a number of authors using monochromators at infrared and farinfrared wavelengths and working at a number of different temperatures e.g. Burstein et al(1956).

Johnson and Dickey(1970) again using monochromators observed cyclotron resonance harmonics, spin-flip cyclotron resonance, and phonon assisted cyclotron resonance; and in 1973 Kaplan et al published a study of cyclotron resonance linewidths as a function of magnetic field.

Kaplan, in agreement with later work by McCombe et al(1976), found that the linewidth went through a minimum as the resonant field was increased. This was attributed to a change at the minimum in the dominant scattering mechanism controlling the linewidth from nonadibatic scattering by ionised impurities at low field to adibatic scattering at high field. However this minimum is only found in InSb and it is possible that the broadening at higher fields could be due to nonparabolicity effects.

Hot electron cyclotron resonance has also been studied extensively. For example Kobayashi and Otsuka(1974) have studied the resonance conditions in a hot electron gas created by a d.c. electric field. From the shift in the

position of the resonance field and the appearance of higher Landau level transitions they were able to obtain information about electron temperatures and the mechanism for energy relaxation. Similar information has been obtained from cyclotron emission.

Gornik et al(1978), using pulsed lasers to create a nonequilibrium distribution of electrons measured the lifetime of electrons in upper Landau levels by saturation absorption. He concluded that the relaxation was dominated by scattering from L.O. phonons assisted by a form of electron-electron scattering. One electron would be excited up by one Landau level and the other simultaniously de-excited. If the electron which had gained energy found itself above the optical phonon energy then it would be relaxed much more effectively because of the strong polar mode coupling.

5.2 Effect of Hydrostatic Pressure

The band structure of InSb is shown in figure 5.2. The conduction band consists of the gamma minimum and higher lying minima at the 'L' and 'X' points of the Brillouin zone. Impurity states appear below all of these minima and because of the high effective mass of the higher order minima the impurity states are quite deep even on an effective mass model. These ground states are highly localised and are not well described by a hydrogenic model

Band Structure of InSb

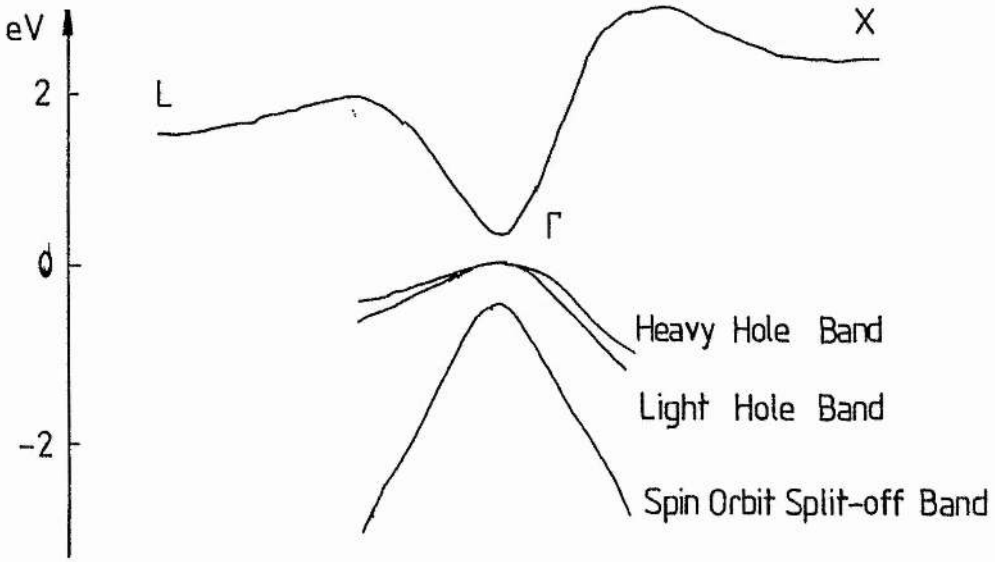

and the local potential around certain of the impurity states is strongly attractive. In particular, a donor species believed to be oxygen is found to have a central cell deepening of the order of $3cm^{-1}$ at 10T even on the gamma associated states. This would correspond to a value of $0.025cm^{-1}$ at 0T (Yafat et al(1957)). If perturbation theory can be applied, this corresponds to a value of $500cm^{-1}$ on the assumption that the electron mass at the 'X' minima is $0.4m_e$ $[(m^*_x/m^*_\Gamma)^3 \sim 2x10^4]$. This is likely to be a lower estimate because the chemical shift is of the order of the effective mass binding energy and therefore the perturbation theory is unlikely to be accurate. Thus, for the 'A' donor at least, the impurity states associated with higher order minima are deep with respect to them. It is likely, therefore, that the states will be rather delocalised in k-space and will contain substantial admixture from other minima.

The effects of hydrostatic pressure are to:

1. Increase the fundamental band gap
2. Increase the effective mass at the gamma point
3. To lower the 'L' and 'X' conduction band minima and associated impurity states with respect to the gamma conduction band minima.

The conduction band and impurity states are shown schematically in figure 5.3. and 5.4. as a function of pressure. figure 5.3 shows the ground and excited states of a single donor species. figure 5.4 shows the ground states for the four common residual donors in InSb usually written as A, B, C and D (A is thought to be oxygen). From effective mass theory one might expect the ground state at the 'X' and 'L' minima to have a degeneracy corresponding to the number of subsidiary minima (4 for the 'X' minima and 3 for the 'L' minima). However in both cases the degeneracy is lifted by valley orbit splitting and the lowest lying state is singly degenerate. The interesting effects begin to occur when some impurity states associated with the subsidiary minima move into the band gap from being resonant with the conduction band . It is not surprising that the deepest donor undergoes this change first at around 7kbar for both subsidiary minima impurity states and in fact, with presently available pressures it is the only one observed to do so.

In material where the acceptor concentration exceeds the total concentration of B,C and D impurities it is possible to see dramatic changes in carrier concentration as carriers are frozen out onto donor states associated with subsidiary minima (see Porowski et al (1974), (1976)and (1980)).

Schematic Diagram Showing The Conduction Band and Impurity States in InSb

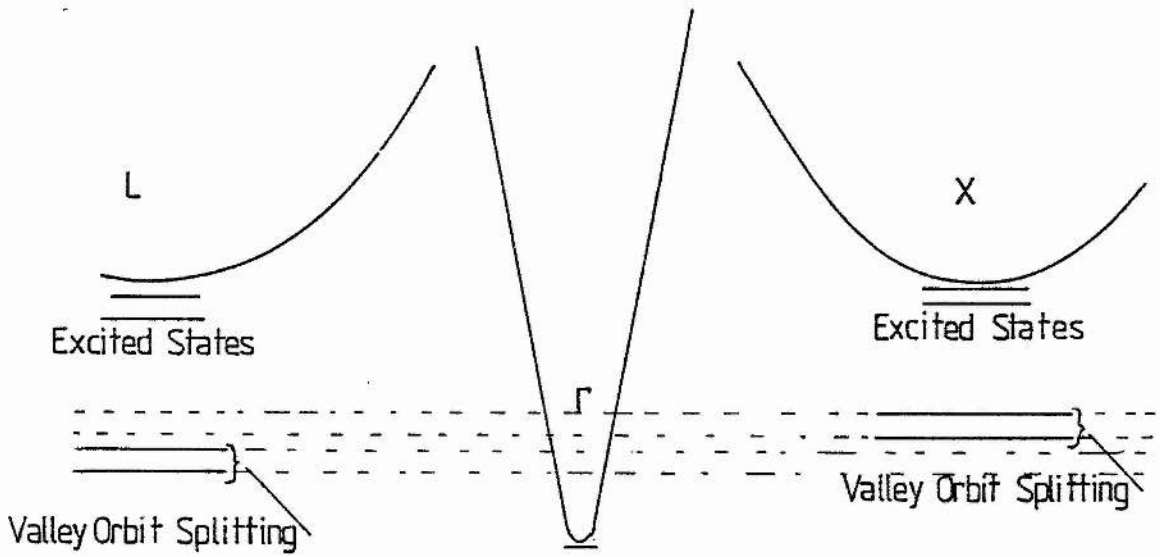

Effect of Pressure on the Conduction Band of InSb and on Ground Impurity States

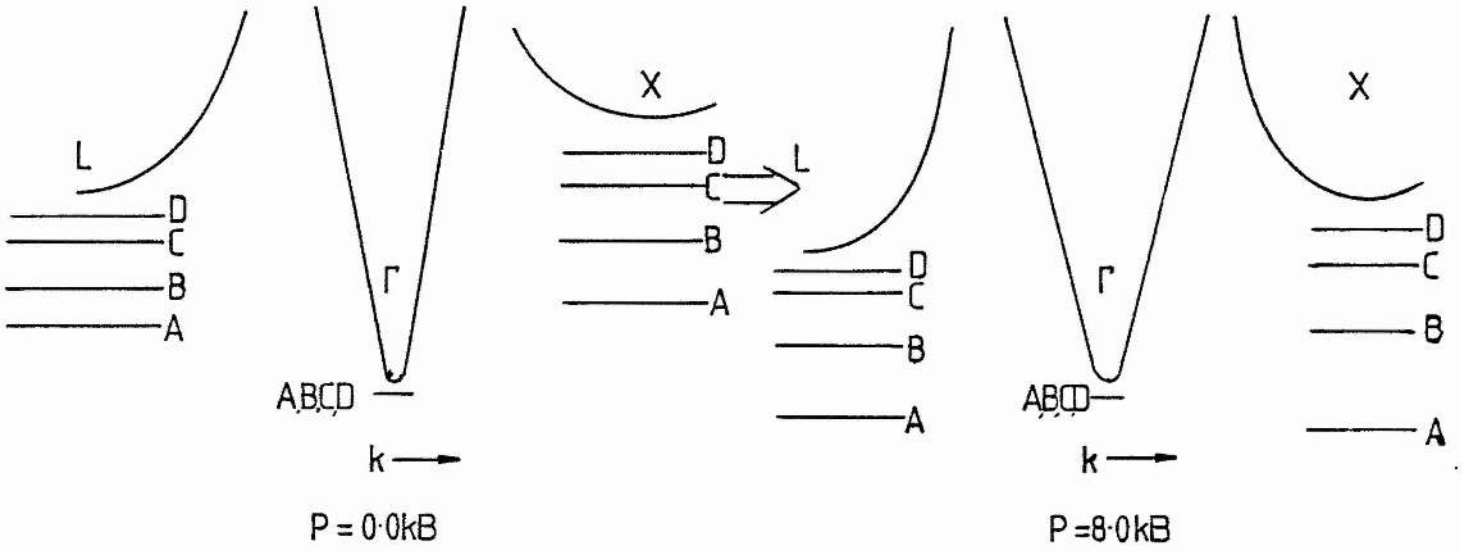

P = 0·0kB

P = 8·0kB

Similar effects have been observed in GaSb (A.Ya.Vul' et al (1971)) CdTe (Isler et al (1971)) and in GaAs (Armistead et al (1984)).

In the case of the lowest state of the 'oxygen' donor associated with the 'X' minima strong lattice relaxation effects can occur giving rise to a potential barrier of 0.3eV in the relaxed state (see figure 5.5.). This means that it is only possible to obtain a thermal equilibrium population of this state at temperatures above about 120K and that the state becomes metastable below that temperature.

An interesting confirmation of the level crossing of the conduction band by the impurity states associated with the 'L' minima was obtained in a magnetooptical study of impurity spectra as a function of pressure (Wasilewski (1982)). In this case the electrons were frozen onto the 'L' minima impurity state and anti-crossing effects were observed, i.e., two branches in the photoconductivity spectrum could be observed near to the cross over region and the intensity of the two components changed smoothly on passing through the crossing condition.

Configuration Coordinate Diagram Showing Lattice Relaxation After Electron Transfer

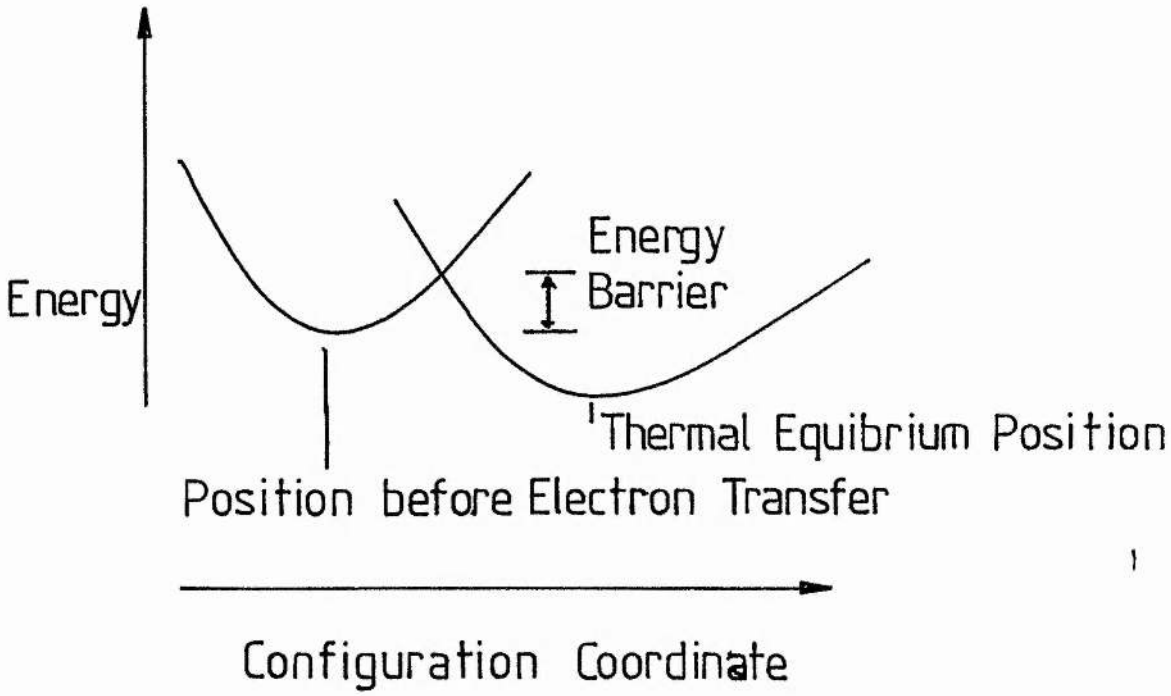

The motivation for studying cyclotron resonance and emission is that cyclotron resonance has previously been observed to narrow substantially after depopulation effects have occurred (Wasilewski et al(1982)) and that preliminary investigations of cyclotron emission have shown similar effects (Gornik(1982)) and (Wasilewski(1980)).

5.3 Experimental

The experimental method and equipment were similar to that described in chapter 3. Two samples, one 1000um thick and the other 50um thick were cut on the wire saw, etched and contacted in the usual way. The material had a 77K mobility of 600000cm^2/Vs and a carrier concentration of around $8x10^{13}cm^{-3}$ at 77K. The samples were mounted in the clamp cell. Cyclotron resonance with electrons in thermal equilibrium at 4.2K and cyclotron emission experiments were done on the samples. Mostly the thin sample was used to avoid over absorption effects but useful results were also obtained from the thicker sample. Cyclotron resonance data were taken using the far-infra-red laser system and cyclotron emission experiments were done using the double magnet system. Both experimental set-ups are described in the chapter 3 as is the clamp cell.

5.4 Cyclotron Resonance

Cyclotron resonance measurements were made using photoconductivity at various wavelengths and at a number of pressures in what was a repeat, using a different sample, of a previous set of experiments (Wasilewski et al(1982)).

Problems were encountered because of noisy contacts when the samples developed a high resistance after the depopulation effects had occurred. As a result only cyclotron resonance photoconductivity data were obtained on the thick sample at 699um.

The 699um traces at atmospheric pressure on the thin sample and at a pressure of 8.5kbar on the thick sample are shown in figure 5.6 and figure 5.7 shows traces obtained during a previous set of experiments(Wasilewski et al (1982). It can be seen that in all three experiments the line narrows considerably on applying pressure. In the lowest energy recording the cyclotron resonance and impurity shifted lines are not resolved at atmospheric pressure but are clearly resolved at 8.5kbar.

C.R. in InSb

699μm

IS522

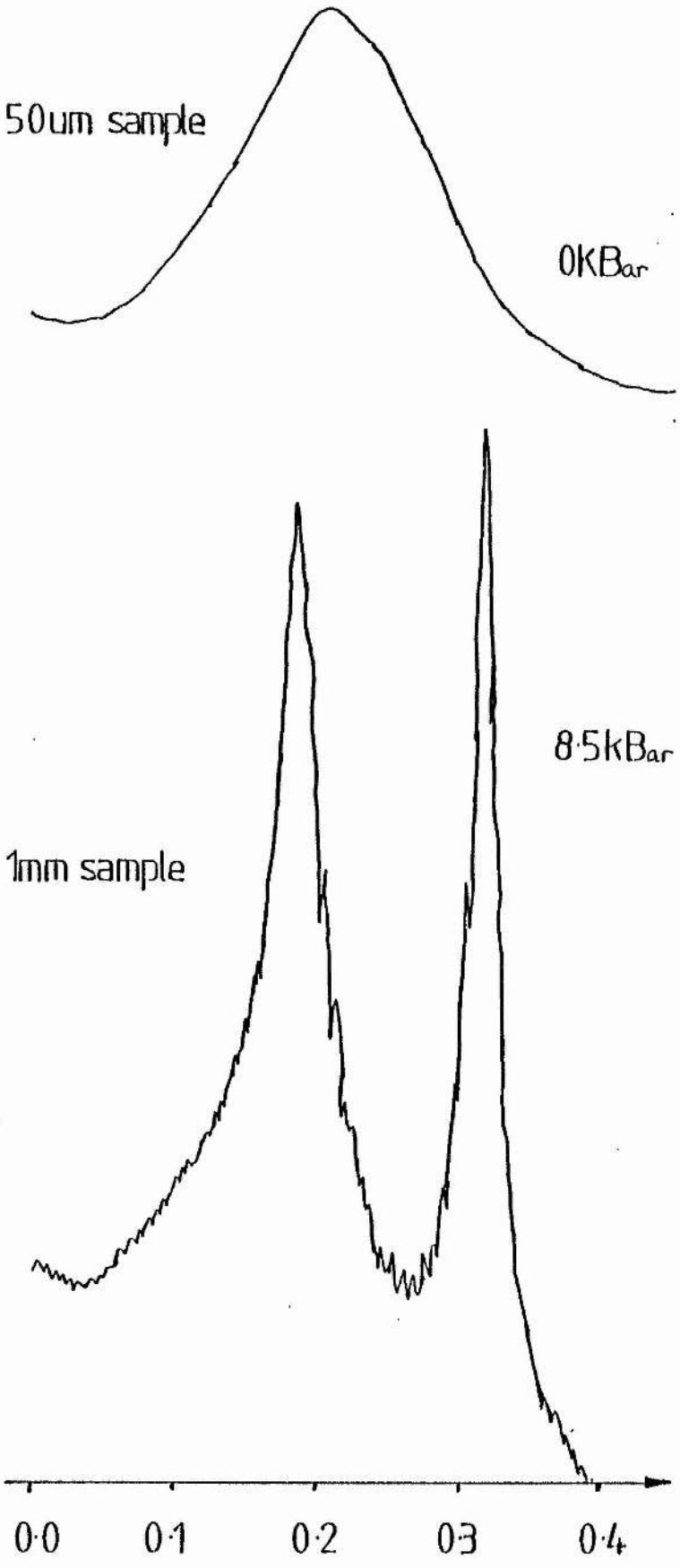

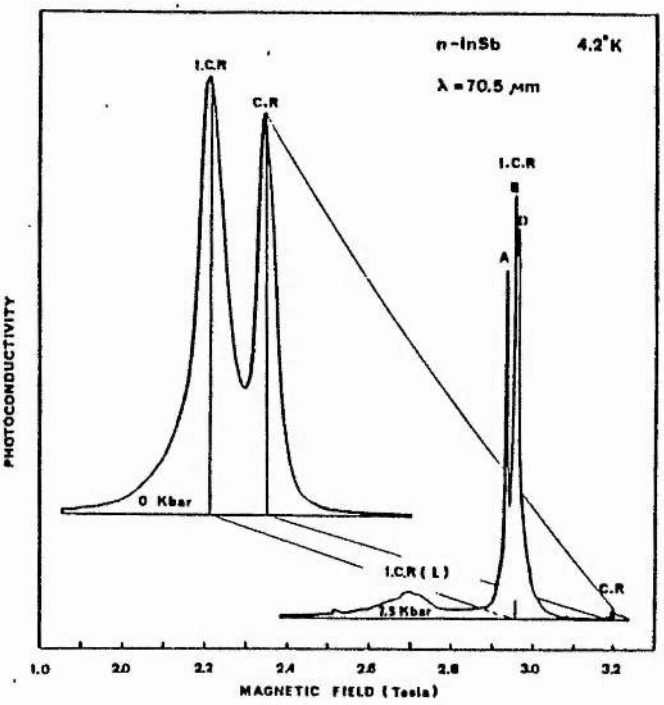

... cyclotron resonance and impurity shifted cyclotron resonance lines taken at 70.5μm wavelength demonstrating the narrowing of the lines obtained on increasing the presence to 7.5kbar and the appearance of L- and Γ-components of donor A together with the resolution of donors B and D.

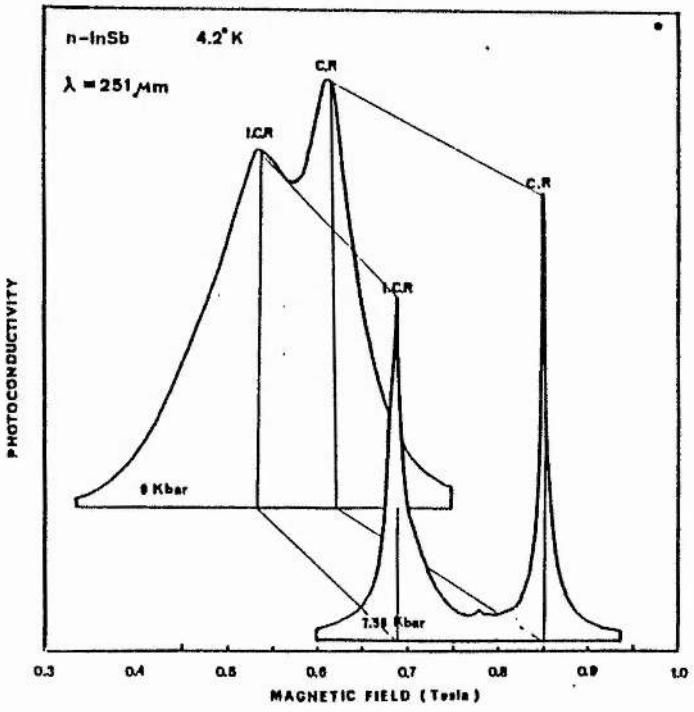

cyclotron resonance and impurity shifted cyclotron resonance lines taken at 251μm wavelength demonstrating nearly an order of magnitude narrowing on going to a pressure of 7.56 kbar.

5.5 Cyclotron Emission

The cyclotron emission experiment was done at a number of pressures between zero and 8kbar and at a detector energy of $35cm^{-1}$. The experiments were done in the transverse (E⊥B) orientation because there was not enough room to mount samples in the longitudinal orientation in the pressure bomb. Emission spectra are shown in figure 5.8 at 0kbar and 8kbar. In figure 5.9 a graph of linewidth against pressure is shown and a considerable narrowing is apparent.

The conditions under which the spectra were taken were quite different. At pressures where no depopulation occurred emission was observed at electric fields below 1V/cm as normal. However once depopulation had occurred no emission was observed until voltage pulses of 50V/cm and greater were applied to the sample. On investigation it was found that a current controlled negative differential resistance characteristic is apparent around this voltage (shown in figure 5.10). This is what one might expect from an impurity breakdown process and it is thought likely that impurity states associated with the 'L' minima are being ionised. At first sight, since these states are thought to involve wavevectors taken from the Brillouin zone close to the 'L' point, it could be argued that impact ionisation to the gamma point would be forbidden without phonon participation. However the donor state at the 'L' minima is

-Effect of Hydrostatic Pressure

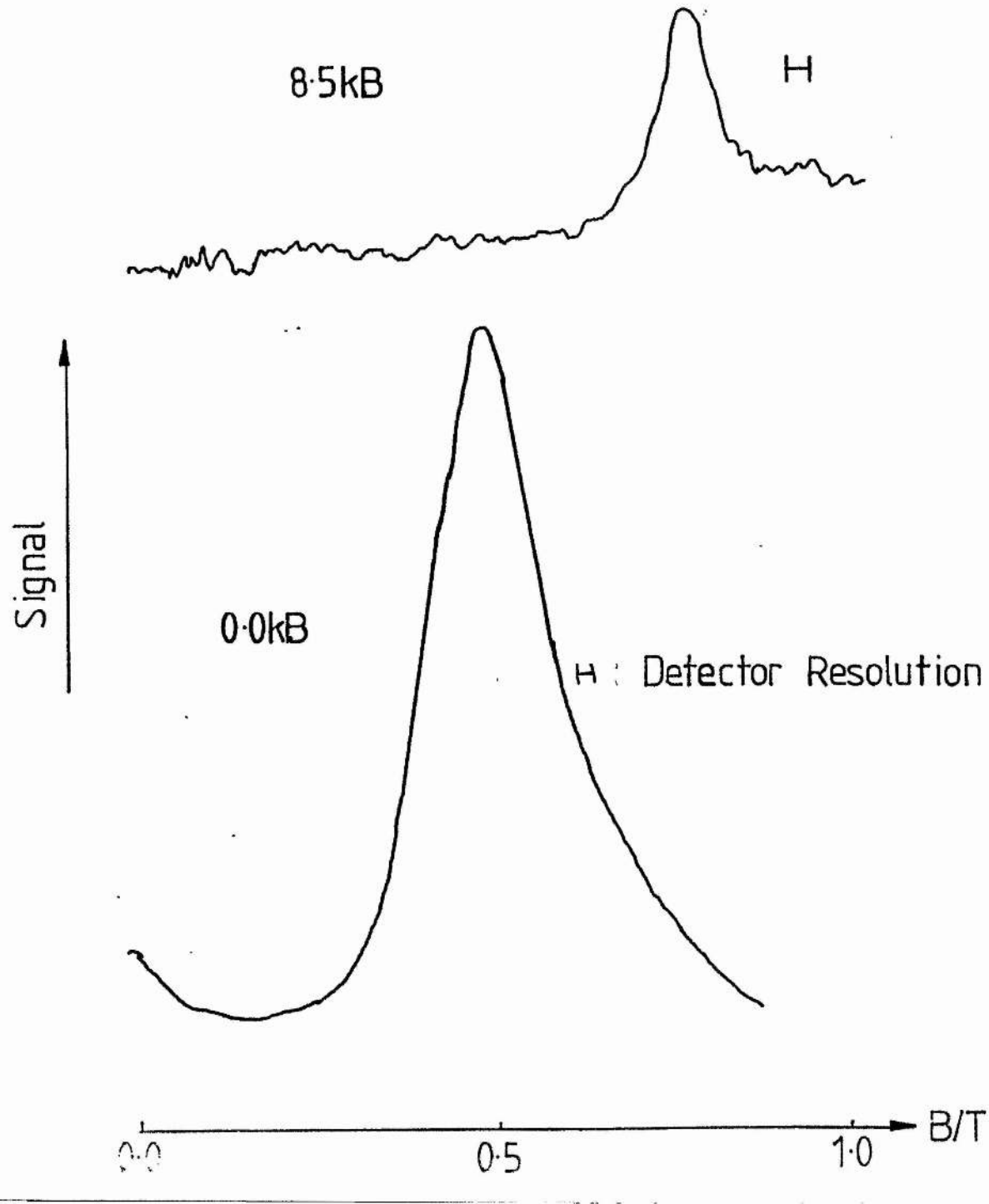

Graph of Linewidth vs. Pressure 5.9

at $35cm^{-1}$

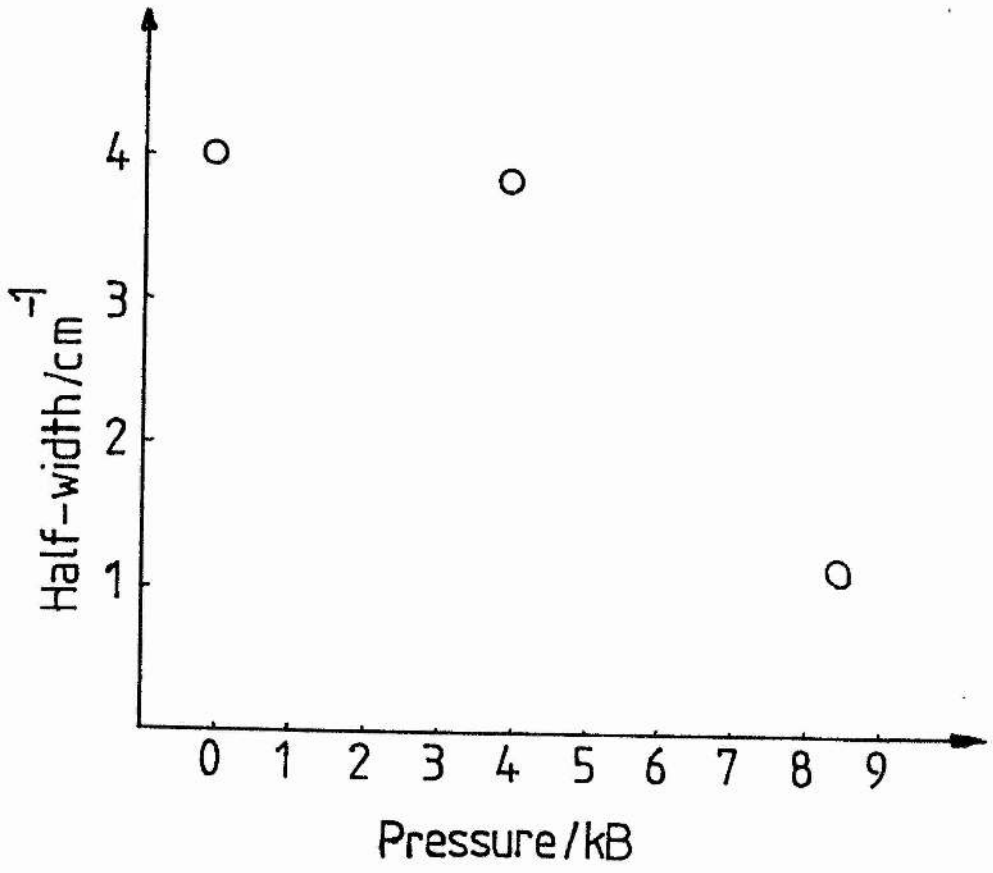

I-V Characteristic of InSb

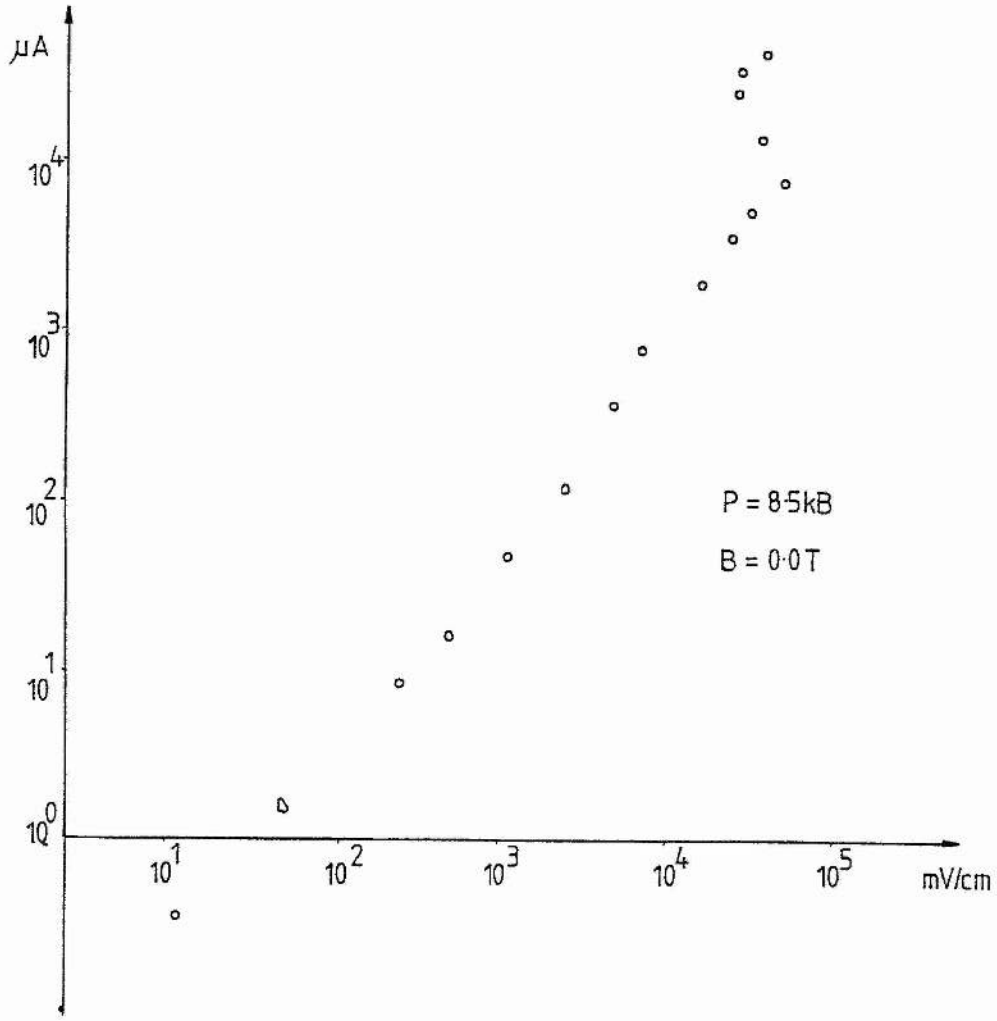

quite localised and therefore cannot be described by effective mass theory. In this case the states will contain quite strong admixtures from other parts of the Brillouin zone allowing the impact ionisation process to occur. No voltage bias dependence of the emission linewidth is observed. This is surprising since for all other emission experiments there was a considerable dependence. A possible explanation might be that above breakdown we are in the linewidth saturation regime observed in the emission experiments on InP and GaAs. The lineshape model for GaAs described in chapter 4 was modified for InSb at 8.5kbar. In the saturation regime the lineshape model yields a linewidth at $35cm^{-1}$ of $1.7cm^{-1}$ with an wT value of 100 for the individual cyclotron transitions (this value means that nonparabolicity mass spread gives the dominant broadening mechanism). This linewidth is considerably broader than the experimental linewidth ($1.2cm^{-1}$) indicating possibly that the electron energy distribution is strongly non-Maxwellian. Indeed we may even be operating under streaming conditions. The time for an electron to be accelerated to the optical phonon energy without scattering is given by Komiyama(1982) as

$$T=(2m^{*}\hbar w_{lo})^{1/2}/eE.$$

For a field of around 100V/cm this is about $5x10^{-12}s$, the the scattering time derived from the cyclotron emission experiment is also found to be $5x10^{-12}s$ and so we are likely to be very close to streaming conditions.

5.6 Discussion of Narrowing Mechanisms

In discussing the narrowing mechanisms it is important to note that they may be different for emission and photoconductivity experiments. For the photoconductivity experiment the narrowing is by a factor of ten at 251um and 8kbar but for the emission it is only by a factor of three.

In all previous experimental and theoretical studies it was assumed that the dominant broadening mechanism in InSb under quantum limit conditions at low temperatures was related to scattering by ionised impurities. However the number of ionised impurities is only reduced by about 30% (typically $N_d \sim 2N_a$ for samples of similar electrical characteristics(McCombe et al(1976))) as a result of the depopulation of the conduction band in the cyclotron resonance experiment. On impact ionisation (i.e. in the emission experiment) virtually all the donor states are ionised so that the number of ionised states would be the same at all pressures (including zero). The reduction in the linewidth can not therefore be explained wholly by a reduction in the number of ionised impurities. It is possible that the narrower line is as a consequence of the increase in the effective mass. Although the effective mass appears explicitly in the formula (e.g. Kawamura et al(1964)) for the relaxation time the dependence is at best proportional to the square root of the effective mass. The effective mass changes only by some 30%, much too small to

explain the drastic reduction in linewidth between 4.1kbar and 8.5kbar. However the effect on electron screening of charged impurities and on electron electron scattering which may contribute to the linewidth could be significant factors. Nonparabolicity broadening will also be reduced as a consequence of the increase in the fundamental band gap and the effective mass.

In the cyclotron resonance experiment one possible mechanism concerns the electrons which remain in the conduction band and shallow donor states, redistributing themselves on the shallow donors. In compensated material at very low temperatures there is a tendancy for electrons not to be bound to donor impurities close to ionised acceptors because of the repulsive potentials that exist. This correlation means that mostly ionised donor acceptor pairs and isolated neutral donors will be left. The dipolar fields from the donor acceptor pairs have a much smaller effect on the scattering than the monopole fields from isolated ionised donors and acceptors. Golka et al (1977) used such a mechanism to explain temperature dependence of the linewidth of impurity transitions in GaAs and CdTe. The tendancy of donor impurities to be located close to acceptor impurities in compensated material could explain the narrowing with pressure since, once depopulation has occurred, the effective compensation of the sample will have increased.

Such a mechanism could not explain a narrowing of the cyclotron emission since in the emission experiment all of the shallow donors are ionised. It is possible, however, that the population of electrons trapped in the metastable states could give rise to the same effect: a tendancy for electrons to neutralise donors in such a way as to minimise stray electric fields. It must be noted that this process is not very likely because the thermal energy of the electrons is high when the metastable states are filled.

Other possible mechanisms could involve the lattice relaxation which can occur when an impurity state associated with electron is trapped on an 'X' or 'L' minima. If this was to involve the displacement of a mobile impurity ion then the narrowing could arise from the resultant cancellation of charge. Such a mechanism is most likely to involve the 'X' minima like state because a lattice relaxation has been observed asociated with that state (Porowski et al(1976)).

A final, unwelcome, possibility presents itself- that the narrowing is due to a reduction in carrier concentration which increases the absorption length and reduces overabsorption broadening. In the cyclotron resonance experiment previous authors have shown (Kaplan et al(1974)) that the absorption length of a sample of very similar

characteristics to the present sample is 50μm at the cyclotron frequency in the farinfrared. This would suggest that, assuming a Lorentzian lineshape, overabsorption could not account for more than about 30% narrowing. Indeed it would take a sample some 600μmthick to account for all the narrowing in this way. A similar argument would have held for the emission experiment except that the resistance after breakdown in the emission experiment at 8.5kbar was 300Ω compared with a resistance of 200Ω (at 1v/cm) at 6kbar suggesting that at least a fair proportion of the the electrons have been impact ionised. This would argue that narrowing from self absorption effects should be even less in emission than absorption.

5.7 Future Work

Clearly the details of the effect of line narrowing in InSb are at the moment not well understood. The first priority in any future study must be to monitor the carrier concentration and mobility as a function of electric field bias and pressure and also to carry out cyclotron resonance absorption measurements in order to check the cyclotron absorption length as a function of electric field bias and pressure to completely eliminate the possibility of self-absorption effects. Another important experiment would be to repeat the present measurements as a function of the population of the metastable state.

CHAPTER 6

MAGNETOIMPURITY EFFECT IN GAAS

Magneto-Impurity Effect

6.1 Introduction

Scattering resulting in energy relaxation of charge carriers is not the predominant mechanism controlling the resistance of a semiconductor. However changes in the resistance of a sample can result when a nonequilibrium energy distribution of charged carriers, created by an electric field, is modified by such a mechanism.

In a magnetic field these energy relaxation processes are strongest when the spacing between two landau levels corresponds to an energy characteristic of the scatterer

i.e. $n\hbar w_c = E_s$

where w_c is the cyclotron frequency

E_s is the energy characteristic of the scatterer

and n is an integer.

The most commonly studied effect is the magneto-phonon effect where electrons are scattered by longitudinal optic phonons

$$n\hbar w_c = \hbar w_{lo}$$

where $\hbar w_{lo}$ is the L.O. phonon energy

Under ohmic conditions the effect results from the momentum relaxation of the charge carriers and, depending on the

material, the effect is strongest between 70K and 200K. The amplitude of the effect decreases strongly at lower temperatures because there are so few carriers having energies around the L.O. phonon energy. Under nonequilibrium electron conditions the energy relaxation of the charge carriers can be observed directly by monitoring the hot electron coefficient described in chapter 2. In this way the effect can be observed at much lower lattice temperatures.

Below 40K a number of other scattering mechanisms also become apparent when the carriers are heated out of equilibrium with the lattice (for review see Stradling(1981)).

Relaxation involving the emission of two transverse acoustic phonons from the high density of states region near the Brillouin zone boundary occurs when:

$$n\hbar w_c = 2\hbar w_{TA}$$

where w_{TA} is the frequency of transverse acoustic phonons at the Brillioun zone boundary.

Momentum is conserved because the two phonons have wavevectors opposite in direction.

Relaxation involving impurity states is also possible. One process, called the impurity-shifted magnetophonon effect, involves the scattering of an electron by a L.O. phonon directly to the ground state of a shallow impurity

$$\hbar w_{LO} = n\hbar w_c + E_i$$

where E_i is the binding energy of a shallow impurity.

Another process is the subject of this chapter. The process is known as the magneto-impurity effect and it occurs when the separation of two Landau levels corresponds to the separation of two impurity levels

i.e. $E_i = n\hbar w_c$.

It is important to realise that this is inelastic scattering from neutral impurities resulting in energy relaxation of charge carriers and not Rutherford scattering from ionised impurities which results in momentum relaxation.

The magnetoimpurity effect has been observed in a number of semiconductors - n-GaAs (Hoult(1974)), n-InP (Eaves(1974)), n-CdTe (Stradling(1981)), p-Te (von Klitzing(1978)), n-Ge(Instone(1977)) and p-Ge(Zverev(1977)). In most of these materials the strongest process involves the 1S -> 2P impurity transition. In InP however the process either results in resonant ionisation from or capture into the impurity ground state and in CdTe the process involves an interexcited state impurity transition. The present study deals with n-GaAs.

6.2 Experimental

In order to study the Magneto-impurity effect traces of resistance against magnetic field were recorded. To highlight fine structure on a monotonically varying background first and second derivatives with respect to magnetic field were obtained by the use of analogue electronic circuits. Traces were taken over a range of

temperatures and electric field biases and on a number of samples.

The sample was put into the longitudinal orientation (current j parallel to magnetic field B), a constant current was applied to the sample and a voltage, assumed to be proportional to the resistance, was measured between the same contacts. The magnetic field was swept linearly and the resistance R, dR/dB, or d^2R/dB^2 was plotted against magnetic field. The derivatives were taken either using sequential passive differential circuits shown in figure 6.1 or an active circuit (a Sallen-Keys filter, see Hoult(1974) for a detailed description). It was found that when using the passive double differential circuit it was necessary to amplify the signal from the first differentiator before it was fed into the second.

The set up yielded many interesting results. However two points need to be bourne in mind when analysing the results:

1. A two contact resistance measurement meant that the contact resistance was included and that a very nonuniform current density occurred in the vicinity of the contacts making it difficult to characterise the electric field in the sample.
2. The experiment used a constant current in the sample. Owing to the strong background magnetoresistance and

Single Differentiator

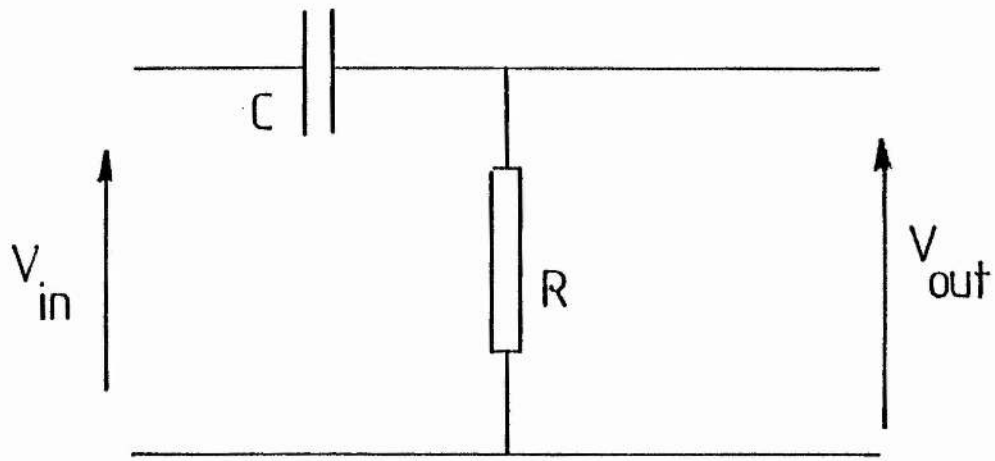

$$V_{in} = CR \, dV_{out}/dt$$

Double Differentiator

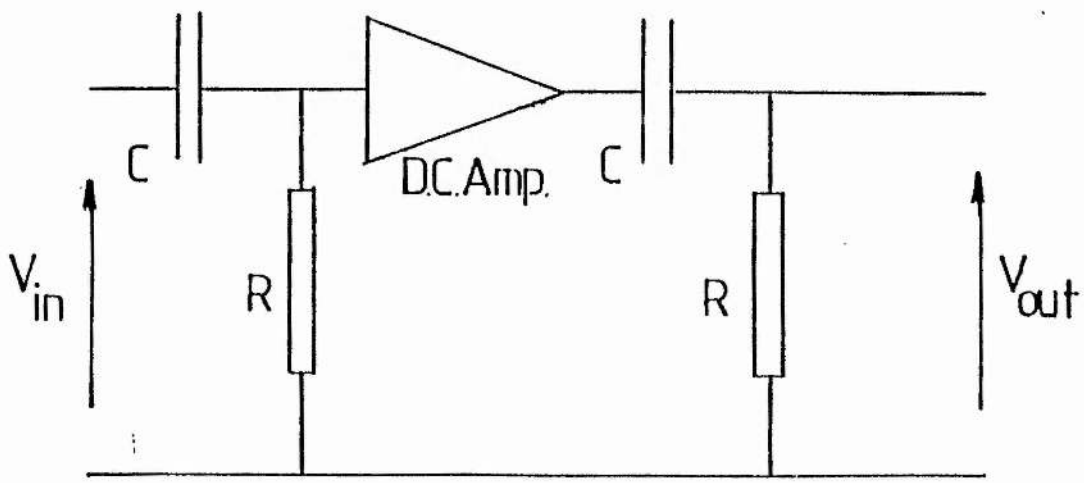

magnetic field dependent impurity freezeout below 10K the electric field bias conditions could change considerably throughout a given sweep. Working at constant voltage is little better as this results in a cooling of the electron gas as the magnetic field is increased.

6.2.1 Sample Characteristics

Three samples were used in the study:

RR133 is typical of the best samples obtained from the Wright-Paterson Air-Force Base. It is grown by the V.P.E. technique and, judging from impurity photoconductivity, had a mobility greater than 150000cm^2/Vs and a carrier concentration of a few times $10^{14}cm^{-3}$ at 77K. RR133 is also very uncompensated material. Impurity photoconductivity results obtained by S.P. Najda showed central cell structure typical of V.P.E. material (i.e. two equally strong donor species called X1 (silicon) and X2 (sulphur) and a third weaker donor X3 (germanium) with a larger binding energy.

Sample 'S2' was obtained from Dr. G.E. Stillman (Univ. of Illinois). It is also V.P.E material of low compensation. However the carrier concentration is somewhat greater and the mobility lower than RR133 judging from photoconductivity results. By reducing the Ga to As ratio during the growth process the incorporation of a group IV element on a group III site is enhanced so that X3 became the dominant impurity species.

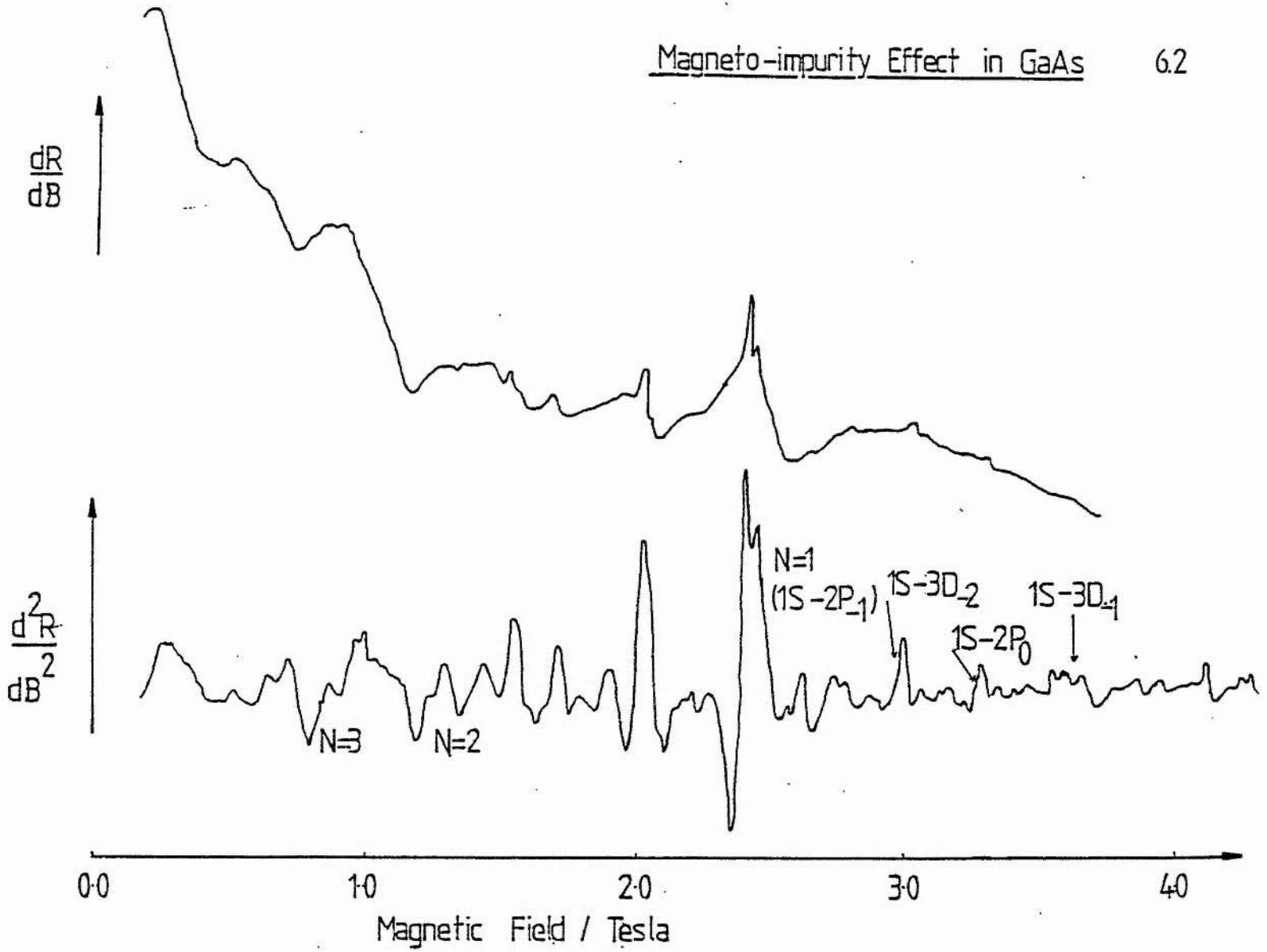
dR/dB
d²R/dB²
N=3
N=2
N=1
(1S-2P-1)
1S-3D-2
1S-2P0
1S-3D-1
0·0
1·0
2·0
3·0
4·0
Magnetic Field / Tesla

Sample E351 is a sample from the Max Plank Institute in Stuttgart. It was grown using liquid phase epitaxy. In contrast to the other materials E351 is highly compensated and a low carrier concentration ($\sim 10^{14} cm^{-3}$). The sample also had a high mobility. The central cell structure, however, was quite different. Three equally intense peaks (Pb, Sn and X2) are observed. Photoconductivity spectra showing central cell structure are shown in figure 6.6.

6.3 Results

Typical experimental results are shown in figure 6.2 for sample RR133; both the first and second derivatives are shown. The fundamental of the strongest magnetoimpurity series associated with the $1S \rightarrow 2P_{-1}$ occurs around 2.3T and the second and third harmonics are clearly shown. Additional peaks corresponding to $1S \rightarrow 2P_{o}$, $3D_{-2}$, and $3D_{-1}$ are all observed at higher fields. These were first observed by Zvereva et al. (1982). Peaks below the fundamental may be harmonics of these transitions or they may correspond to conditions where the spacing of two Landau levels equals the energy difference between two excited states of the hydrogenic impurity; they have not yet been identified properly. The strong feature around 2T has two possible explanations. It may correspond to the second harmonic of the magnetoimpurity series observed in InP where oscillations in the magneto resistance occur when the spacing of two Landau levels corresponds to the ionisation

Transition Energies for the Magnetoimpurity Effect

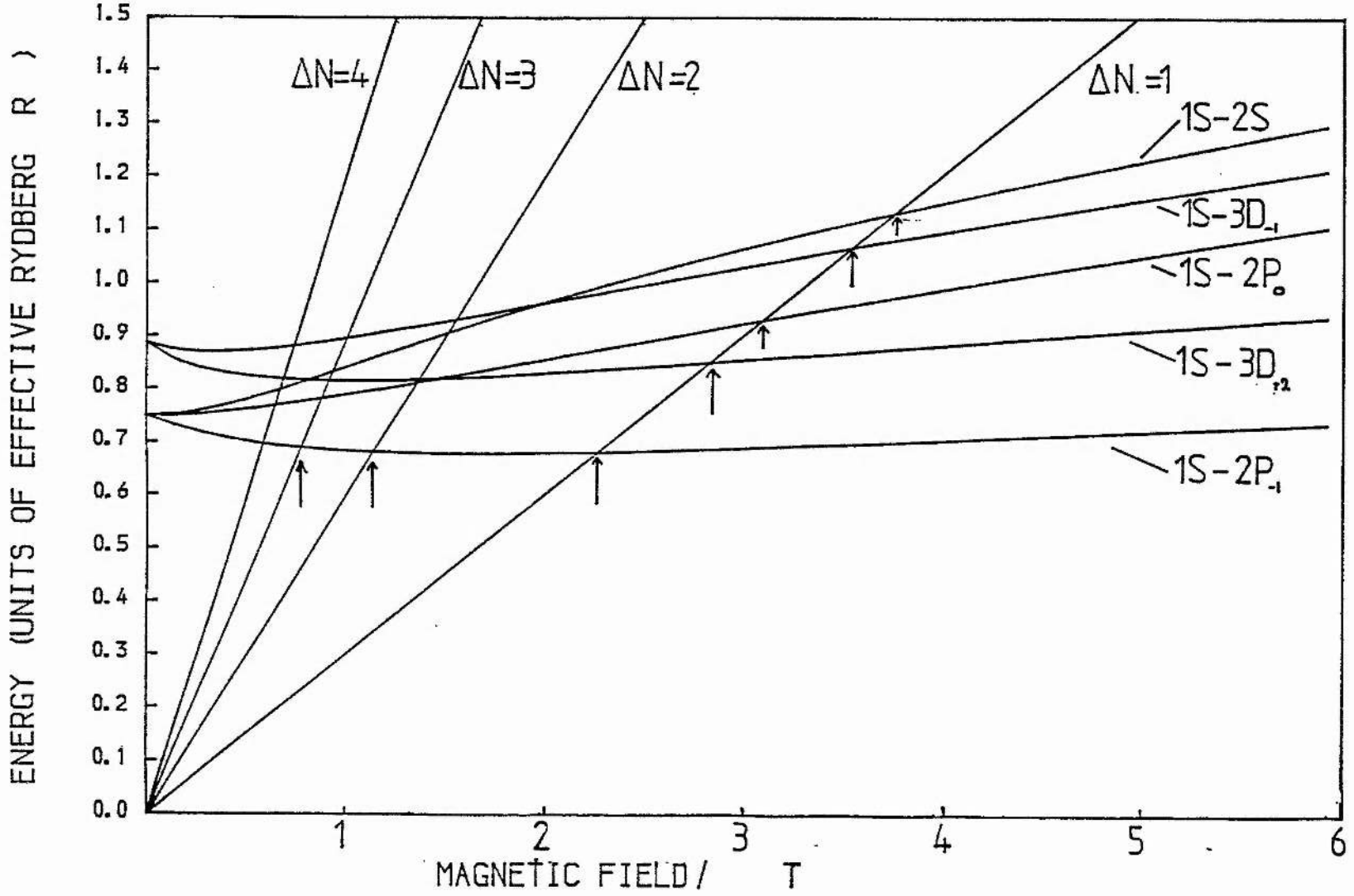

energy of the impurity. Another possibility is that the transfer of electrons to or from the $2P_{+1}$ state as it becomes resonant with the conduction band causes a dip in the resistance. Pidgeon et al(1983) using saturation absorption measurements claim to have observed such a transfer process. It is not clear which of these is actually the cause. However if the former explanation were true one might expect central cell structure to appear on the peak. This is not apparent. Also, we do not observe the fundamental of the impact ionisation series. A graph of transition energies against magnetic field is shown in figure 6.3 (Aldridge and Green(1979)). The points at which the Landau level transitions cross impurity transitions represent resonant conditions.

6.3.1 'Heating' or 'Cooling' ?

An important question arising from the experiment is whether the conduction electrons are heated or cooled by the inelastic scattering process. Nicholas and Stradling (1976) found that the process involved heating of the conduction band electrons at the expense of cooling of the bound electrons. However these experiments were done at much higher temperatures (around 20K) and the relative population of impurity and conduction band electrons is quite different from that at 4K. These authors found that all peaks resulted from a dip in the resistivity and they determined the direction of the process from a study of the hot

electron coefficient B.

In our experiment the situation is somewhat more complex; the n=1 peak of the $1S->2P_{-1}$ transition corresponds to a dip in the resistance and the higher harmonics to an increase. This reversal has also been observed in InP (see Nicholas and Portal (1979)).

Without a study of the hot electron coefficient it is difficult to determine exactly which way the process is going. In order to explain the reversal of sign of the peaks between the n=1 and n=2 peaks of the $1S->2P_{-1}$ transition it seems likely that the process changes direction with increasing field. It is important to note that if we are warming the impurity electrons and cooling the conduction electrons then a process akin to photothermal ionisation can take place where the electron is thermally excited from the upper impurity state into the conduction band. According to Stillman et al (1973) the probability of thermal ionisation from excited impurity states is very high. In other experiments , performed at St. Andrews by me, it was found that the fundamental peak changed sign at 1.8K.

6.3.2 Effect of Electric Field

At all temperatures the electric field bias is an important parameter when studying the magnetoimpurity effect. At 4.2K it is particularly important. It was explained earlier that the characterisation of the electric field bias is difficult in a given sample or over a particular sweep. Nevertheless the effect was studied as a function of bias. In figure 6.4 magneto impurity traces are shown as the bias is increased. The magnetoimpurity effect disappears below a certain bias and at high biases the magnetoimpurity effect is obscured by sharp structure, seen on the top trace in figure 6.4, corresponding to the impact ionisation of impurity states (Trager (1984)). The existence of a voltage threshold below which no oscillations are seen indicates that we are indeed dealing with a warm electron effect. The bottom trace in figure 6.4 is taken in the region of threshold and the middle two show magnetoimpurity oscillations. Since we are operating below impurity breakdown and there are few electrons in the conduction band it is unlikely that a Maxwellian approximation to a warm electron energy distribution would be valid.

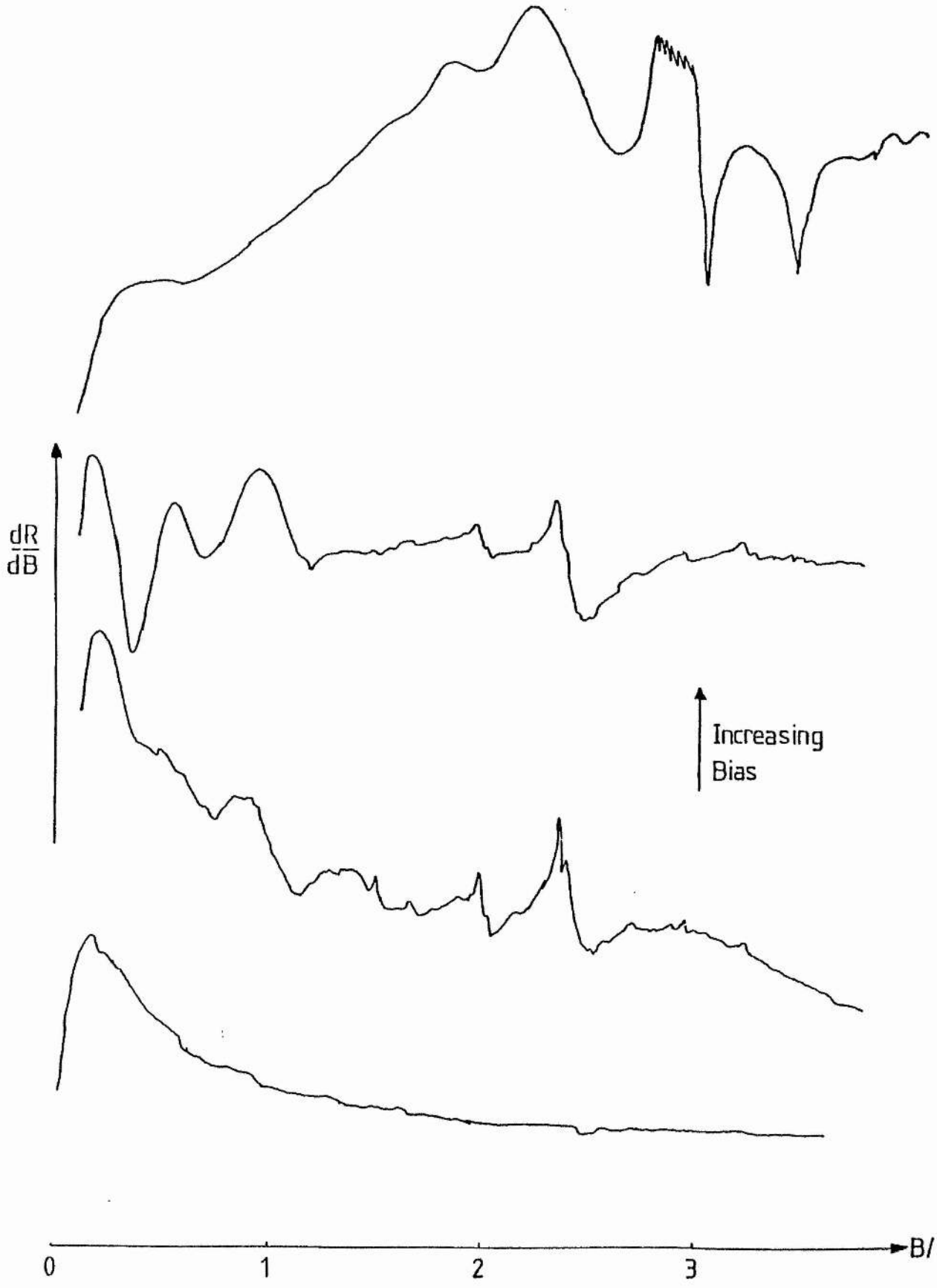
dR/dB
Increasing Bias
0
1
2
3
B/T

6.3.1 Central Cell Structure

The 1S ground state impurity wavefunction has a finite amplitude at the impurity atom and as a result it is sensitive to the chemical nature of the particular impurity present. This can result in a change of as much as $2cm^{-1}$ in the energies of electrons bound to different shallow donor species in GaAs. Chemical shifts of this magnitude should therefore be apparent in the fundamental of the magnetoimpurity series since

$$\hbar eB/m^* = \Delta E_i$$

E_i is different for different impurity species so that the splitting in the field is related to the central cell splitting of impurities by

$$B_{cc}/B = E_{cc}(B)/E_{1S->2P-}(B)$$

where B is the mean field, E the mean energy and B_{cc} and E_{cc} are the central cell splittings in field and energy respectively.

Previously central cell structure was observed in InP but not in GaAs. This is probably because the fundamental of the series in GaAs is obscured by magnetophonon oscillations at the higher temperatures at which the experiments were performed.

The central cell structure is shown quite clearly on all traces in figure 6.5. In RR133 the donors X1, X2 and X3 are shown clearly and in the S2 sample a broader peak is located in the position of X3 in sample RR133. In sample E351 three strong peaks are observed and are identified as Pb, Sn and X2 by comparison with far infra red photoconductivity measurements. All of this is consistent with photoconductivity measurements which are shown in figure 6.6 (from S.P. Najda).

A summary of all the results is given in Table 1 below.

Magneto-Impurity Effect in GaAs 6.5

-Central Cell Structure

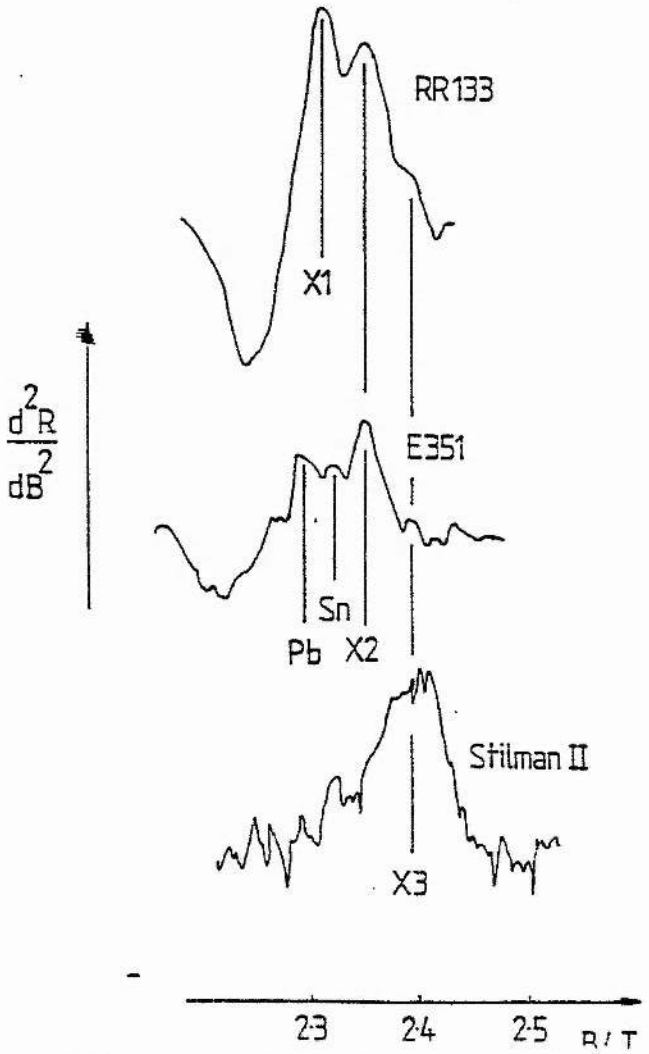

Central Cell Structure in GaAs 6.6

Photoconductivity 118μm

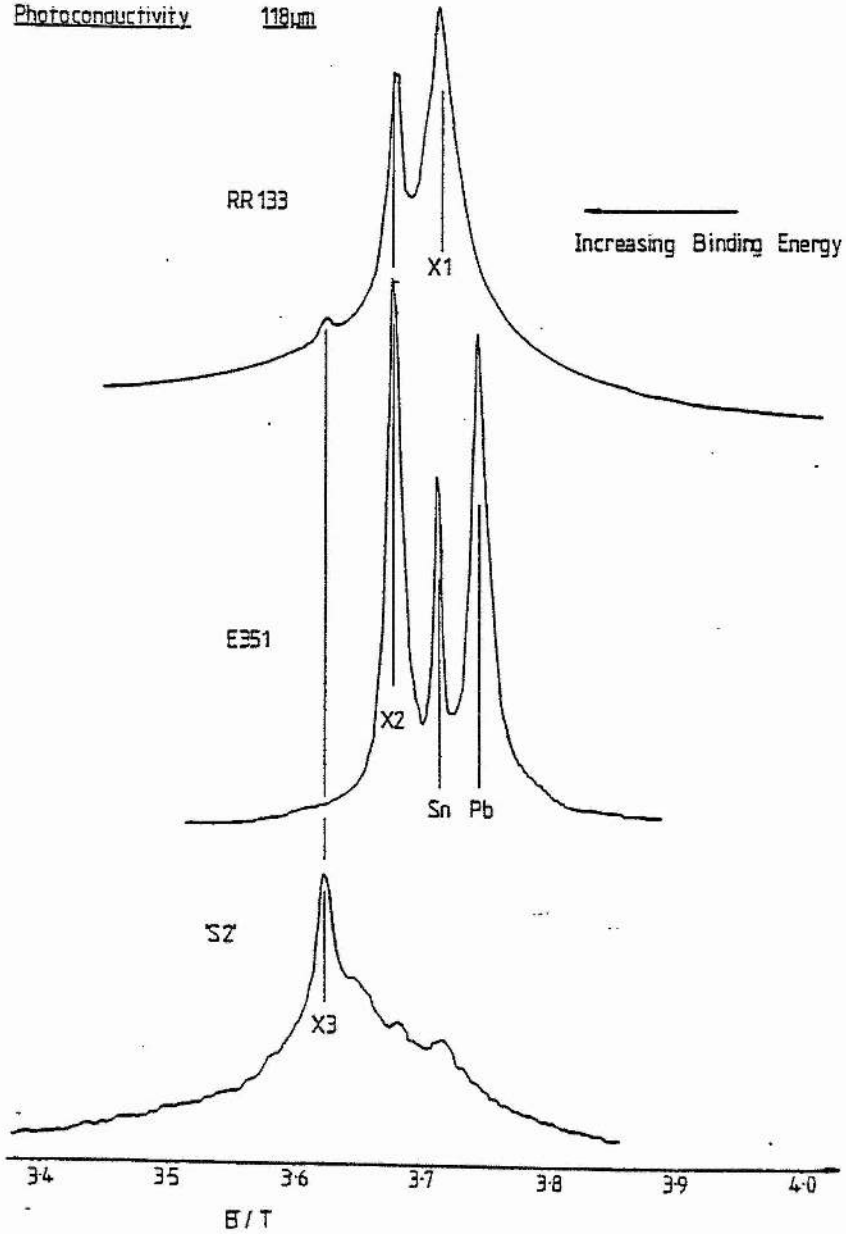

Table 1

Transition	Peak Position (in Tesla)	Theory (in Tesla)
$1S->2P_{-1}$	2.30	2.24
$1S->3D_{-2}$	2.87	2.81
$1S->2P_{o}$	3.15	3.06
$1S->3D_{-1}$	3.56	3.51
N=2	1.14	1.12
N=3	0.76	0.75

Central Cell Splitting	Magnetoimpurity (in cm^{-1})	Photoconductivity (in cm^{-1})
X1 to X2	0.55	0.50
X1 to X3	1.23	1.20

The difference between the theoretical and experimental results can be explained by nonparabolicity corrections to the band edge effective mass ($m^*/m = 0.0665$) and by the deepening of the 1S state due to central cell corrections. Nonparabolicity accounts for shifts of the order of +0.015T and central cell shifts of the order of +0.05T with respect to the theoretical value at 2.3T and so the difference between the experimental and theoretical values is readily explained.

6.4 Relevance of the Magnetoimpurity Effect to Cyclotron emission

It was explained in the introductory chapter that it was not possible to make a steady state cyclotron emission laser because energy relaxation times increased towards the band edge. Thus it is not possible to obtain a population inversion because the upper Landau level always empties faster than the lower Landau level. With this in mind the magnetoimpurity effect was studied because it provides a mechanism whereby a Landau level can be emptied resonantly. That such a small effect, in terms of resistance change could possibly be used as a mechanism to produce a population inversion may be surprising. However very few electrons are in excited states and in the conduction band at 4.2K. If the magnetoimpurity effect causes heating of the conduction band electrons there are few electrons in the impurity excited states to cause scattering. Similarly if the effect causes a cooling of the free electrons there will be very few in the n=1 Landau Level. Also the experiment does not measure populations directly but merely the changes of mobility of electrons as they move from one Landau level to the next. Therefore, large changes in population could result in possibly only small changes in conductivity. The recent results of Allan et al(1984) using far-infra-red absorption measurements indicate that large changes in

population can occur.

It seems possible therefore that the magnetoimpurity effect could provide a mechanism to empty a particular Landau level if, with appropriate optical pumping, the numbers of electrons in impurity and conduction band states were optimised.

6.5 Conclusions

The magnetoimpurity effect in nGaAs has been studied. A large number of transitions are observed the strongest corresponding to $1S->2P_{m=-1}$. The problem of whether the magnetoimpurity effect is a heating or cooling process is discussed and the observation of central cell structure on the fundamental peak is demonstrated.

CHAPTER 7

CYCLOTRON RESONANCE IN C.M.T. UNDER HYDROSTATIC PRESSURE

C.R. and Transport Properties of C.M.T. under Pressure

7.1 Introduction

$Cd_xHg_{1-x}Te$ (C.M.T.) is an alloy of CdTe and HgTe. HgTe has a small negative band gap and CdTe has a large positive band gap. By choosing different proportions of Cd and Hg materials of different band gaps can be grown and used as intrinsic detectors at frequencies corrosponding to the band gap. It is this feature which makes C.M.T. a technologically important material. A schematic diagram of the way the bandgap varies with cadmium concentration is shown in figure 7.1 (after Seeger (1982)).

In the previous paragraph it was mentioned that HgTe has a negative band gap. The meaning of this is that the band structure has inverted and the effective masses and energies (with respect to the heavy hole band at the gamma point) of the light hole and conduction bands have both changed sign. The light hole and heavy hole bands are still degenerate at the gamma point and so no actual gap between filled and empty states exists.

Much of the interest lies in material with a cadmium concentration ,x, of about 0.2 corresponding to the 9-11um atmospheric window and it was this narrow gap material which was used in the study.

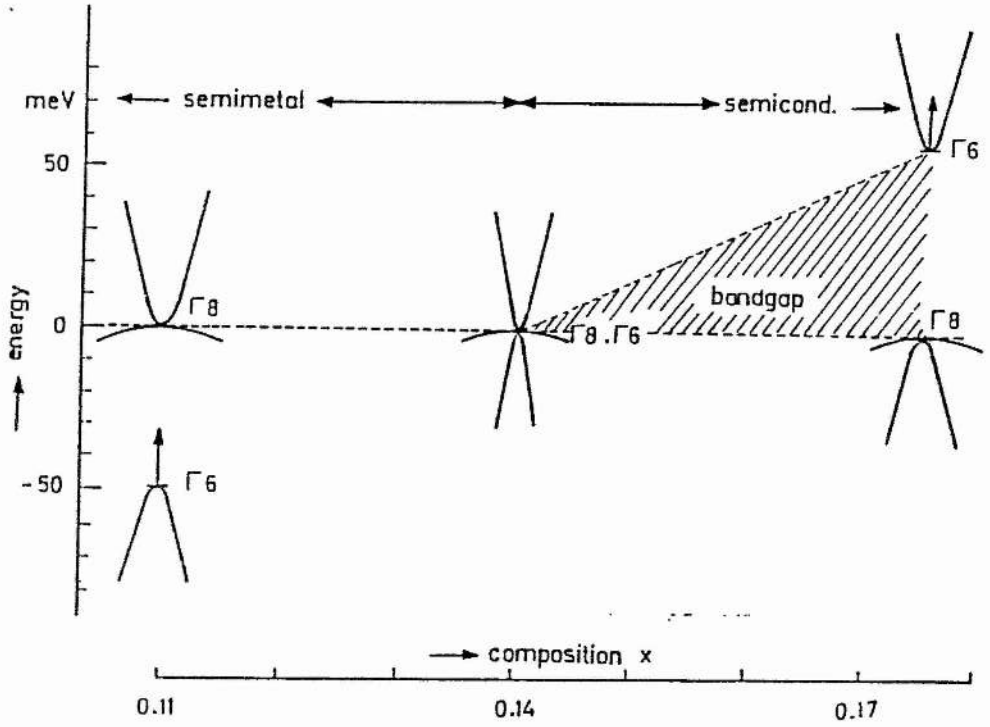

Band structure of $Cd_xHg_{1-x}Te$ alloys near the semimetal-semiconductor transition.

At the gamma point the effective masses in narrow gap materials are given by Kane (1957) in the limit that $E_g << E_{so}$ (E_{so} is the energy difference between the spin-orbit split off band and the valance band edge at the gamma point).

$$m^*_{co} = 3\hbar E_g/4P^2$$

$$m^*_{ho} \rightarrow \infty$$

$$m^*_{lo} = 3\hbar E_g/4P^2$$

where m^*_{co}, m^*_{ho} and m^*_{lo} are the effective masses of the conduction, heavy hole and light hole bands at the band edges

and P is the interband momentum matrix element.

Away from the gamma point the conduction band is strongly nonparabolic and electron energies are given by

$$E = E_g/2 + (E_g^2/4 + E_g(\hbar^2k^2/2m^*_{co}))^{1/2}.$$

7.2 C.R. and the Effect of a Magnetic Field

Cyclotron resonance was first observed by Straus et al in 1962 at 77k and a considerable amount of effort has been expended since in the determination of band edge effective masses e.g.Knowles et al (1978) and Poeler et al (1970). The band edge effective mass may also be detemmined from the fundamental band gap e.g. Willey and Dexter(1969). Magnetophonon oscillations have also been observed as have Shubnikov de Haas oscillations in the bulk material (Bauer

et al (1973)).

The conduction band energies in c.m.t. in a magnetic field are given in chapter 2 as

$$E(n,k_z,+/-) = E_g/2 + (E_g^2/4 + E_g D(n,k_z,+,-))^{1/2}$$

where

$$D(n,k_z,+/-) = \hbar^2 k^2/2m^*_{co} + (n + 1/2)\hbar eB/m^*_{co} +/- g^*_{co}B\mu_B$$

In c.m.t. the conduction band is very nonparabolic and when considering far-infra-red cyclotron resonance one has to calculate transition energies

$$\hbar w_c = E(n+1,k_z,+/-) - E(n,k_z,+/-)$$

and average over the electron energy distribution to calculate the position of the cyclotron resonance line. C.M.T. (x=0.2) has a high effective g-factor which leads to a spin splitting very close to one half of the cyclotron energy (in the limit $E_g << E_{so}$ the spin splitting is exactly one half of the cyclotron energy at the band edge according to Zawadski (1963)). As a consequence, at 4.2k and for cyclotron energies greater than about $30cm^{-1}$, the lowest spin split subband is the only one which is occupied and the electron gas is located mostly close to the gamma point . The expression for the cyclotron resonance energy simplifies to

$$\hbar w_c = E(1,0,+) - E(0,0,+)$$

and it is this expression which must be used in an analysis of cyclotron resonance.

7.3 Surface Electronic States

During device preparation the surface of c.m.t. is often treated so that an insulating oxide layer is grown on the surface. The surface charge that this introduces results in the sample being strongly accumulated (n-type) or inverted(p-type) even without the application of a gate voltage.

As a consequence of charge neutralisation and screening electrons are trapped in a thin surface layer and, for sufficiently good material, their energies are are quantised in direction perpendicular to the surface. The electrons are free to move in a plane parallel to the surface and they thus have energies, neglecting nonparabolicity of

$$E = \hbar^2/2m^*(k_x^2 + k_y^2) + E_{zi}$$

forming a series of electric subbands.

E_{zi} is the energy corresponding to the bottom of the ith subband.

The subbands are filled up to the Fermi level of the bulk material which for an n-channel accumulation layer corresponds to the bottom of the conduction band at low temperatures. The situation is shown schematically in figure 7.2. In a magnetic field (aligned perpendicular to the surface) the electrons move in cyclotron orbits and so their energies can be written as

Schematic Diagram of an Accumulation Layer

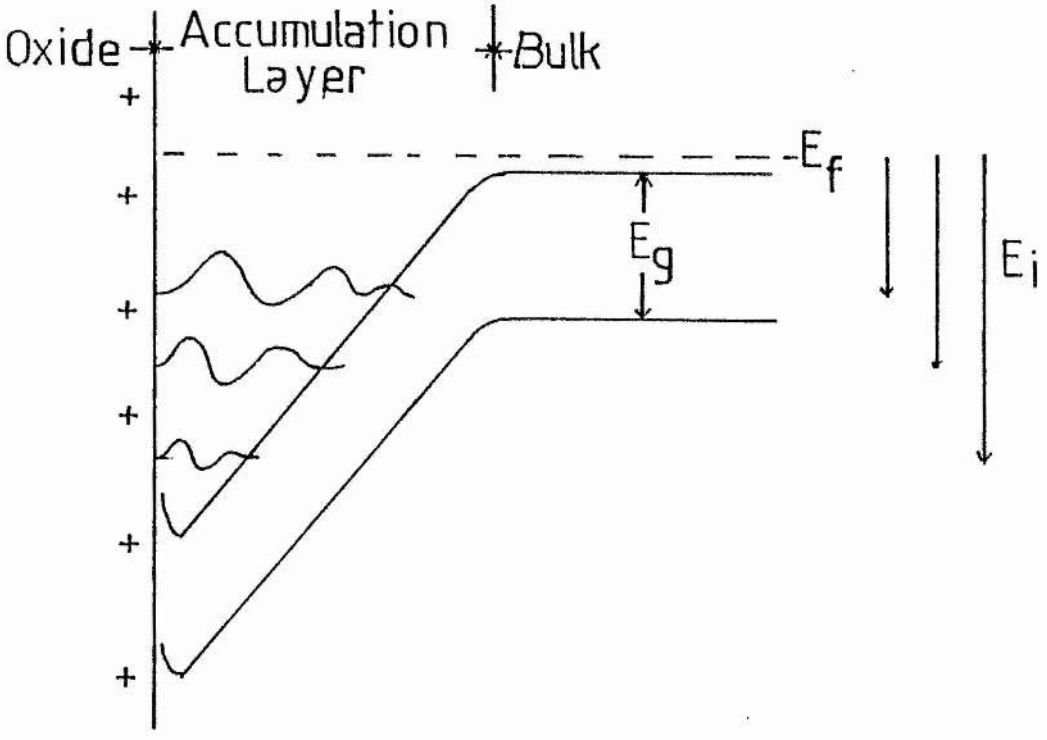

$$E = (n+1/2)\hbar w_c + E_{zi}$$

neglecting nonparabolicity, spin splitting and possible coupling with the valence band. If nonparabolicity and spin splitting were included the energy levels could be writen as

$$E = E_{zi} - E_g/2 + (E_g^2/4 + E_g((n + 1/2)\hbar eB/m^*_{co} \pm g^*_{co}B\mu_B))^{1/2}$$

where the energies are measured from the bottom of the conduction band.

Cyclotron resonance of the surface electrons has been observed by Koch et al (1984) and Nicholas et al (1984). The resonance involves only electrons close to the Fermi level since all the surface Landau states below the Fermi level will be occupied. Shubnikov de Haas oscillations have also been observed. This results from the increase in the number of states available for scattering when Landau levels pass through the Fermi level (Koch et al (1984), Nicholas et al (1984)).

7.4 Experimental

The sample used in this experiment was donated by G.E.C. It consisted of a 10um thick layer of c.m.t. grown on bulk CdTe using l.p.e.. The sample had a nitrogen temperature mobility of $100000 cm^2/vs$ and a carrier concentration at 77K of $10^{14} cm^{-3}$. The surface was chemically treated and the c.m.t. was strongly accumulated.

The sample was mounted in the pressure bomb as shown in figure 7.3. A hole in the stage allowed light to be transmitted to a bolometer as shown. The bolometer, consisting of a carbon resistor ground very thin, worked well in the pressure bomb (Wasilewski et al (1984)).

The cyclotron resonance results were taken using a far-infra-red laser described in the chapter 3 and the Shubnikov de Haas results were taken using the single differential circuit described in the chapter 6. Shubnikov de Haas and C.R. data were taken at 0kbar, 2.9kbar, 4.2kbar and 6.7kbar.

7.5 Results and Analysis

7.5.1 C.R. Data

Experimental recordings of the cyclotron resonance at the four pressures studied are shown in figure 7.4 and a graph of the cyclotron effective mass was shown in figure 7.5 The band edge effective mass is then calculated by solving the equation

$\hbar\omega_c = E(0,0,+) \quad - E(0,0,+)$ (see p100)

graphically for m^*_{co}. The calculated band edge effective masses are also shown in figure 7.5 as are the band gaps derived using a three band model. In the calculation it was assumed that the energy gap was related to the effective

Diagram Showing Set-up for

Transmission Experiments in Pressure Bomb

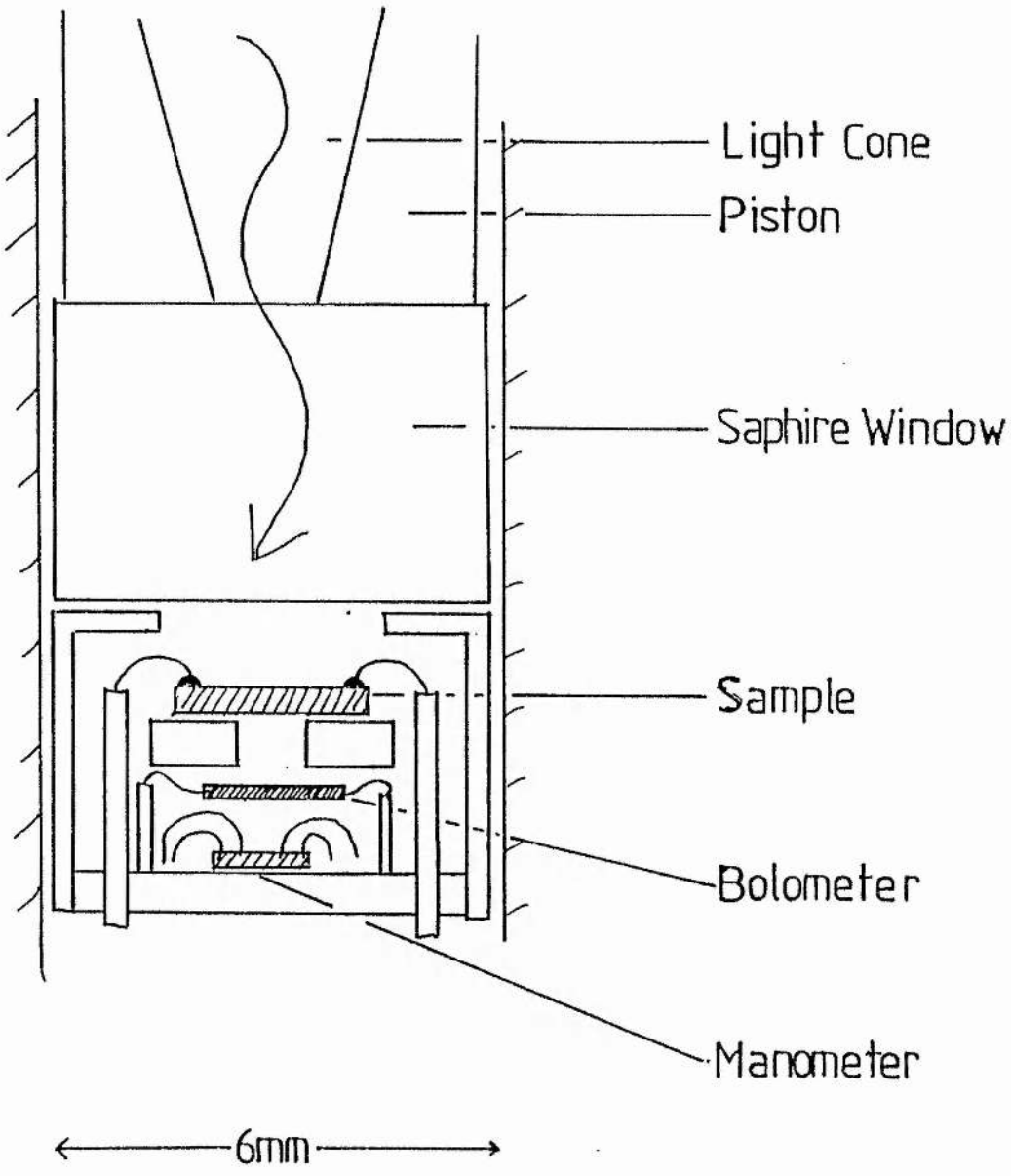

CR. in C.M.T. under Pressure
118μ

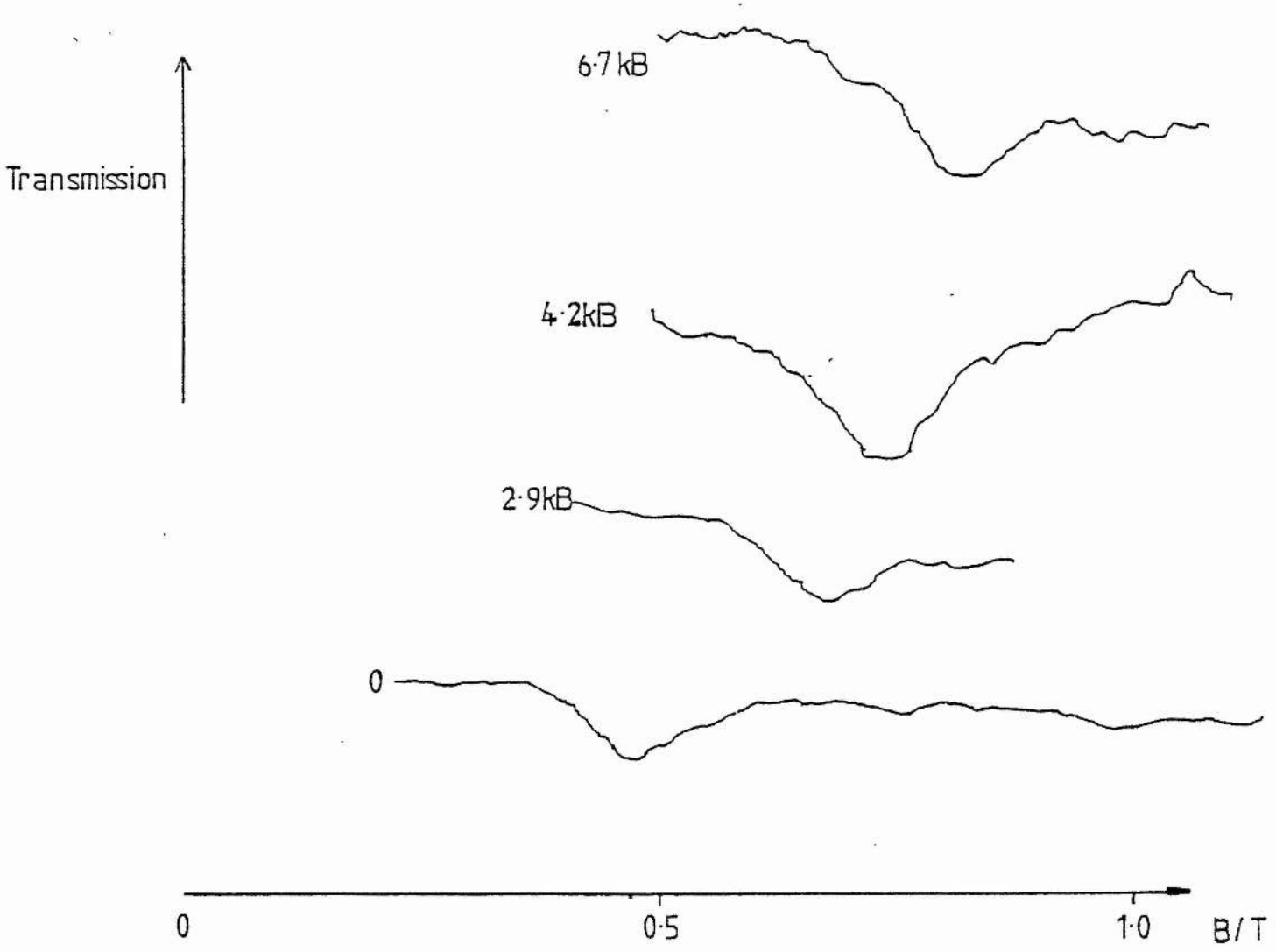

Graph of Pressure vs. Effective Mass and Band Gap

for C.M.T. ($x \sim 0{\cdot}2$)

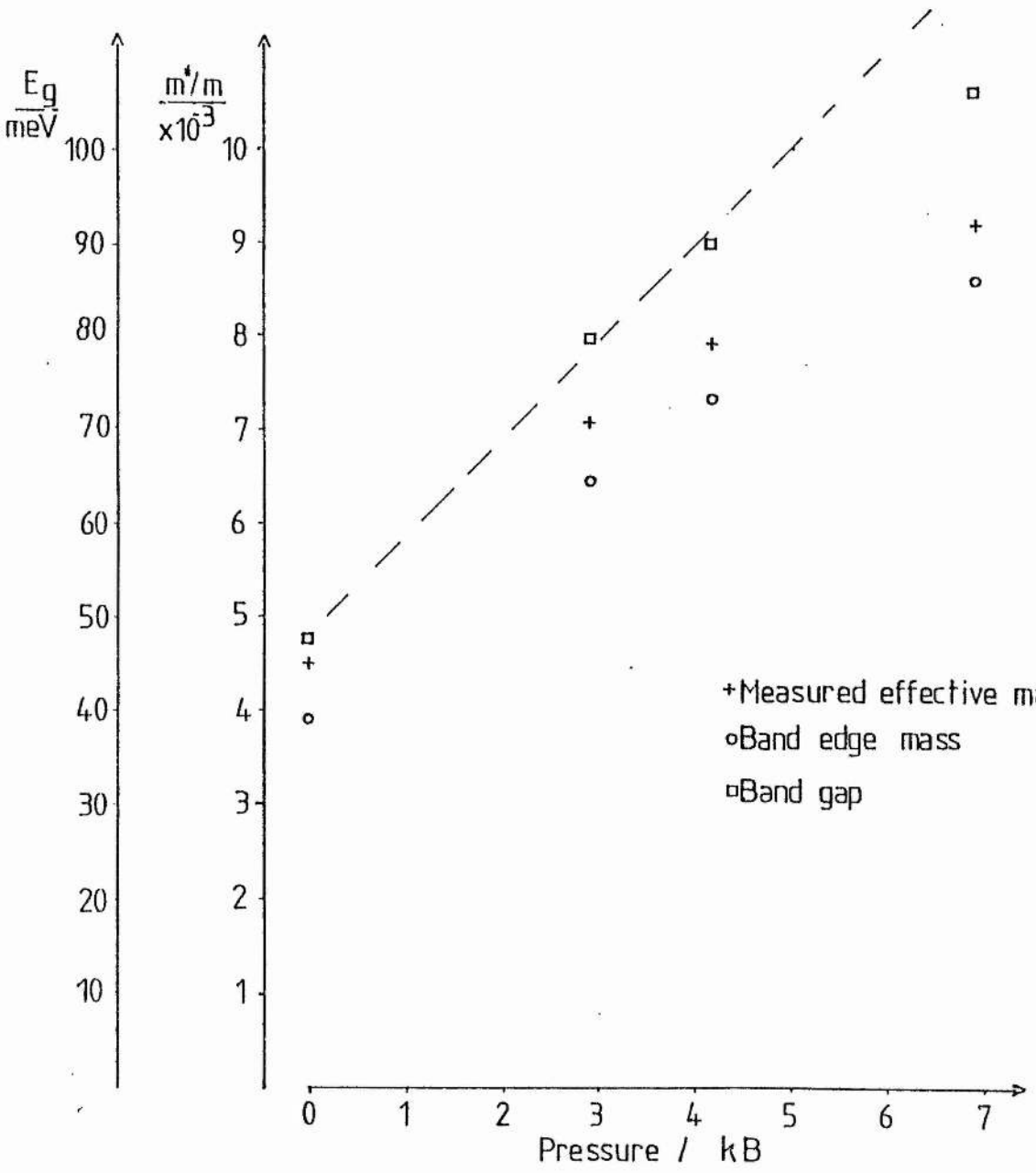

mass by

$$E_g = 4P^2 m^*_{co}/3\hbar,$$

that the energy $E_p = P^2/2m$ was accurately given by (18+3x)eV where x is the cadmium concentration (Willey and Dexter(1969)) and that P was insensitive to hydrostatic pressure. It seems unlikely that all of these assumptions particularly the last will be exact. Never-the-less the calculated increase in the bandgap, at least at low pressures seems to be in reasonable agreement with the pressure dependence given by Martinez(1979) shown as the dotted line.

7.5.2 Accumulation Layer Data

Shubnikov de Haas measurements shown in figure 7.6 were taken at each of the pressures. That the oscillations resulted from a 2-D electron gas on the surface was demonstrated by Walker(1984) who observed a $1/\cos\theta$ dependence for the positions of the oscillations (θ is the angle between the magnetic field and the normal to the surface). A Fourier transform analysis was attempted and in fact for the zero pressure results four periods were observed in the oscillations and it was assumed that these resulted from four subbands. This is in agreement with theoretical results by Takada et al (1981) and experimental results by Koch et al (1984) and Nicholas et al (1983).

Shubnikov de Haas Oscillations in C.M.T. under Pressure

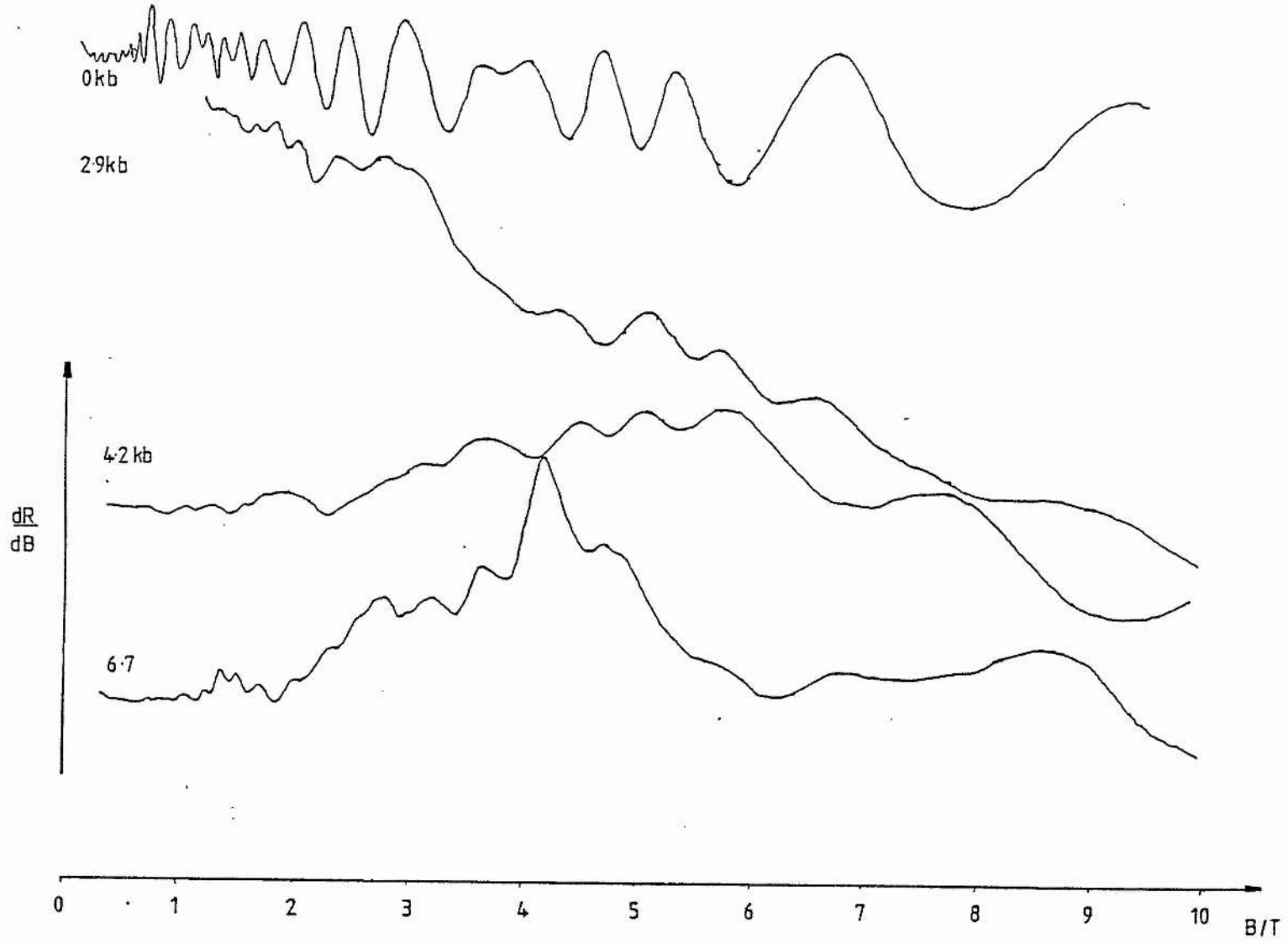

Once pressures were applied poorer signal to noise ratios were achieved which in conjunction with the reduction in amplitude of the signal made it impractical to apply Fourier transform techniques meaningfully and so the results were not analysed.

Surface subband cyclotron resonance shown in figure 7.7 is also observed at atmospheric pressure. It is also assumed that the four absorptions corresponded to four subbands, It can be seen that reasonable agreement between the subband energies determined from the two sets of experiments.

The subband energies in the cyclotron resonance experiment were calculated using the expression for the effective mass given by Zawadzki (1963) at an given energy away from the band edge.

i.e. $$m^*_c = m^*_{co}(2E_c/E_g + 1)$$

where m^*_c is the effective mass at an energy E_c into the conduction band. In our case the surface cyclotron resonance occurs at the Fermi energy which is pinned to the edge of the bulk conduction band so that the measured effective mass will be the mass at an energy E_i away from the subband edge. (E_i is the subband energy). The subband energies can be found by simply rearranging the equation for the effective mass.

i.e. $$E_i = E_g(m^*_c/m^*_{co} - 1)/2$$

Subband Cyclotron Resonance 7.7

118µ

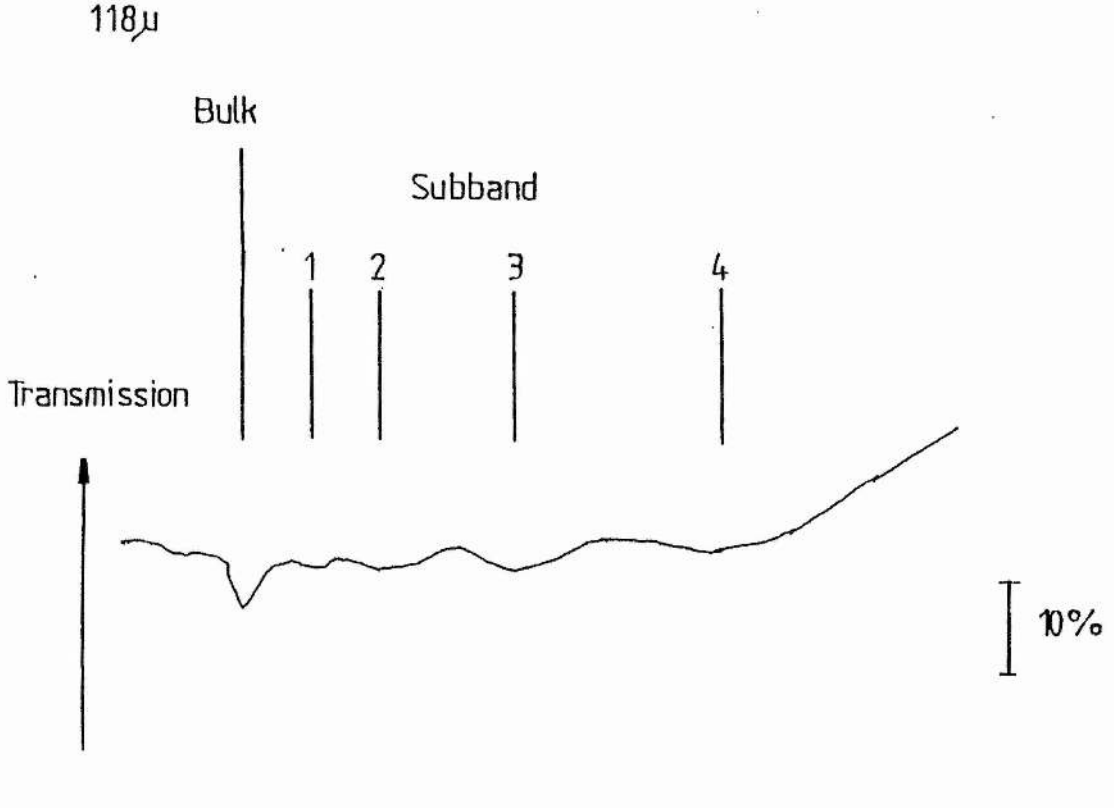

In the Shubnikov de Haas experiment resistance maxima occur when the bottom of each Landau level passes through the Fermi level. This applies to both 2-D and 3-D systems and is consequence of the maximum in the density of states which occurs at the bottom of each Landau level. When these maxima corrospond to Fermi level there are large numbers of adjacent full and empty electron states causing a maximum in electron momentum relaxation and therefore resistance. The wavevector perpendicular to the magnetic field is given by

$$k = 2e(n + 1/2)B/h$$

so that resonance occurs when $k = k_f$ (k_f is the wavevector at the Fermi level). The fundamental field (obtained from a Fourier transform of the oscillations), B_f occurs when n=1 i.e.

$$B_f = hk_f^2/3e$$

From k the number of electrons can be found directly and the Fermi energy can be estimated from the equation on

page 99. The Fermi energies were calculated using that equation and the effective mass and band gap obtained from the cyclotron resonance experiment. For material (like that used) where the Fermi level is close to the bottom of the bulk conduction band the Fermi energy is the same as the subband energy.

Table 7.1 shows the subband energies calculated from the Subnikov de Haas and from the cyclotron resonance data.

Table 7.1.

Subband	Cyclotron resonance		Shubnikov de Haas	
	m^*/m	E_i	B_f	E_i
1	0.0079	24meV	1.33T	26meV
2	0.0105	44meV	4.50T	55meV
3	0.0168	79meV	12.0T	108meV
4	0.0243	128meV	17.0T	133meV

7.6 Conclusions

In this chapter the cyclotron resonance in C.M.T. is studied as a function of pressure, the band edge mass is determined and variation of the band gap (estimated from the band edge mass) agrees well with standard values. The surface subbands are studied at zero pressure and Shubnikov de Haas oscillations and cyclotron resonance are observed. The subband energies are obtained from both experiments and reasonable agreement is achieved.

CHAPTER 8

CYCLOTRON EMISSION AS A SPECTROSCOPIC SOURCE

Cyclotron Emission as a Spectroscopic Source

8.1 Description of Source

In a magnetic field the conduction band of a semiconductor is split into Landau levels whose energies are given by

$$E=(N+1/2)\hbar w_c = (N+1/2)eB\hbar/m^*$$

If an electric pulse is applied to the material the electrons are excited into or within the conduction band and, as they try to decay back into equilibrium, radiative transitions occur at the cyclotron frequency and this constitutes the source. Since the spacing of the Landau levels is proportional to B the source is tunable with magnetic field.

Two materials are competitive for source applications : InSb and GaAs, though InP also yields narrow lines. There is little difference between the materials in terms of power output (this is of the order of microwatts and depends on the individual samples). The linewidth and tunability are, however, of some importance.

InSb is tunable up to $200cm^{-1}$ with a field of 3 Tesla, limited only by the energy of the L.O. phonon, and has a linewidth of $3cm^{-1}$. The application of hydrostatic pressure can, however, narrow the linewidth to about $1cm^{-1}$.

GaAs is tunable up to $110cm^{-1}$ with a field of 8 Tesla, limited by the field, and can have a linewidth as low as $0.5cm^{-1}$.

The lower frequency is limited by the linewidth of the emission.

8.2 Detectors

The ideal detector for a spectrometer application would be one with a completely flat response over the frequency range of interest i.e. a carbon or germanium bolometer. These were tried on a number of occasions but little success was achieved. This is probably because the ambient pressure and temperature used was unsuitable.

Instead the broadband response of Ga- doped Ge and n-GaAs detectors were used. The spectral response of these functions is shown in figure 8.1. The Ga doped Germanium detector opperates from $70cm^{-1}$ to $200cm^{-1}$, and the GaAs from $30cm^{-1}$ to $80cm^{-1}$ thus the entire range from $30cm^{-1}$ to $200cm^{-1}$ is covered. Some effort has been expended in the development of these detectors (see for example Stillman (1969) on GaAs and Moore and Shenker(1965)on germanium).

Spectral Responce of Broadband Detectors

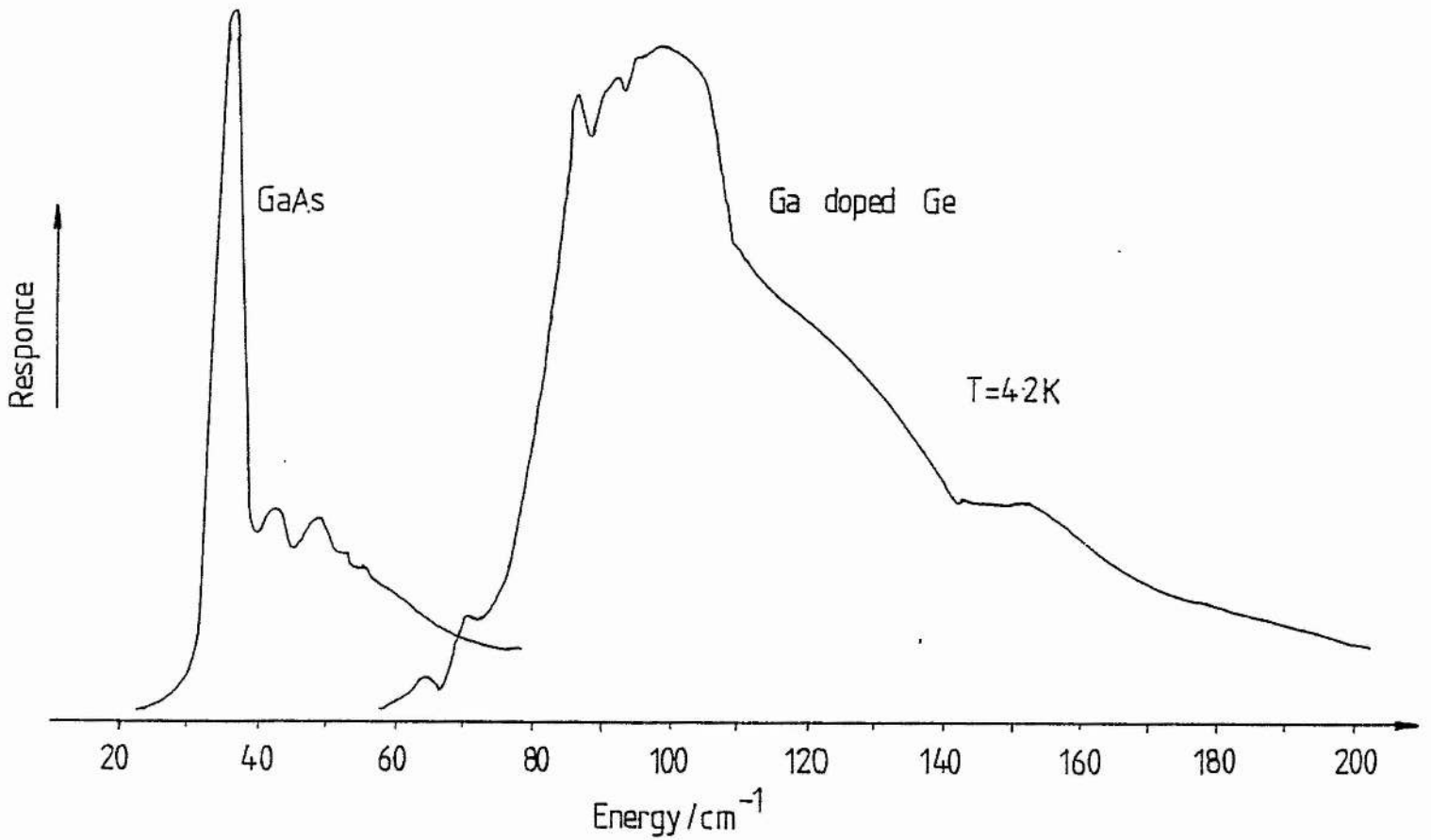

8.3 Spectrometer

A schematic diagram of the spectrometer is shown in figure 2. A sample sits in the emitter magnet producing photons of energy

$$E=eB\hbar/m^*.$$

This photon flux is allowed to fall on the sample and, by varying some experimental parameter (e.g., radiation energy, magnetic field, gate voltage,etc.), a spectrum can be taken.

In principle it is possible to take absorption, reflectivity and photoconductivity spectra using polarised or unpolarised light. So far we have used the spectrometer for absorption and photoconductivity spectra with unpolarised light.

8.4 Spectrometer Modes

8.4.1 Fixed Wavelength Mode

In this mode the emitter field is held constant and some parameter associated with the sample under study is changed. This could be the magnetic field in the case of the magnetooptics of semiconductors or the gate voltage in the study of two-dimensional devices. This operation is akin to that of the far-infra-red laser spectrometer which operates at a number of fixed frequencies, and in which some

Cyclotron Emission Spectrometer

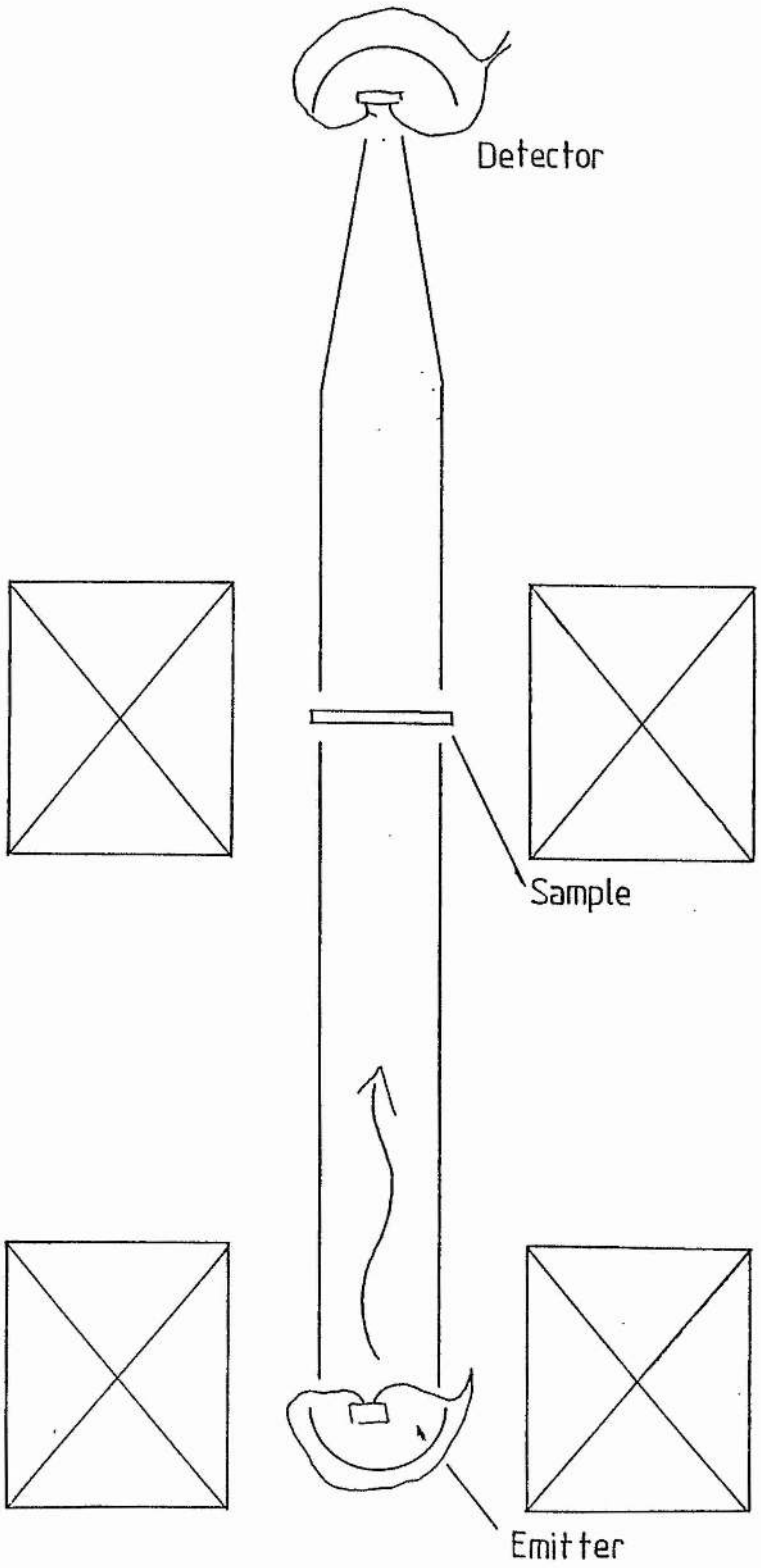

parameter of the sample is changed to produce spectra. The laser has two advantages over cyclotron emission; it produces much greater power (as high as 100mW) and has virtually zero linewidth. Cyclotron emission has a maximum power of 1μW and a minimum linewidth of $0.5cm^{-1}$.

In many applications ,however, cyclotron emission is still competitive with the laser spectrometer for the following reasons:

1. It is cheaper: the cost of an 8T superconducting magnet system to tune the emitter is less than £10K; that of a laser is (around £40K) and a superconducting magnet can be used for other things as well, such as transport experiments.

2. It is continuously tunable, whereas the laser is limited to discrete frequencies. It also allows spectra to be taken at small increments of frequency with an almost constant emission intensity in a region of particular interest.

It will be particularly useful in the study of relatively broad lines in the magneto-optics and impurity spectra of ternary and quaternary semiconductors and narrow gap materials. It could also be used in the study of phonon spectra using the Fourier transform mode discussed in the next section.

Signal to noise ratios using the existing detectors are quite good, and using existing techniques it should be possible to see absorptions as small as, say, 1%.

Cyclotron Resonance in InSb

In order to demonstrate the use of cyclotron emission as a spectroscopic source in the laser mode of operation cyclotron resonance in InSb was studied. The InSb had a carrier concentration (N_d-N_a) of $8x10^{13}cm^{-3}$ and mobility $700,000cm^2/Vs$ at 77K. A 50μm slice was cut, etched and placed in the second magnet. A GaAs detector was placed out of the field behind the InSb . Figure 8.3 shows the cyclotron resonance in InSb at three frequencies. At the highest frequency the splitting between the impurity-shifted cyclotron resonance and the cyclotron resonance is becoming resolved.

8.4.2 Swept Frequency Mode

In this mode the sample is held under constant conditions and the emitter field is swept giving a spectrum directly as a function of emitter energy. In this respect it is comparable to the Fourier Transform Spectrometer (F.T.S.) or to a grating spectrometer.

Cyclotron Emission as a Spectroscopic Source–

C.R. in InSb at an Arbritary Energy

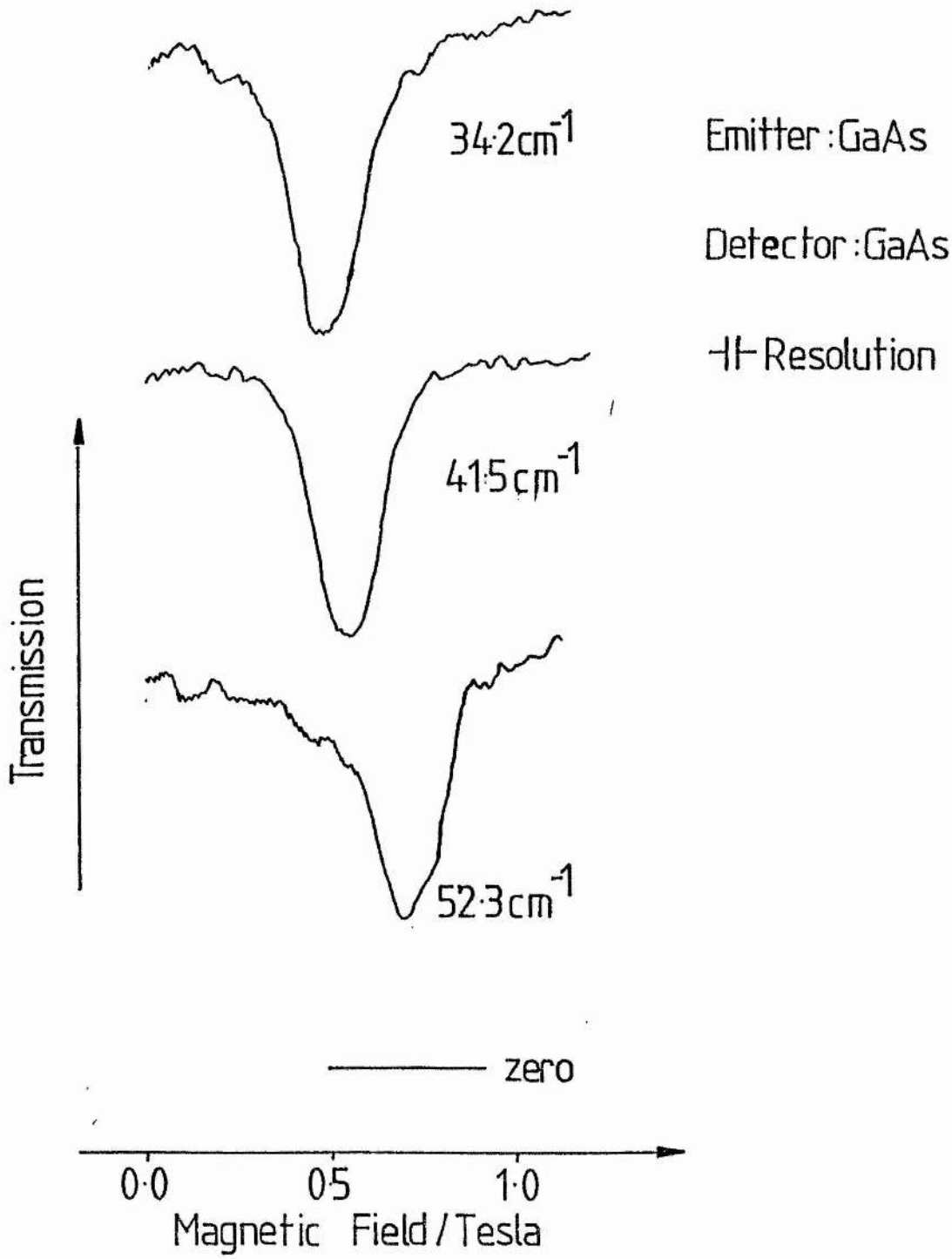

The F.T.S. is basically a Michelson interferometer. A broadband source is used and the response of the detector is recorded as one of the mirrors is swept. The Fourier transform of this recording gives an energy spectrum.

The relative merits of the two spectrometers are listed:

1. Cyclotron Emission has a much higher power output (1μw compared with 1nw in a $1cm^{-1}$ bandwidth centered at $30cm^{-1}$ for the F.T.S.).

2. Cyclotron Emission has a worse resolution: $0.5\ cm^{-1}$ at best compared with $0.1cm^{-1}$ typically on the F.T.S.

3. The F.T.S. covers a greater energy range than Cyclotron Emission (up to $1000cm^{-1}$ compared with $200cm^{-1}$). It is possible to have F.T.S.'s which also work in the near-infra-red and the visible.

4. Cyclotron emission is cheaper: a superconducting magnet costs less than £10K; compared with much more for a F.T.S. and does not require computer back-up.

5. With the F.T.S., complex beamsplitter interference patterns and absorptions arise. With cyclotron emission for absorption spectra only the broadband detector response

functions need be considered.

Impurity and Phonon Spectra in CdTe

To demonstrate the use of the spectrometer in this mode a spectra was taken of n-CdTe shallow impurity lines and phonon absorptions were also observed. The CdTe was 1mm thick and had a nominal carrier concentration of $5 \times 10^{13} cm^{-3}$ at 77K.

The 1s-2p impurity transition should occur at $84 cm^{-1}$ and the 2-TA phonon absorption band occurs at $72 cm^{-1}$ (see Carter et al(1977)). Figure 8.4 shows the spectra taken with a n-GaAs detector. Two lines can be clearly seen, one at $72 cm^{-1}$ and one at $86 cm^{-1}$, and these are identified as the phonon and impurity transitions respectively.

8.5 Other Examples of Spectrometer Application

8.5.1 Ion Implanted Silicon

An unusual example of a spectrometer application was the observation of interference fringes in the far-infra-red absorption spectrum of ion implanted silicon. A colleague, Mr A Thorley, has been modelling the optical properties of this material in an attempt to characterise implants. His theory and results on the F.T.S. were compared with results using cyclotron emission.

Absorption in CdTe 8.4

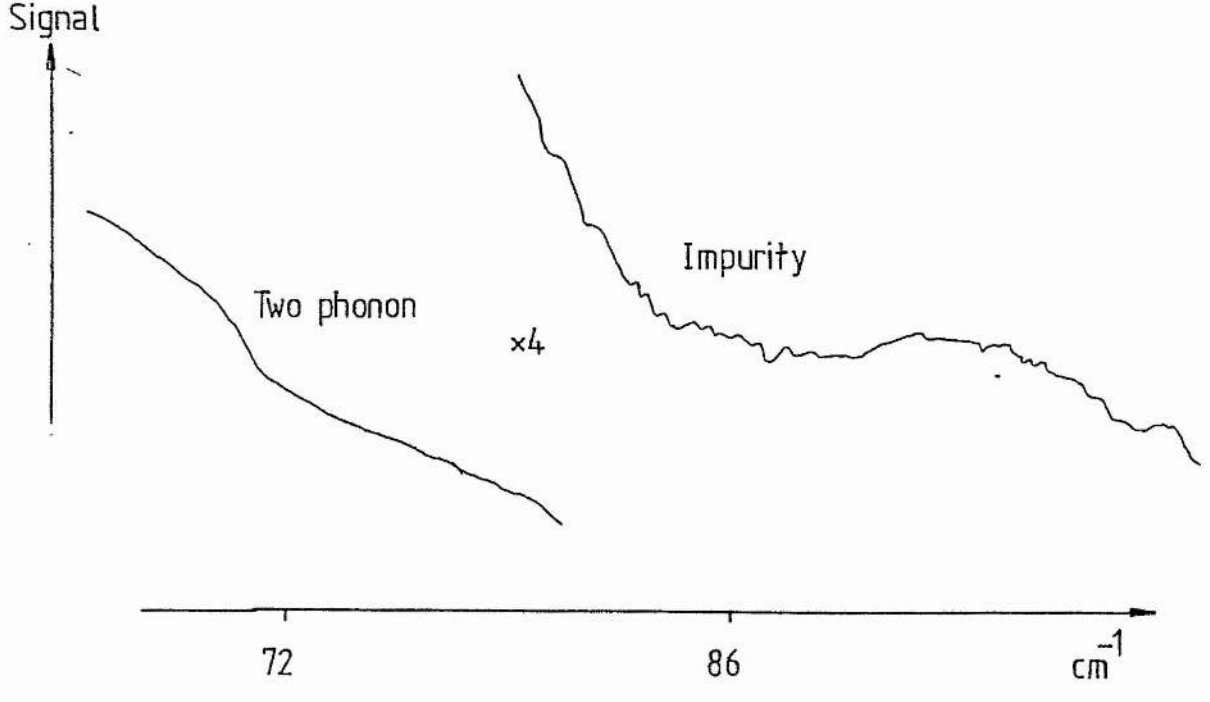

The silicon was placed between the emitter and detector and a spectrum was taken. Little change in the spectrum is expected as the sample is cooled to helium temperatures because the implant concentration results in the sample being well above the metal insulator transition . It turned out that the depth of modulation of the interference fringes is much less than that given by the theory or obtained on the F.T.S. This is partly due to the finite linewidth of the emission and partly due to the non-parallel radiation in the light pipe. It was concluded therefore that the F.T.S. was a more appropriate instrument or this application. The emission, background and ratioed spectrum is shown in fig.8.5.

8.5.2 Central Cell Structure

Although none of our samples produced lines which were narrow enough to resolve central cell structure in n-GaAs. E.Gornik(1982) has in fact done this in St. Andrews. Using an extreamly pure sample he has obtained emission lines with half-widths as low as $0.35cm^{-1}$. With this he was able to resolve the central cell structure of an n-GaAs sample. His result is shown in figure 8.6.

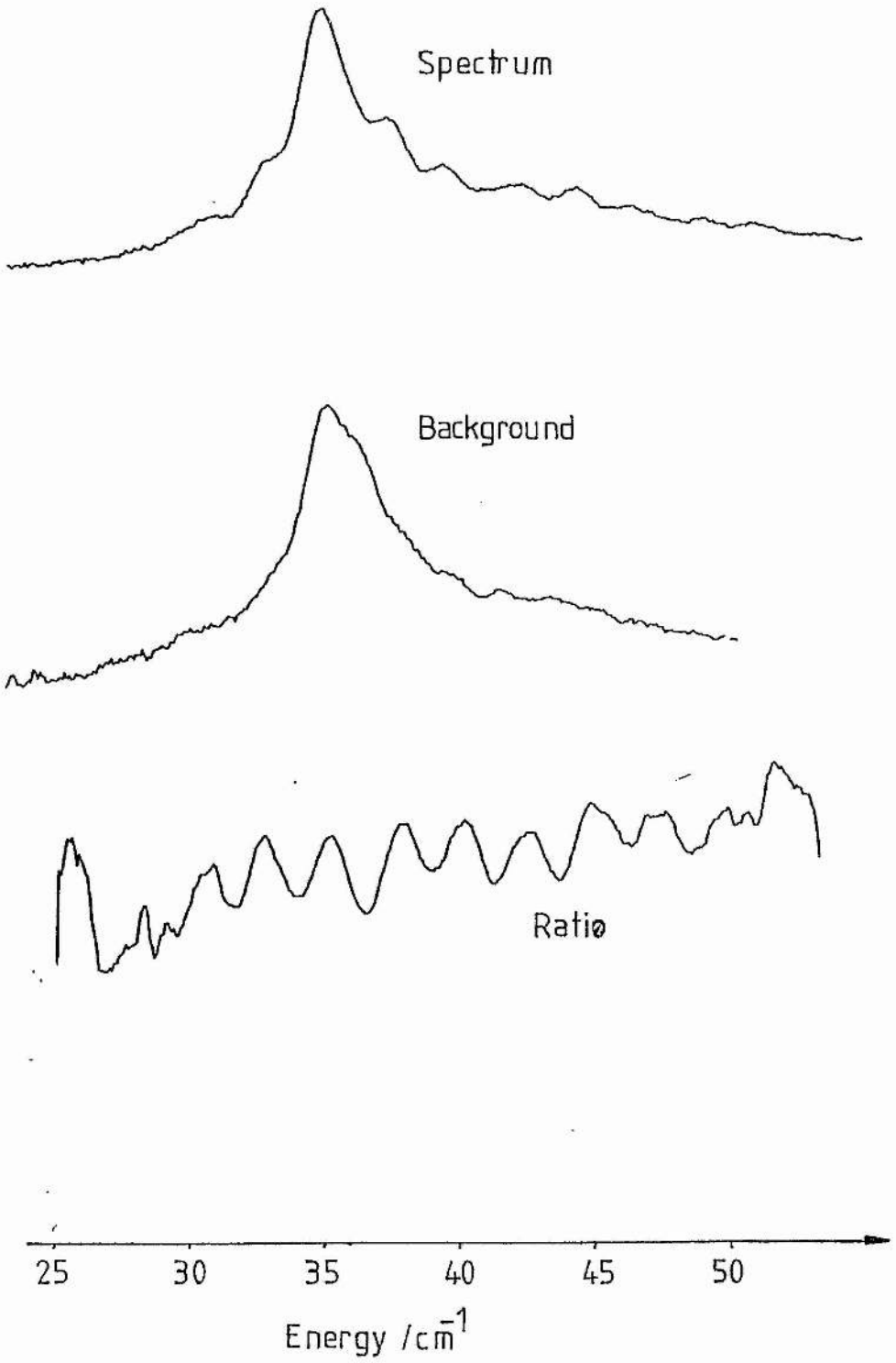
Spectrum
Background
Ratio
25
30
35
40
45
50
Energy /cm^{-1}

8.7

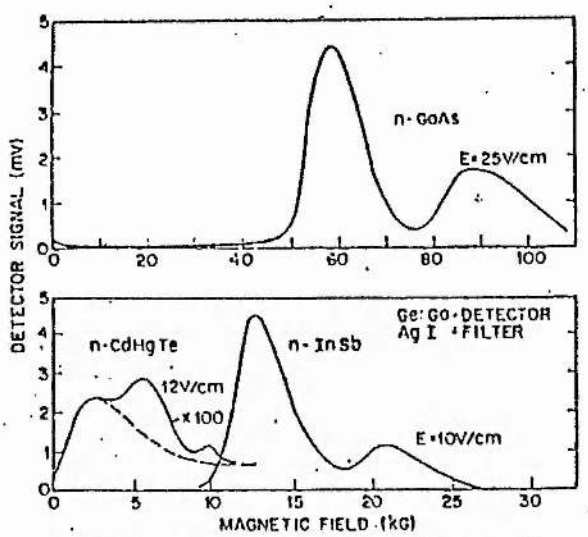

. Photoconductive signals of a Ge:Ga detector with a AgI filter inserted between detector and emitter. The emission frequency is tuned with the magnetic field.

8.6

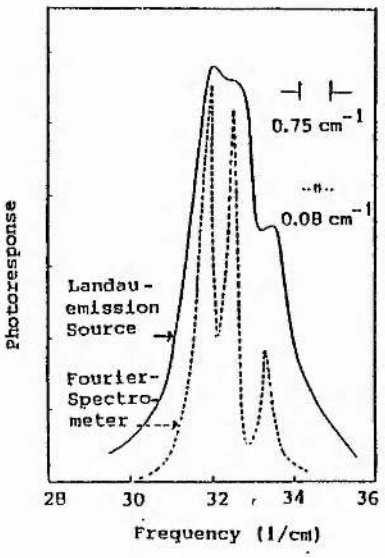

Photoconductive spectrum of the lowest impurity line (see fig. 2) of a GaAs sample (doping level $N_I \sim 3 \times 10^{14} cm^{-3}$) as obtained with a narrowband GaAs Landau source and a Fourier Spectrometer.

8.5.3 Phonon Spectra

The restrahlen bands of a number of crystals have also been observed using emitters GaAs, InSb and C.M.T. The absorption of AgI is shown in figure 8.7 for different emitters (after Gornik(1979)).

8.6 Conclusions

In this chapter the use of cyclotron emission as a spectroscopic source has been demonstrated. It has been compared with other spectroscopic techniques and it has been found that, under certain circumstances it is competitive with both the laser spectrometer and the Fourier transform instrument.

References

Aldridge and Greene
"Hydrogen Like systems in strong magnetic fields"
Phys. Stat. Sol., Vol 93, p 343, 1979

Allan, Black, Pidgeon, Seidenbush and Colter
"Impurity and Landau level electron lifetimes in n-GaAs"
to be published

Armistead, Kuchar, Najda, Porowski, Sotomayor Torres, Stradling and Wasilewski
"The use of hydrostatic pressure as an additional variable in the magnetooptical studies of III-V compounds and alloys"
to be published in Proc. 17th Conf. of Phys. Semicond.

Bajaj
"Polaron in a Magnetic Field"
Phys. Rev., Vol 170, P 694, 1968

Bauer and Kahlert
"Magnetophonon effect in C.M.T."
Phys. Rev. Lett., Vol 30, P 1211, 1973

Burstein
"Cyclotron resonance at infrared frequencies in InSb at room temperature"
Phys. Rev. Vol 103, P 825, 1956

Chamberlain
DPhil Thesis, University of Oxford, 1972

Chamberlain, Simmonds, Stradling and Bradley
"Excited state laser spectroscopy of impurities in III-V and II-VI compounds"
Sol. Stat. Comms., Vol 11, P 463, 1972

Colter, Look and Reynolds
"Low compensation V.P.E GaAs"
App. Phys. Lett. Vol 43, P 282, 1983

Dresselhaus, Kip, Kittel and Wagonner
"Cyclotron and spin resonance in InSb"
Phys. Rev. Vol 98, P 556, 1955

Dornhaus, Happ, Muller, Nimtz, Schlabitz and Zaplinski
"Low temperature galvanometric props of C.M.T."
Proc. 12th Int. Conf. on Phys. of Semicond., P 1157, 1974

Eaves and Portal
"Review of the magnetoimpurity effect in semiconductors"
J. Phys. C, Vol 12, P 2809, 1979

Golka, Trylski, Skolnick, Stradling and Couder
"Temperature dependence of linewidths of shallow impurity spectral lines"
Sol. Stat. Comms. Vol 22, P 623 1977

Gornik
"Recombination radiation from impact ionised shallow donors in InSb"
Phys. Rev. Lett. Vol 29, P 595, 1972

Gornik, Nguyen and Damen
"Radiative transitions of photoexcited electrons between Landau levels in InSb"
App. Phys. Lett. Vol 23, P 169, 1976

Gornik and Tsui
"Cyclotron emission from silicon mosfets"
Surface Science Vol 73, P 217, 1978

Gornik, Pratl, Muller and Kohl
"Hot electron energy distribution in strong magnetic fields"
J. Phys. C Vol 11, P1091, 1978

Gornik, Lindemann, Schawarz and Tsui
"Cyclotron emission in GaAs and InP"
Inst. Phys. Ser. No. 56., Chapter 8, P 631

Gornik, Schawarz, Lindeman and Tsui
"Emission spectroscopy on two-dimensional systems"
Surface Science, Vol 98, P 493, 1980

Gornik
"Magnetically tunable emitters and detectors"
Proc. Conf. on application of high magnetic fields in semiconductor physics., P 248, 1982

Gornik, Lindemann, Lassnig and Seidenbush
"Cyclotron resonance study of polarons in GaAs"
Phys. Rev. B., Vol 28, P 4693, 1983

Holtzman
MSc Thesis, University of St. Andrews, 1981

Hoult
DPhil Thesis, University of Oxford, 1974

Instone, Eaves, Portal, Houlbert, Perrier and Askanasy
"Energy relaxation of photoexcited electrons in n- and p-Ge by magnetoimpurity and magnetophonon processes"
J. Phys. C Vol 10, P 1585, 1977

Isler, Kafalas, Straus Macmillan and Bube
"Non gammma donorlevela and kinetics of electron transport in n CdTe"
Sol. Stat. Comms. Vol 10, P 619, 1972

Johnson and Dickey
"Infrared cyclotron resonance and related experiments in the conduction band on n-InSb"
Phys. Rev. B, Vol 1, P 2676, 1970

Kane
"Band structure of InSb"
J. Phys. Chem. Sol., Vol 1, P 249, 1957

Kaplan, Wagner and McCombe
"Cyclotron resonance linewidth in the quantum limit"
Sol. Stat. Comms., Vol 12, P 967, 1973

Kawabata
"Theory of cyclotron resonance linewidth"
J. Phys. Soc. Jap. Vol 23, P 999, 1967

Kawamura, Saji, Fukai, Sekido and Imia
"Cyclotron resonance line broadening due to carrier carrier scattering in Ge"
J. Phys. Soc. Jap., Vol 288 19649, P 1

von Klitzing
"Impurity spectroscopy on Te by means of magnetoresistance measurements"
Sol. Stat. Elect., Vol 21, P 223, 1978

Kobayashi and Otsuka
"Cyclotron resonance of hot electrons and nonlinear transport in n-InSb"
J. Phys. Chem. Sol., Vol 35, P839, 1974

Koch
Subband physics for narrow gap semiconductor C.M.T."
Proc. Conf. on narrow gap semiconductors, Mauterndorf, P 20, 1984

Komiyama
"Streaming motion and population inversion in crossed electric and magnetic fields"
Adv. in Phys. Vol 31, P 255, 1982

Kubo, Miyake annd Hashitsume
"Quantum theory of the galvanometric effect at extremely high magnetic fields"
Sol. Stat. Phys., Vol 17, P 264, 1965

Lodder and Fujita
"On the cyclotron resonance width due to electron charged impurity interaction"
Physica, Vol 38b, P 117, 1976

McCombe, Kaplan, Wagner, Gornik and Muller
"Absorption and emission studies of cyclotron resonance linewidths in InSb"
Phys. Rev. B, Vol 13, P 2536, 1976

Martinez
"Optical properties of semiconductors under pressure"
in Handbook of Semiconductors, Vol 2 published by North Holland Publishing Company, P 181, 1980

Mengelis, Stillman, Wolfe and Dimmock
"Far infrared recombination radiation from impact ionised shallow donors in GaAs"
Phys. Rev. Lett. Vol 23, P 1111, 1969

Meyer
"On the low temperature limit of mm-wave cyclotron resonance linewidths"
Phys. Lett. Vol 2, P 259, 1962

Nicholas and Stradling
"Energy relaxation in GaAs from magnetophonon spectra"
J. Phys. C, Vol 9, P 1253, 1976

Nicholas and Portal
"Hot electron transport in quantising magnetic fields"
Nato advanced studies institutes series, Series B Physics, Vol 52, P 255, 1977

Nicholas, Singleton and Sarkar
"Tilted field studies of C.M.T. accumulation Layers"
to be published, 1984

Ohyama
"Dynamical behaviour of photoexcited electron system in GaAs"
J. Phys. Soc. Jap. Vol 51, P 1431, 1982

Pidgeon, Vass, Allan, Prettle and Eaves
"Non-linear F.I.R. magnetoabsorption in GaAs"
Phys. Rev. Lett. Vol 50, P 1309, 1983

Poeler and Appel
"F.I.R. cyclotron resonance in C.M.T."
Phys. Lett. A, Vol 32A, P 286, 1970

Porowski, Konizykowski and Chroboczek
"Evidence from transport measurements at high pressures for donor ions occupying nonequivalent lattice positions in InSb"
Phys. Stat. Sol. Vol 63, P 291, 1974

Porowski, Pietrzkowski, Konczykowski and Dmowski
"Pressure induced slow relaxation of free electron concentration in undoped InSb"
Phys. Stat. Sol. Vol 73, P k131, 1976

Porowski, Konczewski, Konczykowski, Aulombard and Robert
"Magnetic freeze out on subsidiary minima associated levels in nInSb under pressure"
Proc 15th Int. Conf. of Phys. of Semiconductors, P 271, 1980

Prasad, Arora, Al-Mass'ari
"Theoretical explanation of observed quantum-limit cyclotron resonance linewidth in InSb"
Phys. Rev. B, Vol 23, P 5619, 1981

Roth and Argyes
Semiconductors and Semimetals, ed Willardson and Beer, Vol 1, P 159, 1966

Seeger
"Semiconductor physics"
Pub. Springer Verlag, 1980

Shin, Argyres, Horing and Lax
"High field anisotropic shielding and cyclotron resonance linewidth in the quantum limit"
Phys. Rev. B, Vol 7, P 5408, 1973

Simmonds
DPhil Thesis, University of Oxford, 1973

Stillman, Wolfe and Dimmock
Proc. 3rd. Symp. on GaAs, Inst. Phys., London, P 212, 1971

Stillman, Wolfe and Korn
"Photothermal ionisation of shallow donors in GaAs"
Proc 11th Conf. Phys. of Semiconds., Warsaw, P863, 1972,

Stillman Wolfe and Dimmock
"Far-infra-red photoconductivity in high purity GaAs"
Semiconductors and Semimetals., ed Willardson and Beer, P , 1976

Stradling
"Quantum transport in semiconductors"
Recent Dev. in Cond. Matt. Phys., ed Devreese, Vol 1, P 155, 1981

Stratton
"Influence of interelectronic collisions on conduction and breakdown in polar crystals"
Proc. Royal Soc., Vol A246, P 406, 1958

Takeda, Arai and Uemura
"2-D subbands in III-V and narrow gap semiconductors"
Proc. Conf. on Phys of Narrow Gap Semiconds., Linz, p 101, 1981

Vul', Bir and Shmartsev
Donor states in GaSb
Sov. Phys. Semicond., Vol 4, P 2005, 1971

Walker Vacation Student, Uni. of St. Andrews
Private communication, 1984

Walukiewicz, Lagowski, Jastrzebski, Rave, Lichtensteiger, Gatos and Gatos
"Electron mobility and free carrier absorption in InP; determination of compensation ratios"
J. App. Phys., Vol 51, P 2659, 1980

Wasilewski
Private communication, 1980

Wasilewski, Davidson, Stradling and Porowski
"Magnetooptical properties of donors under pressure" Proc. Conf. on Appl. of High Mag. Fields in Semicond. Phys., Grenoble, P 233, 1982

Wasilewski, Porowski and Stradling
"High pressure cell for magnetooptical measurements"
to be published, 1984

Willey and Dexter
"Helicons and nonresonant cyclotron absorption in C.M.T."
Phys. Rev., Vol 118, P 1181, 1969

Yafat, Keys and Adams
"Hydrogen atom in a strong magnetic field"
J. Phys. Chem. Sol., Vol 1, P 139, 1957

Yamada and Kurasawa
"Theory of hot electrons in strong magnetic fields" J. Phys. Soc. Jap., Vol 36, P 603, 1973

Zawadzki
"Magnetic moments of conduction electrons in III-V compounds"
Phys. Lett. Vol 4, P 190, 1963

Zverev
"Magnetoimpurity oscillations in Uniaxially stressed Ge"
Sov. Phys. Sol. Stat Vol 19, P 1179, 1977

Zverev
"Magneto-impurity oscillations in the photoconductivity of nGaAs"
Sov. Phys. JETP. Lett., Vol 35, No 2, P 109, 1983.